

SRG/ART-XC all-sky X-ray survey: Catalog of sources detected during the first year*

M. Pavlinsky¹, S. Sazonov^{1**}, R. Burenin¹, E. Filippova¹, R. Krivonos¹, V. Arefiev¹, M. Buntov¹, C.-T. Chen², S. Ehlert³, I. Lapshov¹, V. Levin¹, A. Lutovinov¹, A. Lyapin¹, I. Mereminskiy¹, S. Molkov¹, B. D. Ramsey³, A. Semena¹, N. Semena¹, A. Shtykovsky¹, R. Sunyaev¹, A. Tkachenko¹, D. A. Swartz², and A. Vikhlinin^{1,4}

¹ Space Research Institute, 84/32 Profsozna str., Moscow 117997, Russian Federation

² Universities Space Research Association, Huntsville, AL 35805, USA

³ NASA/Marshall Space Flight Center, Huntsville, AL 35812 USA

⁴ Harvard-Smithsonian Center for Astrophysics, 60 Garden Street, Cambridge, MA 02138, USA

October 1, 2021

ABSTRACT

We present a first catalog of sources detected by the Mikhail Pavlinsky ART-XC telescope on board the *SRG* observatory in the 4–12 keV energy band during its ongoing all-sky survey. The catalog comprises 867 sources detected on the combined map of the first two 6-month scans of the sky (December 2019 – December 2020), ART-XC sky surveys 1 and 2, or ARTSS12. The achieved sensitivity to point sources varies between $\sim 4 \times 10^{-12}$ erg s $^{-1}$ cm $^{-2}$ near the ecliptic plane and $\sim 8 \times 10^{-13}$ erg s $^{-1}$ cm $^{-2}$ (4–12 keV) near the ecliptic poles, and the typical localization accuracy is $\sim 15''$. Of the 750 sources of known or suspected origin in the catalog, 56% are extragalactic (mostly active galactic nuclei, AGN; and clusters of galaxies) and the rest are Galactic (mostly cataclysmic variables, CVs; and low- and high-mass X-ray binaries). For 114 sources, ART-XC has detected X-rays for the first time. Although the majority of these (~ 80) are expected to be spurious (given the adopted detection threshold), there can be a significant number of newly discovered astrophysical objects. We have started a program of optical follow-up observations of the new and previously unidentified X-ray sources, which has already led to the identification of several AGN and CVs. With the *SRG* all-sky survey planned to continue for a total of four years, we can expect the ART-XC survey in the 4–12 keV band to significantly surpass previous surveys that were carried out in similar (medium X-ray) energy bands in terms of the combination of angular resolution, sensitivity, and sky coverage.

Key words. Surveys – Catalogs – X-rays: general

arXiv:2107.05879v2 [astro-ph.HE] 30 Sep 2021

1. Introduction

All-sky X-ray surveys have played a paramount role in the exploration of Galactic and extragalactic astrophysical objects ever since the first such survey was carried out by the *Uhuru* orbital observatory in 1970–1973 (Forman et al. 1978). A revolutionary all-sky survey in soft X-rays was performed in 1990–1991 by the *Röntgensatellit* (*ROSAT*) orbital observatory. The grazing incidence X-ray telescope on *ROSAT* improved the sensitivity by two orders of magnitude with respect to previous surveys, which enabled the detection of $\sim 10^5$ sources in the 0.1–2.4 keV energy band (Voges et al. 1999; Boller et al. 2016).

However, soft X-rays provide a strongly biased view of the Universe because X-ray sources are frequently obscured from our view by gas and dust within the object and/or in the intervening matter. Hence, there is a need for large-area surveys that are performed at energies above a few keV. Since the beginning of the 21st century, a number of such surveys have been performed in the standard (2–

10 keV) and harder X-ray energy bands. Most of them are serendipitous, that is, they are based on a compilation of pointed or slew observations. The *Rossi X-ray Timing Explorer* (*RXTE*) Slew Survey (XSS) achieved a sensitivity $\sim 10^{-11}$ erg s $^{-1}$ cm $^{-2}$ and angular resolution $\sim 1^\circ$ in the 3–20 keV energy band in the extragalactic sky ($|b| > 10^\circ$) (Revnivtsev et al. 2004; Sazonov & Revnivtsev 2004). A somewhat better sensitivity ($\sim 5 \times 10^{-12}$ erg s $^{-1}$ cm $^{-2}$) was recently reached in the 4–10 keV band in the Monitor of All-sky X-ray Image/Gas Slit Camera (MAXI/GSC) all-sky survey (Kawamuro et al. 2018; Hori et al. 2018), which similarly to XSS is conducted by a collimator instrument. A similar average depth in the 2–12 keV band, but with excellent angular resolution (achieved through X-ray mirror optics), characterizes the *XMM-Newton* Slew Survey (XMMSL, Saxton et al. 2008); however, XMMSL has covered the sky highly nonuniformly and not in its entirety (84% by the end of 2014, the time of compilation of the XMMSL2.0 catalog¹). Finally, hard X-ray (above 15 keV) all-sky surveys carried out by the coded-mask Imager on-Board the INTEGRAL Satellite (IBIS) on board the *INTERNATIONAL Gamma-Ray Astrophysics Laboratory* (INTEGRAL) and the Burst Alert Telescope (BAT) on board the Neil Gehrels *Swift* observa-

* The catalog is only available in electronic form at the CDS via anonymous ftp to cdsarc.u-strasbg.fr (130.79.128.5) or via <http://cdsweb.u-strasbg.fr/cgi-bin/qcat?J/A+A/> and at <http://srg.cosmos.ru>.

** E-mail: sazonov@iki.rssi.ru

¹ <https://www.cosmos.esa.int/web/xmm-newton/xmmsl2-ug>

tory have reached a depth $\sim 10^{-11}$ erg s $^{-1}$ cm $^{-2}$ and angular resolution ~ 10 arcmin (e.g., Krivonos et al. 2007, 2012; Bird et al. 2016; Oh et al. 2018). All these surveys together have discovered several hundred new X-ray sources that had not been detected in soft X-rays during the *ROSAT* all-sky survey, in particular, a large number of heavily obscured active galactic nuclei (AGN) and high-mass X-ray binaries (HMXBs). These discoveries have greatly improved our understanding of the corresponding populations of objects in the local Universe and in the Galaxy (e.g., Koss et al. 2017; Kretschmar et al. 2019; Malizia et al. 2020).

The *Spektrum-Roentgen-Gamma (SRG)* orbital observatory² (Sunyaev et al. 2021), launched on 13 July 2019 from the Baikonur Cosmodrome to a halo orbit near the L2 point of the Sun–Earth system, promises to once again revolutionize our understanding of various populations of X-ray sources. The observatory is equipped with two grazing incidence telescopes: the extended ROentgen Survey with an Imaging Telescope Array (eROSITA) (Predehl et al. 2021), and the Mikhail Pavlinsky Astronomical Roentgen Telescope – X-ray Concentrator (ART-XC) (Pavlinsky et al. 2021), which operate in the overlapping 0.2–8 keV and 4–30 keV energy bands, respectively. Since 12 December 2019, *SRG* has been performing an all-sky X-ray survey, which is planned to consist of eight scans of the whole sky, each lasting 6 months.

At energies above 2 keV, eROSITA and ART-XC will for the first time survey the whole sky with subarcminute angular resolution. The ART-XC survey in the 4–12 keV band is expected to significantly surpass previous surveys that were carried out in similar energy bands in terms of the combination of angular resolution, sensitivity, and uniformity. ART-XC is a crucial component of the *SRG* mission because it provides better sensitivity than eROSITA at energies above 6 keV (Sunyaev et al. 2021). ART-XC is particularly important for systematic search and exploration of absorbed X-ray sources.

By December 15, 2020, *SRG* had completed two full scans of the sky. This paper presents a catalog of sources detected by ART-XC during this early stage of the mission.

2. Data analysis

After an initial calibration and performance verification (CalPV) phase, the *SRG* observatory started conducting its all-sky X-ray survey on 12 December 2019. During the survey, the optical axes of the ART-XC and eROSITA telescopes rotate with a period of 4 hours around the spacecraft Z-axis that is pointed approximately toward the Sun (this main regime of observations is hereafter referred to as “survey mode”). This enables full sky coverage every 6 months (see Sunyaev et al. 2021 for further details). By 10 June 2020, the entire sky had been covered for the first time and by 15 December 2020 for the second time. The catalog of sources presented in this paper is based on the ART-XC data accumulated during these two surveys, hereafter referred to as ART-XC sky survey 1 and ART-XC sky survey 2 (or ARTSS1 and ARTSS2 for short), respectively.

We only used the ART-XC data obtained in survey mode and disregarded the data obtained during deep observations of selected regions of the sky in scanning mode (when the ART-XC and eROSITA telescopes perform a raster scan of

a field with a size up to $12.5^\circ \times 12.5^\circ$, see Sunyaev et al. 2021; Pavlinsky et al. 2021 for further details) and during pointed observations³. Time intervals when the calibration sources were inserted into the collimators or when high voltage was switched off on the detectors for depolarization (see Pavlinsky et al. 2021 for details) were also excised. As the ART-XC background has proved to be exceptionally stable (Pavlinsky et al. 2021), no cleaning of ART-XC X-ray data for high background periods was needed. Only events detected in one or two upper detector strips and in one or two lower strips were selected, while events detected in a larger number of strips were not used in the analysis⁴.

We produced a summed map of ARTSS1 and ARTSS2 (the combined first-year survey is hereafter referred to as ARTSS12) in the 4–12 keV energy band. The choice of this band is motivated by the energy dependence of the ART-XC effective area (see fig. 19 in Pavlinsky et al. 2021), namely by a significant and abrupt drop in sensitivity above 12 keV. We then applied to this map a set of algorithms for detection of point and extended X-ray sources that are described in §2.3 and §2.4, respectively, which resulted in a catalog of sources detected during ARTSS12.

2.1. Construction of maps

In order to construct all-sky maps, the ART-XC survey data were split into 4,700 overlapping sky tiles in equatorial coordinates. All tiles have an equal tangential size of 3.6×3.6 degrees, and the overlap between tiles is 0.6 degree in the right ascension and declination directions. This is needed to eliminate edge effects during sky background determination and source detection. The same scheme is used for eROSITA data products (Predehl et al. 2021). For each tile, a set of standard maps were prepared, including an exposure map, particle and photon background maps, and sky images. All maps consist of 1024×1024 pixels of $12.66''$. The maps were prepared for ARTSS1 and ARTSS2 separately and were then combined.

When combining the data of the seven ART-XC telescope modules, we took the misalignment of their optical axes and the actual positions of the optical axes at the detectors into account, which had been calibrated using observations of bright X-ray sources during the survey and a special series of pointed observations of the Crab nebula, respectively. The exposure maps were corrected for the vignetting function, which had been measured using ground calibrations of the mirrors and detector units as well as extensive ray-tracing simulations. We refer to Pavlinsky et al. (2021), where all the instrument calibration activities preceding the construction of maps are discussed in detail.

2.2. Background estimation

To estimate the particle background, we took advantage of the fact that the efficiency of the ART-XC X-ray optics

³ Scanning and pointed observations have taken place not only during the CalPV phase, but also during short recesses in the all-sky survey associated with *SRG* orbit corrections.

⁴ The coordinate resolution of each of the seven ART-XC telescope modules is provided by two mutually perpendicular sets of 48 strips on the two sides of a CdTe crystal. The strip width corresponds to an angular resolution of $45''$ (Pavlinsky et al. 2021).

² <http://srg.cosmos.ru>

vanishes at energies higher than 30 keV, and we used observations of blank-sky fields (i.e., regions without bright X-ray sources). Assuming that all events in these blank sky observations are associated with particle background, we determined the ratio of count rates in the energy bands of 4–12 keV and 30–70 keV for each detector pixel. These ratios were then combined with the measured 30–70 keV count rate for each survey mode observation to determine the expected number of particle background events in the 4–12 keV energy band in each detector pixel during each 1 s time interval of the survey. These values were then projected onto the sky map. Because the particle background measured in the ART-XC orbit is extremely stable, we expect this background estimation to be robust. The cosmic X-ray background provides a negligible contribution to the total background in the 4–12 keV energy band.

The residual background, associated with the uncertainty of the particle background estimation and with possible large-scale X-ray structures in the sky (e.g., the Galactic Ridge X-ray emission), was estimated from X-ray images themselves. To this end, the particle background was subtracted from a given X-ray image and then all significant details at angular scales below 5' are eliminated from the X-ray image using the wavelet decomposition technique (`wvdecomp`, Vikhlinin et al. 1998). This angular scale was chosen so that it is much larger than the full width at half maximum (FWHM) of the ART-XC point spread function (PSF), equal to 53'' (Pavlinsky et al. 2021), but is much smaller than the ART-XC field of view (FoV), 36' in diameter (Pavlinsky et al. 2021).

2.3. Detection of point sources

Convolution of an image with an instrument's PSF is equivalent to a maximum likelihood test for the case of high background when the statistics is Gaussian (e.g., Pratt 1978). However, in X-ray images, the noise statistics is often Poisson, and the optimal filter, which maximizes the probability of detection of real sources and minimizes the probability of false detections of statistical fluctuations, can in this case be written as (The Lynx Team 2018; Ofek & Zackay 2018)

$$\Phi = \ln \left(\frac{f}{b} P + 1 \right), \quad (1)$$

where f is the source flux, b is the background brightness, and P is the PSF image normalized to unity. This approach can be readily extended to the case of any specific spectral flux distribution.

In the case of ART-XC data, the situation is even more complicated because the PSF is not centrally symmetric and the PSF and vignetting strongly vary across the FoV. Therefore we used the following filter for source detection:

$$\Phi(x) = \ln \left(\frac{f(e)v(x,e)}{b(x,e)} P(x_0|x) + 1 \right), \quad (2)$$

where x_0 is the photon coordinates, e is the photon energy, $f(e)$ is the expected spectral energy distribution of X-ray sources, $v(x,e)$ is the vignetting function, $b(x,e)$ is the spectral brightness of the background as a function of coordinates and energy, and $P(x_0|x)$ is the PSF value at x_0 under the assumption that the source is located at x . The optimal filter described by equation (2) thus depends on the

energy of every photon and on the estimated background in every point in the image. Hence, it is applied to ART-XC data on an event-by-event basis.

We adopted the vignetting function from the results of extensive ray-tracing simulations of the ART-XC X-ray mirrors (Pavlinsky et al. 2021). The $P(x_0|x)$ function was precomputed for a fine grid of positions in the ART-XC FoV using the ART-XC PSF model obtained from the results of ground calibrations of the mirror systems (Gubarev et al. 2014; Krivonos et al. 2017; Pavlinsky et al. 2018, 2019a,b, 2021). Interpolation was then used to evaluate $P(x_0|x)$ for a photon at a given position in the ART-XC FoV.

For X-ray sources, we assumed a power-law spectrum with a photon index $\Gamma = 1.4$, which approximately corresponds to the slope of the cosmic X-ray background spectrum in the 4–20 keV energy band considered here (Gruber et al. 1999; Churazov et al. 2007; Krivonos et al. 2021) and to the slope of the cumulative X-ray spectrum of the local population of AGN (Sazonov et al. 2008). This is a reasonable assumption (which can be improved in future analyses of ART-XC all-sky survey data) because nearly half of the ARTSS12 sources prove to be AGN, whereas the remaining ones are mostly X-ray binaries and cataclysmic variables (CVs), whose X-ray spectra are not dramatically different from those of AGN. For the background, we adopted a flat spectrum with a photon index $\Gamma = 0$, which is close to the measured ART-XC particle background spectrum in the 4–20 keV energy band.

To calculate the flux-to-background ratio in equation (2), we assumed that point sources have a diameter of 53'', that is, that the diameter is equal to the FWHM of the ART-XC PSF. Given the ART-XC PSF, this size is also the diameter of the circle within which half of the source photons with angular offsets smaller than 5' are contained (source photons with larger offsets are included in the background, see §2.2 above).

Sources are detected in images that are obtained by convolution of raw ART-XC data with the optimal filter given by equation (2) (hereafter referred to as convolution images) as peaks with values above some specified threshold. In the case of multiple detections within 53'' from each other, only the highest peak is taken into account (with the corresponding coordinates and amplitude).

In order to specify thresholds for source detection in convolution images, we carried out Monte Carlo simulations of empty fields (Burenin et al., in preparation). Only the particle background was simulated because it strongly dominates the ART-XC background. We thus computed the expected number of peaks of a given amplitude per square degree in the convolution image of an empty field, N_f , for different background levels. Using these tabulated results of simulations, we can evaluate the probability for a source detection in a given ART-XC convolution image (with the corresponding background level) to be spurious as $P_f = N_f/N_{tr}$, where N_{tr} is the effective number of trials. The latter can be estimated from the adopted size of pointed sources (53'') as the number of independent cells for source detection per square degree. Finally, the statistical significance (signal-to-noise ratio), S/N , of the source detection can be determined from the likelihood $L = -2 \ln P_f + \text{const}$, where the constant is defined so that the value of the complimentary error function at $S/N = \sqrt{L}$ is equal to P_f .

We adopted the $S/N = 4.5$ level as a threshold for detection of pointed sources. The source flux within the 53''

aperture that corresponds to $S/N = 4.5$ for a given background level must then be substituted into equation (2). The resulting filter is optimal for the detection of weak sources near the adopted S/N threshold, with the corresponding flux threshold depending on the estimated background at a given position in the sky. However, brighter sources will also be confidently detected with this filter (see section A.3.2 in [The Lynx Team 2018](#)). Eventually (in §3.1), we imposed a slightly (by $\sim 7\%$) higher S/N cut to include sources into a final ART-XC catalog to reduce the fraction of spurious detections.

For future versions of the ART-XC source catalog, we plan to further adjust both the characteristic source size and the S/N threshold, which define the optimal filter given by equation (2). They are currently equal to $53''$ and 4.5 , respectively. We will use additional simulations of the source detection procedure in the ART-XC all-sky survey for the adjustment.

[Figure 1](#) shows an example of a detection of a faint source during the all-sky survey; the source with a flux of only a few photons is detected here with high significance. [Figure 2](#) shows a fragment of the resulting convolution image of the Galactic center region.

2.4. Detection of extended sources

The filter given by equation (2) is only optimal for detection of point sources in the ART-XC survey. Sources with an angular size larger than the ART-XC PSF, that is, $\gtrsim 1'$, cannot be detected efficiently with this filter. Therefore we used the standard wavelet decomposition method (`wvdecomp`, [Vikhlinin et al. 1998](#)) to detect sources of large angular size (from ~ 1 arcmin up to approximately half a degree).

Specifically, sources were found as peaks in the stacked decomposition images⁵ of larger than 4.5σ significance (Poisson statistics) at 6th to 8th wavelet scales, corresponding to angular scales approximately from $3'$ to $12'$. The significance of a detection of extended sources was estimated using the noise images produced by `wvdecomp`.

We then correlated the candidate sources with catalogs of galaxy clusters, namely, the Meta-catalog of X-ray detected clusters of galaxies (MCXC, [Piffaretti et al. 2011](#)) and the Second Planck catalog of Sunyaev–Zeldovich sources (PSZ2, [Planck Collaboration et al. 2016](#)), as well as with the catalog of Galactic supernovae remnants (SNRs, [Green 2019](#)). The adopted matching radius is $2'$ for MCXC, $5'$ for PSZ2, and the maximum size of a given remnant for the SNR catalog. In the last case, we also inspected the associations of X-ray sources with SNRs manually. The chosen matching radii take the typical positional uncertainties of object coordinates in the corresponding catalogs into account.

If an extended source was not found in any of these catalogs, we included it in the final ART-XC source list only if its detection significance was higher than 5.5σ . This threshold was chosen so that fewer than one spurious extended source is expected to be found in the survey, given the probability of false detection and the number of indepen-

dent source detection cells (estimated assuming a minimum size of extended sources of 3 arcmin) over the whole sky. Application of the second criterion led to the inclusion of two additional extended sources: the galaxy M31 (namely, unresolved X-ray emission from its central region), and the massive cluster of galaxies IGR J1744–3232.

2.5. Measurement of source X-ray fluxes

X-ray fluxes for detected point sources were measured in a circular aperture of $2'$ radius, which contains approximately 90% of the total X-ray flux from the source at angular scales $< 5'$. The flux was calculated from the count rate of background-subtracted photons in the aperture. As was explained in §2.1, the vignetting effects were taken in account in the calculation of the exposure maps that are used to measure the source fluxes. The corresponding Poisson uncertainties were estimated using the approximate formulae from [Gehrels \(1986\)](#).

We calibrated the ratio of flux to count rate for the 4–12 keV energy band using the available ART-XC observations of the Crab nebula, taking the difference between the slopes of the spectrum of the Crab nebula ($\Gamma = 2.1$) and the fiducial spectrum used in our source detection algorithm ($\Gamma = 1.4$) into account. This resulted in a difference of a few percent in the fluxes. The Crab nebula is observed by ART-XC as an extended source of $\approx 1'$ size, as expected. Its flux was computed from the spectral parameters given in [Madsen et al. \(2017\)](#) and was fixed at this value.

The conversion factor of count rate to flux in general depends on the adopted procedure of selecting various types of ART-XC detector events. For the criteria adopted in this work (see §2), a count rate of 1 cnt s^{-1} corresponds to a flux of $3.34 \times 10^{-11} \text{ erg cm}^{-2} \text{ s}^{-1}$ in the 4–12 keV energy band.

The derived fluxes of some weak sources in the ART-XC catalog are consistent with zero. These cases usually arise when the survey exposure varies significantly across the $2'$ aperture used for flux measurement (see above). We plan to improve our method of measuring source fluxes in future versions of the ART-XC catalog.

The fluxes of extended X-ray sources were roughly estimated from the wavelet decomposition images. The large-scale part of the flux of an extended object that is missing in the decomposition image was estimated as the flux contained in the wings of a β -model ([Cavaliere & Fusco-Femiano 1976](#)) with $\beta = 0.67$, $1'$ core radius, and the same flux in the central region (where the source is detected). The conversion of count rate to flux was made under the assumption of an optically thin $kT = 5 \text{ keV}$ plasma source spectrum.

We compared the X-ray fluxes of galaxy clusters estimated in this way with the corresponding fluxes calculated (in the 4–12 keV band) from the X-ray luminosities presented in the MCXC catalogue ([Piffaretti et al. 2011](#)), using the luminosity–gas temperature relation adopted from [Vikhlinin et al. \(2009\)](#). Our flux estimates prove to be accurate to better than 50% for galaxy clusters. More accurate measurements of X-ray fluxes for extended ART-XC sources must be made using an accurate model of the source image and spectrum. This is beyond the scope of this work.

⁵ A decomposition image is a wavelet convolution image with significant smaller size details subtracted and nonsignificant details of a given characteristic size masked with zeroes. See the `wvdecomp` documentation, available at an online repository archived at [doi:10.5281/zenodo.361034](https://doi.org/10.5281/zenodo.361034)

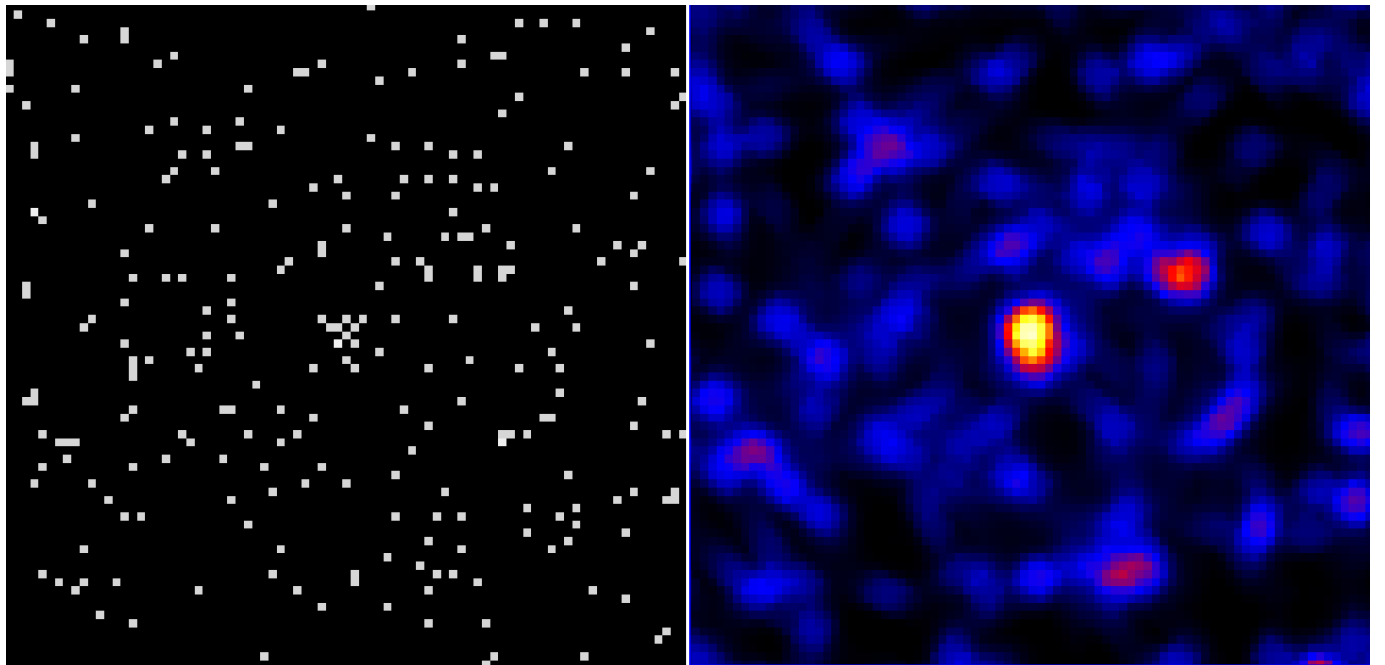


Fig. 1. Example of a detection of a faint source using the Poisson optimal filter, described in §2.3. Left: Raw photon image in the 4–12 keV energy band. Right: Convolution with the optimal filter. The size of the images is approximately $20' \times 20'$.

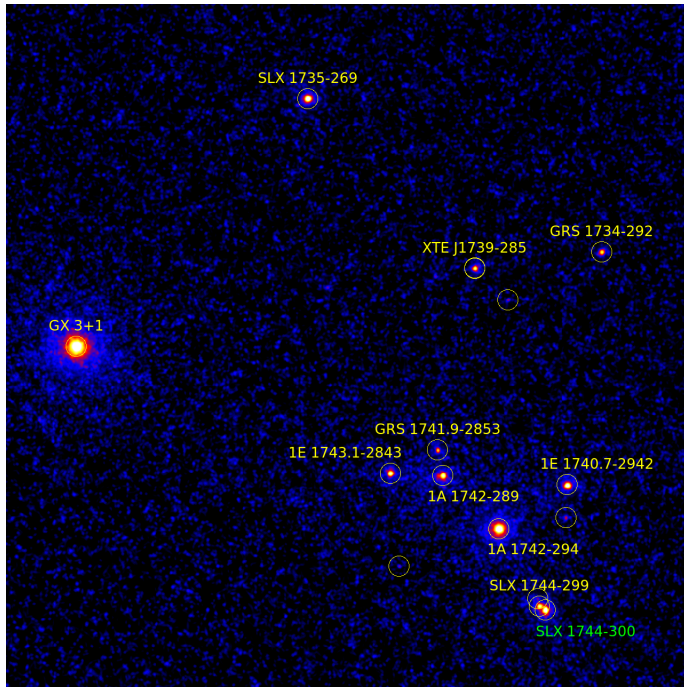


Fig. 2. Map of the sky near the Galactic center obtained in ARTSS12 by convolution with the optimal filter in the 4–12 keV energy band, in Galactic coordinates. The size of the image is approximately $4.5^\circ \times 4.5^\circ$. The detected sources are shown with circles, and the brightest sources ($S/N > 10$) are additionally indicated by their common names.

2.6. Merging X-ray source catalogs of individual sky tiles

Based on the procedures described above, we obtained catalogs of point and extended sources detected in each sky tile. These individual catalogs were then merged into a composite all-sky catalog, taking the overlap of tiles into account.

To this end, we first merged the catalogs of point and extended sources for each tile. If a point and an extended source are found at the same position in the sky (taking the source extent into account), we rejected the source with the lower X-ray flux. This allowed us to eliminate false extended source detections associated with the broad PSF wings of bright point X-ray sources, as well as spurious point sources on top of bright extended sources.

The catalogs of sources detected in each tile were then merged into an all-sky catalog. To this end, sources that are located closer than $3'$ to the tile edge were rejected, and if a source was detected in two or more tiles, the detection at the larger distance from the tile edge was selected.

2.7. Exposure map

The *SRG* observational strategy in sky survey mode is described in Sunyaev et al. (2021). It results in a relatively uniform exposure near the ecliptic plane, which varies from ≈ 30 to ≈ 80 s with a median of ≈ 60 s (vignetting corrected) after one year of the ART-XC survey. In the regions near the ecliptic poles, the exposure is much higher, reaching ~ 17 ks, and it is nonuniform.

Figure 3 shows the all-sky vignetting-corrected exposure map in the 4–12 keV band for the first year of the survey. Zoomed-in fragments of this map near the Galactic center and near the north ecliptic pole (NEP) are shown in Fig. 4.

3. Construction of the final catalog

3.1. Source detection thresholds

The size of the resulting catalog depends on the adopted threshold for source detection. We originally detected point sources down to the $S/N = 4.5$ significance limit, with S/N defined in §2.3. At this level, a large number of spurious sources are expected to appear on the ART-XC all-sky map.

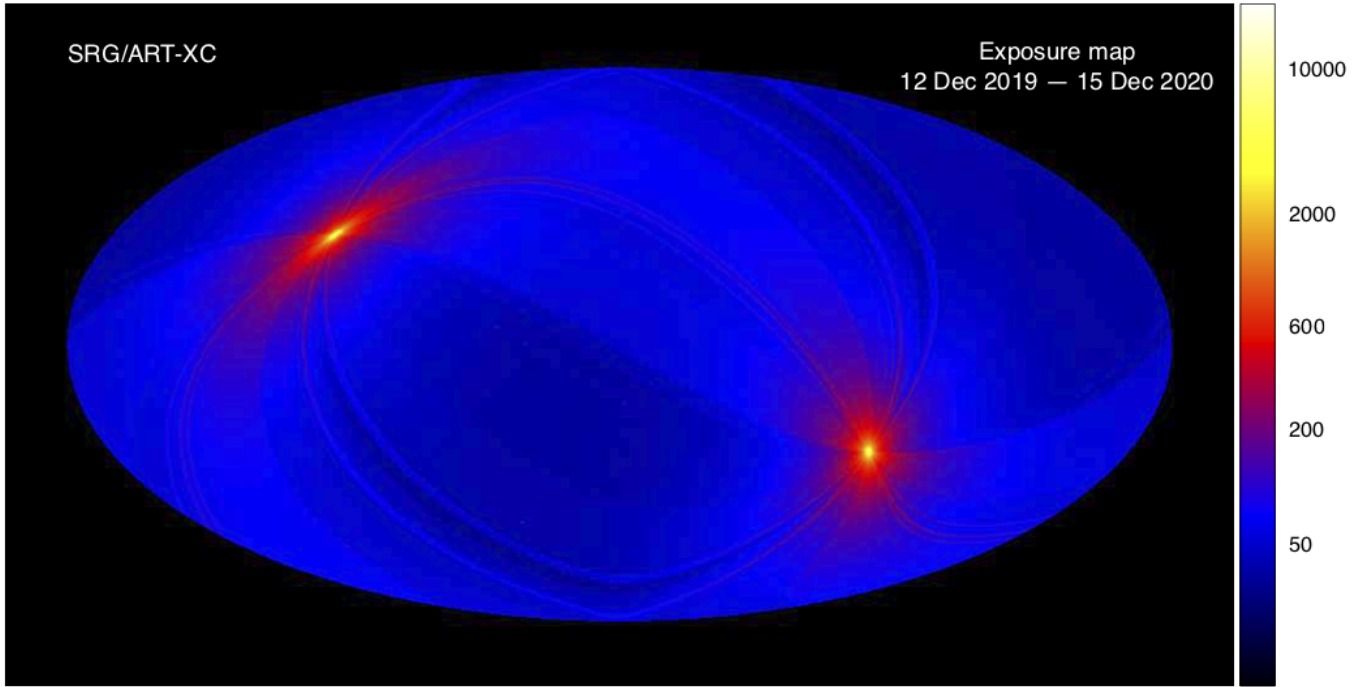


Fig. 3. ART-XC sky exposure map in Galactic coordinates in the 4–12 keV energy band, vignetting corrected, after the first two all-sky surveys (ARTSS12). Exposure time is given in seconds (see the color scale on the right-hand side). Note the very high exposure accumulated near the ecliptic poles (bright spots) compared to the rest of the sky.

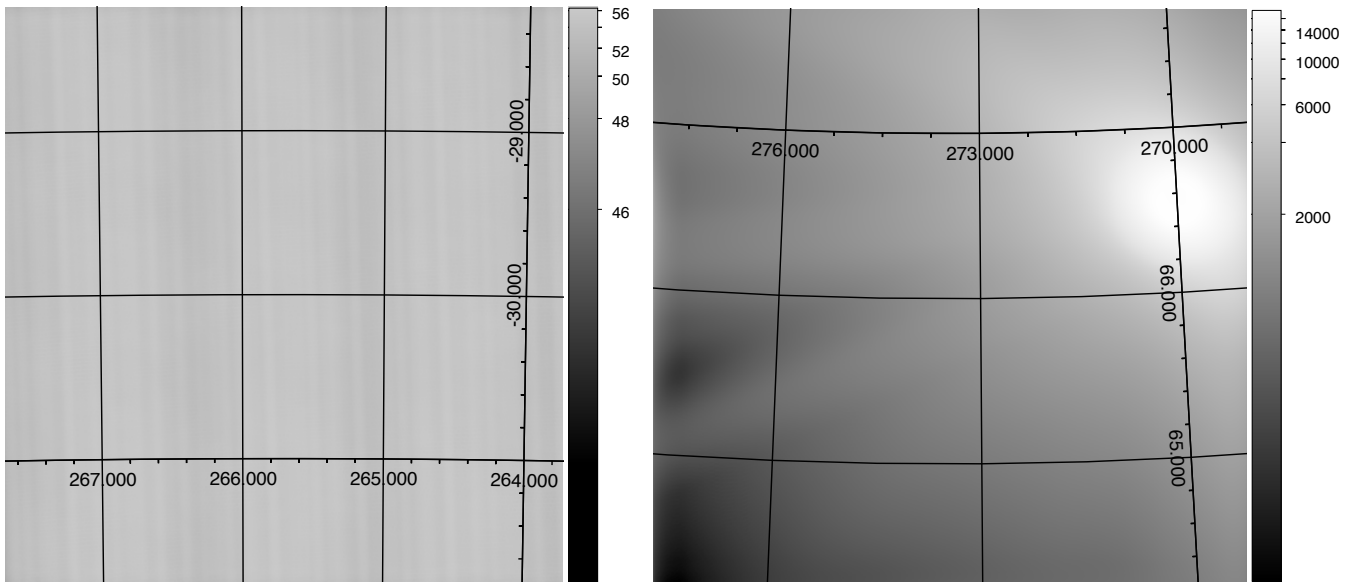


Fig. 4. First-year survey $3^{\circ}.6 \times 3^{\circ}.6$ exposure maps near the Galactic center (left) and near the NEP (right), calculated for the 4–12 keV energy band, vignetting corrected. Exposure time is given in seconds (see the color scales next to the panels). The equatorial coordinate system grid is shown.

By raising the threshold, we can improve the purity of the catalog at the cost of reducing its size.

Figure 5 shows the total number of point sources detected by ART-XC in ARTSS12 in the 4–12 keV band as a function of the significance limit. The total number reaches 1335 for $S/N > 4.5$ when the expected fraction of false detections (thin solid curve in Fig. 5) is as high as $\approx 26.6\%$. This fraction was estimated from the results of extensive Monte Carlo simulations of empty fields (§2.3). We thus decided to raise the detection limit to $S/N = 4.82$, so that the

expected fraction of spurious sources is 10%. At this threshold, the total number of point sources detected in ARTSS12 in the 4–12 keV energy band is 821 (with ≈ 241 real sources expected to be lost compared to the $S/N = 4.5$ threshold). For comparison, a still cleaner sample with 1% of spurious sources consists of 571 point sources with $S/N > 5.34$.

It is difficult to specify a similarly strict statistical threshold for the inclusion of extended sources into the ART-XC catalog. Based on the algorithm described in §2.4, a total of 46 extended sources detected in ARTSS12 were included in

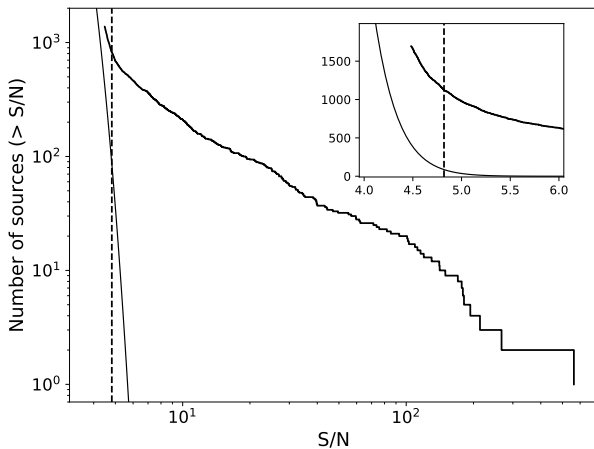


Fig. 5. Number of point sources as a function of detection significance in ARTSS12 in the 4–12 keV band (thick solid line). The dashed vertical line indicates the adopted threshold of $S/N = 4.82$, which corresponds to the expected 10% fraction of spurious sources. The thin solid line shows the expected number of spurious sources as a function of the detection significance. The inset shows a zoom-in near the detection threshold.

the catalog. All of these are previously known astrophysical objects and have been detected in X-rays before.

3.2. Identification and classification of ART-XC sources

The ART-XC localization accuracy is better than 40 arcseconds for the weakest detected sources (see §4.3). This enables a fairly straightforward search for likely counterparts of ART-XC sources in other wavebands.

To this end, we cross-correlated the ART-XC source catalog with the SIMBAD Astronomical Database (Wenger et al. 2000) and NASA/IPAC Extragalactic Database⁶ (NED) as well as with the X-ray astronomy database provided by the High Energy Astrophysics Science Archive Research Center (HEASARC). The search for counterparts was carried out within 40'' from the positions of ART-XC sources. The majority of the ART-XC sources could be unequivocally associated with a single previously known X-ray source within this matching radius. If no known X-ray sources or more than one potential X-ray counterparts from external catalogs were found within the matching radius, we searched the literature in an attempt to identify and classify the ART-XC source. For the same purpose, we also searched (within 40'') for possible counterparts in other wavebands in catalogs of optical, infrared, and radio all-sky surveys, namely Gaia Early Data Release 3 (Gaia EDR3; Gaia Collaboration et al. 2021), AllWISE (Cutri et al. 2021), and the Faint Images of the Radio Sky at Twenty-cm survey (FIRST, Helfand et al. 2015), the NRAO VLA Sky Survey (NVSS, Condon et al. 1998), and the Sydney University Molonglo Sky Survey (SUMSS, Mauch et al. 2003).

The resulting identifications and classifications for ART-XC sources as well as redshifts for extragalactic sources were adopted from SIMBAD and/or NED. In the case of dubious

identification or classification, for recently discovered X-ray sources, and for newly discovered ART-XC sources, we used additional information found in the literature and/or inferred from our multiwavelength cross-correlation analysis described above. All these cases are discussed in detail in Appendix A, where the corresponding references are also provided.

3.3. Follow-up campaign

We have set up a program of optical follow-up observations for new X-ray sources discovered by ART-XC and for the ART-XC sources that were known as X-ray sources from previous missions, but whose nature remained unknown or uncertain. In the northern part of the sky, this program is being carried out at two telescopes that compose the ground segment of the SRG mission: the Sayan observatory 1.6 m telescope (AZT-33IK, Burenin et al. 2016), operated by the Institute of Solar-Terrestrial Physics of the Siberian branch of the Russian Academy of Sciences, and the Russian-Turkish 1.5 m telescope (RTT-150), operated jointly by the Kazan Federal University, the Space Research Institute (IKI, Moscow), and the TUBITAK National Observatory (TUG, Turkey).

The first results of this program, including a number of newly identified AGN and CVs, have been reported by Zaznabin et al. 2021b,a; Zaznabin et al., in preparation. This information has been included in the ART-XC source catalog and in the corresponding notes to the catalog.

4. Source catalog

The content of the catalog is as follows:

Column (1) “Id”: The source sequence number in the catalog.

Column (2) “Name”: The source name in the ART-XC catalog (prefix “SRGA” followed by the source coordinates). New X-ray sources, that is, sources detected for the first time in X-rays by SRG/ART-XC, are highlighted in bold text.

Columns (3,4) “RA, Dec”: The equatorial (J2000) coordinates of the source.

Columns (5) “S/N”: The detection significance of the source.

Column (6) “Flux”: The time-averaged source flux in the 4–12 keV energy band and the corresponding lower and upper uncertainties (in parentheses). For some sources, only an upper limit on the (aperture) flux is reliably obtained (the cases for which the quoted lower error is equal to the flux), even though the source has surpassed the detection significance threshold (see §2.5).

Column (7) “Common name”: The common name of the source, if available.

Column (8) “Redshift”: The source redshift (for extragalactic objects), if known.

Column (9) “Class”: The general astrophysical class of the object: LMXB (HMXB), that is, low- (high-) mass X-ray binary; X-RAY BINARY, that is, X-ray binary of uncertain type; CV, that is, cataclysmic variable or symbiotic binary; SNR, that is, supernova remnant; SNR/Pulsar, that is, supernova remnant with a central pulsar (when both may contribute to the X-ray emission); MAGNETAR, that is, a magnetar (anomalous X-ray pulsars and soft gamma-ray

⁶ The NASA/IPAC Extragalactic Database is funded by the National Aeronautics and Space Administration and operated by the California Institute of Technology.

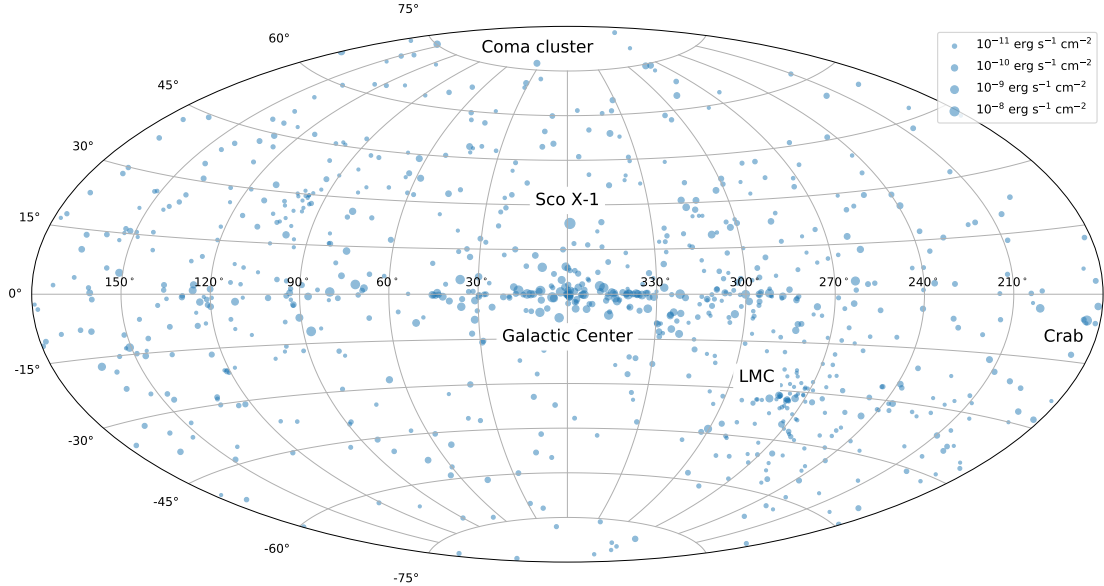


Fig. 6. Positions (in Galactic coordinates) of the X-ray sources detected by ART-XC in the 4–12 keV energy band during the first year of the all-sky survey. The symbol size reflects the X-ray brightness of a source, as indicated in the legend in the top right corner.

repeaters); STAR, that is, an active star (of various types, excluding the previously listed types of stellar objects); SFR, that is, a star-forming region; SEYFERT, that is, AGN of the Seyfert or (rarely) LINER type; AGN, that is, unclassified AGN; BLAZAR, that is, a beamed AGN (BL Lac or flat-spectrum radio quasar); and CLUSTER, that is, a cluster of galaxies. UNIDENT lists an unclassified source. A question mark indicates that the quoted classification is tentative; see comments on all these cases in Appendix A.

In addition to this key information, we plan to maintain an extended online version of the ART-XC catalog at <http://srg.cosmos.ru> where additional information will be presented. Specifically, we plan to provide cross-matches with external catalogs in X-ray and other wavebands for each ART-XC source as well as ART-XC maps of the corresponding region of the sky. Figure 6 shows the celestial distribution of the ART-XC sources detected during the first year of the all-sky survey.

4.1. Source number–flux function and the sensitivity of the survey

Figure 7 shows the cumulative and differential flux distributions of the point sources detected in ARTSS12 in the 4–12 keV energy band. The median flux of point sources (above the adopted threshold of $S/N = 4.82$) is $7.6 \times 10^{-12} \text{ erg s}^{-1} \text{ cm}^{-2}$.

Figure 8 shows the distribution of the point sources on the plane of ecliptic latitude – X-ray flux. It is evident that the sensitivity of the survey monotonically increases from $\sim 4 \times 10^{-12} \text{ erg s}^{-1} \text{ cm}^{-2}$ near the ecliptic plane (at $|b_{\text{ecl}}| < 30^\circ$) to $\sim 8 \times 10^{-13} \text{ erg s}^{-1} \text{ cm}^{-2}$ near the ecliptic poles (at $|b_{\text{ecl}}| > 80^\circ$). The quoted values are the median fluxes of the sources (excluding the few for which only upper limits on the flux are available) detected with $4.82 < S/N < 5$, that

Table 1. Statistics of the sources listed in the combined catalog.

Type	Count (Notes)
LMXB	89
HMXB	72
X-ray binary (unclassified)	6
CV	102
Star	34
Magnetar	5
SNR, SNR/Pulsar	15
Star-forming region	3
Galaxy	1 (M31)
ULX	1 (M82 X-1)
Seyfert galaxy	243
AGN (unclassified)	40
Blazar	87
Galaxy cluster	52
Unidentified	117

Table 2. Statistics of sources by category.

Category	Count
Galactic	313
Local Group	18
Extragalactic	419

is, near the adopted threshold. More accurate estimates of the sky coverage as a function of sensitivity for the ART-XC survey will be made through extensive Monte Carlo simulations of the source detection procedure and will be presented elsewhere.

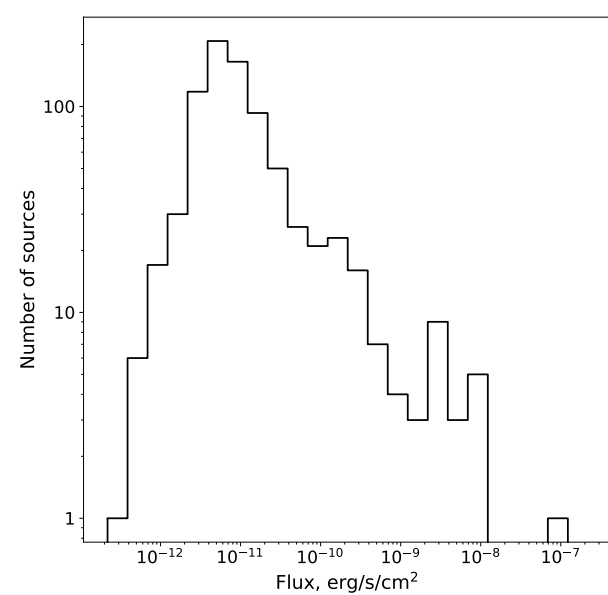
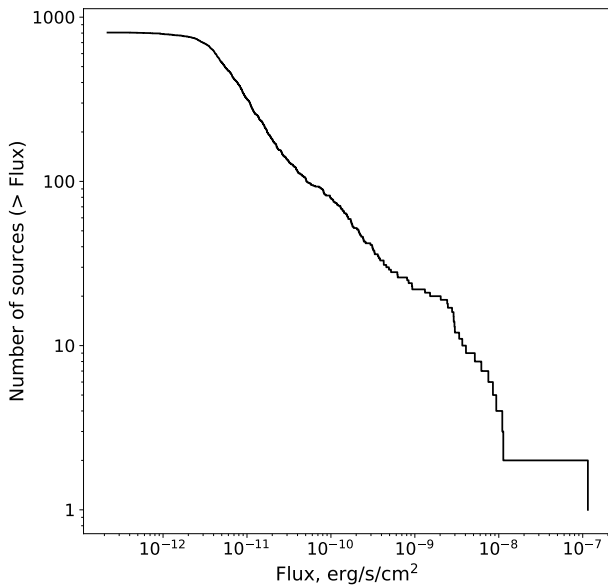


Fig. 7. Cumulative (top) and differential (bottom) flux distributions of the point sources detected in ARTSS12 in the 4–12 keV energy band. Sources with only upper limits on the flux were excluded. The differential distribution peaks at a flux of $(4.1 \pm 0.5) \times 10^{-12}$ erg s $^{-1}$ cm $^{-2}$.

4.2. Source classes

Table 1 summarizes the statistics of objects of various classes present in the ART-XC catalog. One hundred seventeen sources, or 13%, remain unidentified or unclassified so far, and many of these may be spurious. Most of the remaining 750 sources, namely 56%, have an extragalactic nature (including objects located in the Local Group of galaxies, see Table 2), but the number of Galactic objects is not much lower. The largest groups within the Galactic category are CVs (and symbiotic binaries), LMXBs, and HMXBs,

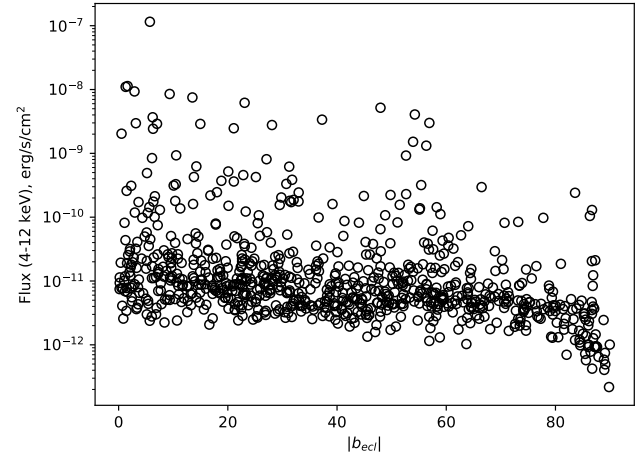


Fig. 8. Distribution of the point sources detected in ARTSS12 in the 4–12 keV energy band over the flux in this band, and the ecliptic latitude. Sources with only upper limits on the flux were excluded.

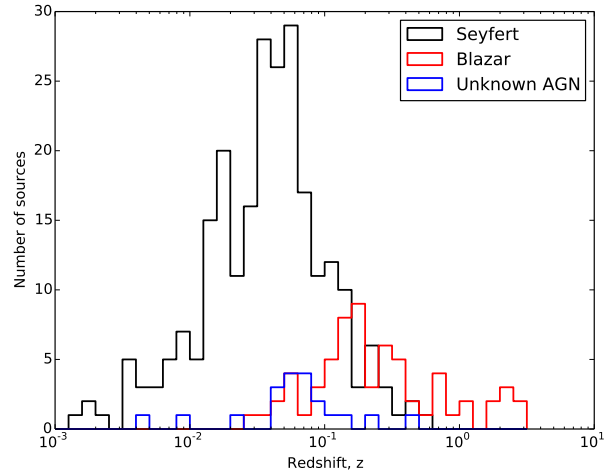


Fig. 9. Redshift distribution of the AGN detected by ART-XC: Seyfert galaxies (black), blazars (red), and unclassified AGN (blue).

although there are also a significant number of hot stars and supernova remnants/pulsars. The extragalactic objects are dominated by AGN, including relativistically beamed ones (i.e., blazars). The second largest group consists of clusters of galaxies.

Figure 9 shows the redshift distribution of the AGN. The median redshift of the unbeamed (i.e., Seyfert-like) AGN is 0.04, and it is 0.19 for the blazars. This shows that ART-XC mainly probes the AGN population in the nearby Universe. Redshifts are still missing for 40 AGN and AGN candidates in the ART-XC catalog.

4.3. Localization accuracy

To evaluate the localization accuracy of ART-XC during the all-sky survey, we selected those sources from the ART-XC catalog that are associated with a point-like Galactic object (i.e., a star, CV, X-ray binary, etc.) and whose optical

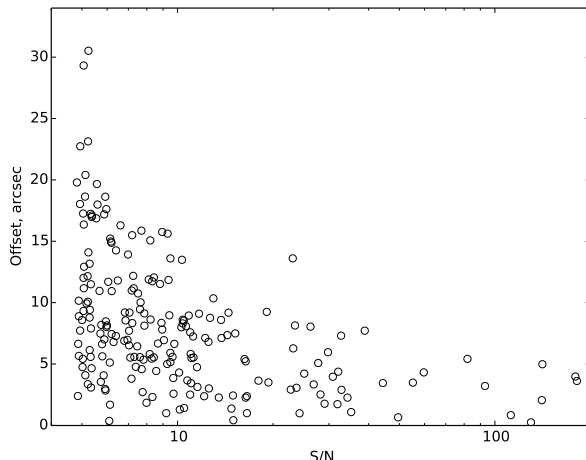


Fig. 10. X-ray-optical offsets as a function of source detection significance for ART-XC sources with point-like Galactic counterparts.

counterpart (found in SIMBAD or in the literature cited in Appendix A) is present in the Gaia DR3 catalog (i.e., has a visual magnitude $G \lesssim 21$). We then compared the ART-XC positions of these X-ray sources with the Gaia positions of their optical counterparts. In total, 209 objects were included in this test.

Figure 10 shows the resulting X-ray-optical positional offsets as a function of source detection significance. The typical accuracy is $\leq 15''$ for $S/N > 6$ and it does not exceed $35''$ for the weakest sources. Based on this, we adopt $40''$ as a minimum search radius for cross-matching with external source catalogs.

4.4. Cross-match with other X-ray and gamma-ray catalogs

The majority of sources in the ART-XC catalog were already known from previous X-ray missions. To evaluate this quantitatively, we cross-correlated the 821 point sources from the ART-XC catalog with a number of all-sky or nearly all-sky X-ray and gamma-ray surveys, namely the Second *ROSAT* all-sky survey (2RXS; Boller et al. 2016), the *XMM-Newton* slew survey (XMMSL2; Saxton et al. 2008, table XMMSLEWCLN in HEASARC), the combined MAXI/GSC 7-year all-sky source catalog (3MAXI; Kawamuro et al. 2018; Hori et al. 2018, table MAXIGSC7YR in HEASARC), the 105-month *Swift*/BAT all-sky survey (hereafter, Swift105mo; Oh et al. 2018), the *INTEGRAL*/IBIS 17-year all-sky survey (hereafter, INTEGRAL17yr; Krivonos et al., in preparation), and the *Fermi*/LAT 10-year all-sky survey (4FGL-DR2; Abdollahi et al. 2020; Ballet et al. 2020). We excluded the extended ART-XC sources from the cross-matching analysis to avoid complications related to the uncertainty in their size and morphology. All these 46 extended objects are well-known X-ray sources (see §2.4).

We regarded the outcome of cross-matching a given ART-XC source with a given external catalog as positive if at least one source from that catalog was found within $40''$ from the ART-XC position or if the ART-XC source proved to lie within the 90% localization region of a source from the external catalog. Hence, the adopted cross-matching algorithm can be described as follows: if $S < 40''$ OR $S < E_{90}$, where

S is the angular separation between an ART-XC source and a candidate counterpart, and E_{90} is the 90% position error of the counterpart. The first of these conditions mainly pertains to 2RXS and XMMSL2 because the position errors of the sources in these catalogs are comparable to or better than those of ART-XC sources (§4.3), while the second criterion mainly governs the cross-matching with the other catalogs mentioned above, which are characterized by larger positional uncertainties.

For a number of 3MAXI sources at a low Galactic latitude without a reported position error in Hori et al. (2018), we estimated E_{90} as $114'/S_{\text{det}, 4-10}$, where $S_{\text{det}, 4-10}$ is the MAXI/GSC source detection significance in the 4–10 keV band. We found that this dependence describes the correlation between these two quantities for 3MAXI sources well. The position error radii for Swift105mo were estimated from eq. (1) in Oh et al. (2018), with an additional factor of 1.42 to convert from 1σ into 90% confidence. The positional uncertainties for INTEGRAL17yr were estimated in different ranges of source detection significance according to Krivonos et al. (2007). For simplicity, we converted the ellipsoidal position errors provided in the 4FGL-DR2 catalog into effective error radii corresponding to the same area of the localization region and excluded extended 4FGL-DR2 sources from the cross-matching analysis.

There are no cases of multiple cross-matches (i.e., more than one counterpart for a given ART-XC source) with the 2RXS, 3MAXI, Swift105mo, INTEGRAL17yr, and 4FGL-DR2 catalogs. However, two ART-XC sources SRGA J174726.0–300002 and SRGA J174726.2–300245 (associated with SLX 1744–299 and SLX 1744–300, respectively) are blended into one *INTEGRAL* source (we counted this case as 2 cross-matches). Additionally, there are 36 multiple cross-matches with XMMSL2 when at least two *XMM-Newton* sources are found within the search region around a given ART-XC source (each such group is regarded as one cross-match). The vast majority of these cases are evidently caused by the imperfect merging of individual *XMM-Newton* slew detections into “unique sources” in the XMMSL2 catalog.

Table 3 provides the results of our cross-matching analysis. The largest overlap of the ART-XC survey is observed with the 2RXS, Swift105mom, and XMMSL2 catalogs. The result of cross-matching with the 4FGL-DR2 catalog of gamma-ray sources is particularly interesting. Eighty-seven ART-XC sources associated with *Fermi* sources have known identifications, including 16 Galactic objects (3 SNRs/pulsars, 8 LMXBs, 3 HMXBs, the star eta Car, and the ART-XC source SRGA J181637.1–391248, which is probably associated with variable star V371 CrA at $414''$ from 4FGL J1816.1–3908), 68 extragalactic objects (9 Seyfert galaxies, 58 blazars, and one ULX – M82 X-1), and 3 SNRs/pulsars in the Large Magellanic Cloud (LMC; SNR J052501–693842, PSR J0537–6910, and PSR B0540–69). The ART-XC catalog includes 87 blazars and blazar candidates, and the majority of them (58) have a *Fermi* gamma-ray counterpart. Additionally, one unidentified ART-XC source, SRGA J101132.4–442258, is spatially consistent with 4FGL J1011.1–4420.

The vast majority of the cross-matches are expected to be real. To estimate the number of accidental matches, we can make the crude assumption that the sources in all of the catalogs under consideration (including the ART-XC catalog) are distributed uniformly over the sky. Then the

expected number of spurious matches can be found as the area of the search region that was used for cross-correlation divided by the area of the sky and multiplied by the number of sources in the ART-XC catalog and by the number of sources in the matching catalog. As mentioned before, the search radius is typically $40''$ for 2RXS and XMMSL2. For the other catalogs, we can use the median radius of the 90% localization regions, which is equal to $613'', 343'', 179'',$ and $192''$ for 3MAXI, Swift105mo, INTEGRAL17yr, and 4FGL-DR2, respectively. In this way, we predict that the number of spurious matches with ART-XC point sources is $\sim 1.0, \sim 0.2,$ $\sim 1.6, \sim 0.9, \sim 0.1,$ and ~ 1.0 for 2RXS, XMMSL2, 3MAXI, Swift105mo, INTEGRAL17yr, and 4FGL-DR2, respectively, which is lower than 2 in each case.

However, the assumption of a uniform distribution of X-ray sources over the sky might be too crude because the Galactic sources are concentrated around the Galactic plane and the Galactic center (see Fig. 6) and because an additional several dozen ART-XC sources are concentrated around the ecliptic poles (see §4.5 below) because these regions receive a deeper exposure in the *SRG* survey. We can try to take this spatial nonuniformity into account by shifting the positions of the ART-XC point sources by some small amount and repeating our cross-matching analysis. Specifically, we shifted the ART-XC positions in random directions by $45'$ because this angular distance, on the one hand, is larger than the median 90% position uncertainty of the 3MAXI catalog by a factor of ≈ 4.4 and by larger factors for the other catalogs considered here, and on the other hand, it is small compared to the effective thickness of the distribution of X-ray sources near the Galactic plane and the effective size of the ART-XC deep fields near the ecliptic poles. Using this alternative method, we found somewhat larger numbers of spurious cross-matches of the ART-XC catalog with the external catalogs, namely 2, 0, 3, 1, 0, and 4 for 2RXS, XMMSL2, 3MAXI, Swift105mo, INTEGRAL17yr, and 4FGL-DR2, respectively. Although in most of these cases the position error of the matching source is much smaller than its angular distance from the original (unshifted) position of the ART-XC source, some of the 3MAXI and 4FGL-DR2 matches have position errors $\sim 1/3\text{--}1/2$ of that distance and thus might be real associations with the ART-XC sources. Therefore the derived numbers for 3MAXI and 4FGL-DR2 should be considered upper limits. Taking this into account, we provide in Table 3 our final estimates of the number of random coincidences of ART-XC sources with sources from the external catalogs.

One hundred forty-one ART-XC point sources have not been detected in any of the six all-sky surveys listed in Table 3. In this context, we recall that ~ 80 of these are expected to be spurious sources.

We finally note that all of the surveys listed in Table 3, except for 2RXS, were carried out over at least 8 years. Some of them are characterized by a very low duty cycle. In particular, XMMSL2 spans 13 years, and the net exposure time was just a few months. For comparison, the ART-XC catalog reported here is based on just the first year of the *SRG* all-sky survey, which is characterized by a duty cycle of more than 97%.

4.5. Ecliptic poles

The regions around the ecliptic poles receive a far higher exposure than the rest of the sky. They may therefore be

regarded as deep extragalactic surveys within the ART-XC all-sky survey. It is worthwhile to discuss the statistics of the detected X-ray sources separately for these zones. Specifically, we focus on the regions $b_{\text{ecl}} > 82^\circ$ and $b_{\text{ecl}} < -82^\circ$ (with a total area of ≈ 200 square degrees) around the north and south ecliptic poles (SEP), respectively.

The NEP region contains 18 ART-XC sources, with fluxes ranging between $\sim 2 \times 10^{-13} \text{ erg s}^{-1} \text{ cm}^{-2}$ (blazar SRGA J180147.2+663835=RJ1801.7+6638, at just $0.2''$ from the NEP) and $\sim 2 \times 10^{-11} \text{ erg s}^{-1} \text{ cm}^{-2}$. All of these X-ray sources have been known before, and the majority of them are AGN, except for two clusters of galaxies and one Galactic star. The SEP region contains 37 ART-XC sources, with fluxes ranging between $\sim 5 \times 10^{-13} \text{ erg s}^{-1} \text{ cm}^{-2}$ and $\sim 2 \times 10^{-10} \text{ erg s}^{-1} \text{ cm}^{-2}$. A significant fraction of these sources, namely 13 (9 HMXBs and 4 SNRs), belong to the LMC. In addition to these, there are 18 AGN (confirmed or suspected), one cluster of galaxies, one Galactic HMXB, one star, and three unidentified sources (previously known 1RXS J061617.6–705237 and two newly discovered X-ray sources).

Because of the detection threshold we chose ($S/N = 4.82$, as for the rest of the sky), we expect ≈ 0.5 spurious sources to be present in each of the NEP and SEP samples. This means that these samples should be highly pure, and it is possible to further lower the detection threshold near the ecliptic poles. We plan to do this in future work.

5. Summary

We have presented the catalog of sources detected by the ART-XC telescope during the first year of the ongoing *SRG* all-sky survey. It comprises 867 sources detected on the combined map of the first two half-year surveys in the 4–12 keV energy band. The achieved sensitivity to point sources after the first year of the survey is between $\sim 4 \times 10^{-12} \text{ erg s}^{-1} \text{ cm}^{-2}$ near the ecliptic plane and $\sim 8 \times 10^{-13} \text{ erg s}^{-1} \text{ cm}^{-2}$ (4–12 keV) near the ecliptic poles. The typical depth of the ART-XC survey is comparable to that achieved in a similar energy band (4–10 keV) in the recent MAXI/GSC all-sky survey (Hori et al. 2018; Kawamuro et al. 2018) and is slightly worse than the sensitivity of the *XMM-Newton* Slew Survey in the 2–12 keV band (Saxton et al. 2008). However, the ART-XC survey greatly improves on the former in terms of angular resolution and provides full and well-behaved sky coverage in contrast to the latter.

Extragalactic sources (mostly AGN and clusters of galaxies) somewhat dominate Galactic sources among the sources of known nature in the catalog. For 114 sources, ART-XC has detected X-rays for the first time. Although the majority of these (~ 80) are expected to be spurious, there can be a significant number of newly discovered astrophysical objects. We have started a program of optical follow-up observations of the new and previously unidentified sources, which has already led to the identification of several AGN and CVs (Zaznabin et al. 2021b,a). The expected fraction of spurious sources in the catalog drops from 10% at the significance level $S/N \approx 4.8$ to just 1% at $S/N \approx 5.3$, which can be taken into account in planning follow-up activities on new ART-XC sources.

With the *SRG/ART-XC* all-sky survey planned to continue for a total of four years (until December 2023), we can expect the number of detected sources to be growing with the completion of each next half-year scan of the sky.

Table 3. Cross-match of the point sources from the *SRG*/ART-XC first-year 4–12 keV all-sky survey with selected X-ray and gamma-ray catalogs.

X-ray survey	Energy band	Reference	Cross-matches	Spurious matches
<i>ROSAT</i> (2RXS) 1 year	0.1–2.4 keV	Boller et al. (2016)	478	~ 2
<i>XMM-Newton</i> SL2	0.2–12 keV	Saxton et al. (2008)	454	≤ 1
MAXI/GSC 7 years	4–10 keV	Kawamuro et al. (2018); Hori et al. (2018)	148	≤ 3
<i>Swift</i> /BAT 105 months	14–195 keV	Oh et al. (2018)	458	~ 1
<i>INTEGRAL</i> 17 years	17–60 keV	Krivonos et al., (in prep.)	345	≤ 1
<i>Fermi</i> /LAT 10 years	50 MeV–1 TeV	Abdollahi et al. (2020)	88	≤ 4

The number of newly discovered sources is expected to increase particularly quickly. We plan to regularly update the ART-XC source catalog. The next release will be based on the data of the first two years of the survey (December 2019 – December 2021) and will include additional information on source fluxes in various energy bands and different *SRG*/ART-XC scans of the sky.

Acknowledgements

The Mikhail Pavlinsky ART-XC telescope is the hard X-ray instrument on board the *SRG* observatory, a flagship astrophysical project of the Russian Federal Space Program realized by the Russian Space Agency in the interests of the Russian Academy of Sciences. The ART-XC team thanks the Russian Space Agency, Russian Academy of Sciences, and State Corporation Rosatom for the support of the *SRG* project and ART-XC telescope. We thank Lavochkin Association (NPOL) with partners for the creation and operation of the *SRG* spacecraft (Navigator). We thank Acrorad Co., Ltd. (Japan), which manufactured the CdTe dies, and Integrated Detector Electronics AS – IDEAS (Norway), which manufactured the ASICs for the X-ray detectors. This research was supported by grant 19-12-00396 from the Russian Science Foundation. We thank the referee for the useful comments.

References

- Abdollahi, S., Acero, F., Ackermann, M., et al. 2020, ApJS, 247, 33
 An, H., Hascoët, R., Kaspi, V. M., et al. 2013, ApJ, 779, 163
 Annuar, A., Alexander, D. M., Gandhi, P., et al. 2020, MNRAS, 497, 229
 Bahramian, A., Gladstone, J. C., Heinke, C. O., et al. 2014, MNRAS, 441, 640
 Ballet, J., Burnett, T. H., Digel, S. W., & Lott, B. 2020, arXiv e-prints, arXiv:2005.11208
 Barnard, R., Stiele, H., Hatzidimitriou, D., et al. 2008, ApJ, 689, 1215
 Barrière, N. M., Tomsick, J. A., Wik, D. R., Chaty, S., & Rodriguez, J. 2015, ApJ, 799, 24
 Bassani, L., Ursini, F., Malizia, A., et al. 2021, MNRAS, 500, 3111
 Bird, A. J., Bazzano, A., Malizia, A., et al. 2016, ApJS, 223, 15
 Boller, T., Freyberg, M. J., Trümper, J., et al. 2016, A&A, 588, A103
 Burenin, R. A., Amvrosov, A. L., Eselevich, M. V., et al. 2016, Astronomy Letters, 42, 295
 Callingham, J. R., Tuthill, P. G., Pope, B. J. S., et al. 2019, Nature Astronomy, 3, 82
 Campbell, H., Fraser, M., Hodgkin, S. T., et al. 2015, The Astronomer's Telegram, 7177, 1
 Cavaliere, A. & Fusco-Femiano, R. 1976, A&A, 500, 95
 Chang, Y. L., Arsioli, B., Giommi, P., Padovani, P., & Brandt, C. H. 2019, A&A, 632, A77
 Churazov, E., Sunyaev, R., Revnivtsev, M., et al. 2007, A&A, 467, 529
 Clavel, M., Tomsick, J. A., Bodaghee, A., et al. 2016, MNRAS, 461, 304
 Clavel, M., Tomsick, J. A., Hare, J., et al. 2019, ApJ, 887, 32
 Coleiro, A., Chaty, S., Zurita Heras, J. A., Rahoui, F., & Tomsick, J. A. 2013, A&A, 560, A108
 Condon, J. J., Cotton, W. D., Greisen, E. W., et al. 1998, AJ, 115, 1693
 Cusumano, G., Segreto, A., La Parola, V., et al. 2015, MNRAS, 446, 1041
 Cutri, R. M., Wright, E. L., Conrow, T., et al. 2021, VizieR Online Data Catalog, II/328
 D'Abrusco, R., Álvarez Crespo, N., Massaro, F., et al. 2019, ApJS, 242, 4
 Degenaar, N., Starling, R. L. C., Evans, P. A., et al. 2012, A&A, 540, A22
 Forman, W., Jones, C., Cominsky, L., et al. 1978, ApJS, 38, 357
 Gaia Collaboration, Brown, A. G. A., Vallenari, A., et al. 2021, A&A, 649, A1
 Gehrels, N. 1986, ApJ, 303, 336
 Goodwin, A. J., Galloway, D. K., in't Zand, J. J. M., et al. 2019, MNRAS, 486, 4149
 Goulding, A. D. & Alexander, D. M. 2009, MNRAS, 398, 1165
 Green, D. A. 2019, Journal of Astrophysics and Astronomy, 40, 36
 Greiner, J., Schwarz, R., Tappert, C., et al. 2010, Astronomische Nachrichten, 331, 227
 Gruber, D. E., Matteson, J. L., Peterson, L. E., & Jung, G. V. 1999, ApJ, 520, 124
 Gubarev, M., Ramsey, B., Kolodziejczak, J. J., et al. 2014, Society of Photo-Optical Instrumentation Engineers (SPIE) Conference Series, Vol. 9144, The calibration of flight mirror modules for the ART-XC instrument on board the SRG mission, 91444U
 Haberl, F., Maitra, C., Carpano, S., et al. 2020, The Astronomer's Telegram, 13609, 1
 Halpern, J. P. & Thorstensen, J. R. 2015, AJ, 150, 170
 Healey, S. E., Romani, R. W., Taylor, G. B., et al. 2007, ApJS, 171, 61
 Helfand, D. J., White, R. L., & Becker, R. H. 2015, ApJ, 801, 26
 Hori, T., Shidatsu, M., Ueda, Y., et al. 2018, ApJS, 235, 7
 Itoh, R., Utsumi, Y., Inoue, Y., et al. 2020, ApJ, 901, 3
 Karasev, D. I., Lutovinov, A. A., & Burenin, R. A. 2008, Astronomy Letters, 34, 753
 Kawamuro, T., Ueda, Y., Shidatsu, M., et al. 2018, ApJS, 238, 32
 Kennea, J. A., Evans, P. A., Beardmore, A. P., et al. 2019, The Astronomer's Telegram, 13195, 1
 Klutsch, A., Frasca, A., Guillout, P., et al. 2020, A&A, 637, A43
 Koss, M., Trakhtenbrot, B., Ricci, C., et al. 2017, ApJ, 850, 74
 Kretschmar, P., Fürst, F., Sidoli, L., et al. 2019, New A Rev., 86, 101546
 Krivonos, R., Revnivtsev, M., Lutovinov, A., et al. 2007, A&A, 475, 775
 Krivonos, R., Tkachenko, A., Burenin, R., et al. 2017, Experimental Astronomy, 44, 147
 Krivonos, R., Tsygankov, S., Lutovinov, A., et al. 2012, A&A, 545, A27
 Krivonos, R., Wik, D., Grefenstette, B., et al. 2021, MNRAS, 502, 3966
 Kumar, H. S., Safi-Harb, S., Slane, P. O., & Gotthelf, E. V. 2014, ApJ, 781, 41
 Landi, R., Bassani, L., Bazzano, A., et al. 2017, MNRAS, 470, 1107
 Lo, K. K., Farrell, S., Murphy, T., & Gaensler, B. M. 2014, ApJ, 786, 20
 Lutovinov, A. A., Tsygankov, S. S., Mereminskiy, I. A., et al. 2021, arXiv e-prints, arXiv:2107.05587
 Maccarone, T. J., Yukita, M., Hornschemeier, A., et al. 2016, MNRAS, 458, 3633

- Madsen, K. K., Forster, K., Grefenstette, B. W., Harrison, F. A., & Stern, D. 2017, ApJ, 841, 56
- Maeda, Y., Mori, H., & Dotani, T. 2013, Advances in Space Research, 51, 1278
- Malizia, A., Sazonov, S., Bassani, L., et al. 2020, New A Rev., 90, 101545
- Maselli, A., Massaro, F., Cusumano, G., et al. 2013, ApJS, 206, 17
- Masetti, N., Bassani, L., Palazzi, E., et al. 2018, The Astronomer's Telegram, 11414, 1
- Masetti, N., Parisi, P., Palazzi, E., et al. 2013, A&A, 556, A120
- Massaro, F., Giroletti, M., D'Abrusco, R., et al. 2014, ApJS, 213, 3
- Mauch, T., Murphy, T., Buttery, H. J., et al. 2003, MNRAS, 342, 1117
- McCollum, B. & Laine, S. 2019, The Astronomer's Telegram, 13211, 1
- Mereminskiy, I., Medvedev, P., Lutovinov, A., et al. 2020a, The Astronomer's Telegram, 14206, 1
- Mereminskiy, I., Medvedev, P., Semena, A., et al. 2020b, The Astronomer's Telegram, 13571, 1
- Mereminskiy, I. A., Dodin, A. V., Lutovinov, A. A., et al. 2021, arXiv e-prints, arXiv:2107.05588
- Negoro, H., Nakajima, M., Sakamaki, A., et al. 2018, The Astronomer's Telegram, 12254, 1
- Ofek, E. O. & Zackay, B. 2018, AJ, 155, 169
- Oh, K., Koss, M., Markwardt, C. B., et al. 2018, ApJS, 235, 4
- Parisi, P., Masetti, N., Jiménez-Bailón, E., et al. 2012, A&A, 545, A101
- Pavlinsky, M., Tkachenko, A., Levin, V., et al. 2021, A&A, 650, A42
- Pavlinsky, M., Tkachenko, A., Levin, V., et al. 2018, Experimental Astronomy, 45, 315
- Pavlinsky, M., Tkachenko, A., Levin, V., et al. 2019a, Experimental Astronomy, 47, 1
- Pavlinsky, M., Tkachenko, A., Levin, V., et al. 2019b, Experimental Astronomy, 48, 233
- Piffaretti, R., Arnaud, M., Pratt, G. W., Pointecouteau, E., & Melin, J. B. 2011, A&A, 534, A109
- Planck Collaboration, Ade, P. A. R., Aghanim, N., et al. 2016, A&A, 594, A27
- Pratt, W. K. 1978, Digital image processing, New York: Wiley-Interscience
- Predehl, P., Andritschke, R., Arefiev, V., et al. 2021, A&A, 647, A1
- Revnivtsev, M., Sazonov, S., Jahoda, K., & Gilfanov, M. 2004, A&A, 418, 927
- Reynolds, C. S., Lohfink, A. M., Babul, A., et al. 2014, ApJLett, 792, L41
- Ritter, H. & Kolb, U. 2003, A&A, 404, 301
- Russell, H. R., Fabian, A. C., Sanders, J. S., et al. 2010, MNRAS, 402, 1561
- Saxton, R. D., Read, A. M., Esquej, P., et al. 2008, A&A, 480, 611
- Sazonov, S., Krivonos, R., Revnivtsev, M., Churazov, E., & Sunyaev, R. 2008, A&A, 482, 517
- Sazonov, S. Y. & Revnivtsev, M. G. 2004, A&A, 423, 469
- Schwope, A., Hasinger, G., Lehmann, I., et al. 2000, Astronomische Nachrichten, 321, 1
- Semena, A., Mereminskiy, I., Lutovinov, A., Molkov, S., & Pavlinsky, M. 2020, The Astronomer's Telegram, 13415, 1
- Spurauskas, J., Deveikis, V., & Tokovinin, A. 2019, A&A, 626, A31
- Starling, R. L. C., Wildy, C., Wiersema, K., et al. 2017, MNRAS, 468, 378
- Stephen, J. B., Bassani, L., Malizia, A., Masetti, N., & Ubertini, P. 2018, The Astronomer's Telegram, 11341, 1
- Stiele, H., Pietsch, W., Haberl, F., et al. 2011, A&A, 534, A55
- Sunyaev, R., Arefiev, V., Babyshkin, V., et al. 2021, arXiv e-prints, arXiv:2104.13267
- The Lynx Team. 2018, <https://www.lynxobservatory.com/report>
- Tomsick, J. A., Bodaghee, A., Chaty, S., et al. 2012, ApJ, 754, 145
- Tomsick, J. A., Lansbury, G. B., Rahoui, F., et al. 2017, ApJS, 230, 25
- Torrejón, J. M., Negueruela, I., Smith, D. M., & Harrison, T. E. 2010, A&A, 510, A61
- Townsley, L. K., Broos, P. S., Garmire, G. P., et al. 2014, ApJS, 213, 1
- Tsujimoto, M., Morihana, K., Hayashi, T., & Kitaguchi, T. 2018, PASJ, 70, 109
- van Roestel, J., Groot, P. J., Kupfer, T., et al. 2019, MNRAS, 484, 4507
- Véron-Cetty, M. P. & Véron, P. 2010, A&A, 518, A10
- Vikhlinin, A., Burenin, R. A., Ebeling, H., et al. 2009, ApJ, 692, 1033
- Vikhlinin, A., McNamara, B. R., Forman, W., et al. 1998, ApJ, 502, 558
- Voges, W., Aschenbach, B., Boller, T., et al. 1999, A&A, 349, 389
- Warwick, R. S., Saxton, R. D., & Read, A. M. 2012, A&A, 548, A99
- Webb, N. A., Coriat, M., Traulsen, I., et al. 2020, A&A, 641, A136
- Wenger, M., Ochsenebein, F., Egret, D., et al. 2000, A&AS, 143, 9
- Wilms, J., Kreykenbohm, I., Weber, P., et al. 2020, The Astronomer's Telegram, 13416, 1
- Xu, X., Shao, Y., & Li, X.-D. 2019, MNRAS, 489, 3031
- Yao, Y., Kulkarni, S. R., Burdge, K. B., et al. 2020, arXiv e-prints, arXiv:2012.00169
- Young, A. J., Wilson, A. S., Terashima, Y., Arnaud, K. A., & Smith, D. A. 2002, ApJ, 564, 176
- Zaznobin, I., Sazonov, S., Burenin, R., et al. 2021a, arXiv e-prints, arXiv:2107.05611
- Zaznobin, I. A., Uskov, G. S., Sazonov, S. Y., et al. 2021b, Astronomy Letters, 47, 71
- Zhekov, S. A., Gagné, M., & Skinner, S. L. 2014, ApJ, 785, 8

Appendix A: Notes on individual sources

Here, we provide comments on the identification and classification of some sources in the ART-XC catalog, namely, those with dubious identification or classification and recently discovered sources. In addition to the references provided for individual sources, we note that the matches with *XMM-Newton* sources for a number of objects were found using the *XMM-Newton* slew survey (XMMSL2, [Saxton et al. 2008](#)) and the fourth *XMM-Newton* serendipitous source catalogue ([Webb et al. 2020](#)).

SRGA J000132.7+240242

Associated with 2MASX J00013232+2402304. Blazar candidate based on radio and infrared properties ([D'Abrusco et al. 2019](#)).

SRGA J001315.3+774824

A blazar candidate ([D'Abrusco et al. 2019; Itoh et al. 2020](#)), but also classified as Seyfert 2 ([Véron-Cetty & Véron 2010](#)).

SRGA J002202.7+254008

A Seyfert 1.2 at $z = 0.1292$ ([Starling et al. 2017](#)).

SRGA J004144.3+413415

Likely an LMXB in the globular cluster Bol 45 in M31 ([Stiele et al. 2011](#)).

SRGA J004241.1+411603

The central region of M31, unresolved into individual X-ray sources.

SRGA J004506.7+620747

Associated with the galaxy LEDA 2631101, likely an AGN based on infrared (WISE) colors.

SRGA J004546.3+413951

An X-ray binary in the globular cluster Bo 375 in M31, likely with a neutron star ([Barnard et al. 2008; Maccarone et al. 2016](#)).

SRGA J005456.3-722646

In the SMC.

SRGA J005642.5+604302

A Be star.

SRGA J011511.9+882912

Likely associated with the bright star Gaia EDR3 576260267526450048, a spectroscopic binary in a young stellar association ([Klutsch et al. 2020](#)). Hence, likely a coronally active star.

SRGA J011704.7-732637

In the SMC.

SRGA J015639.0-835828

Likely associated with the star Gaia EDR3 4617143036371460864 at $D \sim 500$ pc. Possibly a CV based on X-ray and optical photometric properties.

SRGA J022235.8+250816

A changing-look AGN ([van Roestel et al. 2019](#)).

SRGA J022624.9+592741

A radio galaxy with unknown AGN optical type and redshift ([Bassani et al. 2021](#)).

SRGA J022745.0-693133

A giant star at $D \sim 240$ pc. The exact nature of the X-ray emission is unknown.

SRGA J025234.3+431004

Associated with the galaxy LEDA 90641, with infrared colors (WISE) typical of AGN.

SRGA J030838.1-552041

Associated with the galaxy LEDA 410289. Present in the catalogue of quasars and active nuclei, 13th edition ([Véron-Cetty & Véron 2010](#)), without detailed classification.

SRGA J031102.9-440232

Likely a blazar ([Chang et al. 2019](#)).

SRGA J031131.8-315251

A CV (nova-like and/or polar, [Ritter & Kolb 2003](#)).

SRGA J035023.8-501802

A Seyfert 2 ([Koss et al. 2017](#)).

SRGA J040850.8-791418

Likely associated with the star Gaia EDR3 4625832751643853696 at $D \sim 1300$ pc. Possibly a CV based on X-ray and optical photometric properties.

SRGA J041328.3-061446

A flat-spectrum radio source ([Healey et al. 2007](#)).

SRGA J041732.7-525316

Likely associated with the galaxy LEDA 14813.

<i>SRGA J042616.9–592322</i>	<i>SRGA J052505.4–693853</i>
Associated with the galaxy LEDA 371722, with infrared (WISE) colors typical of AGN.	In the LMC.
<i>SRGA J043209.5+354927</i>	<i>SRGA J052947.3–655645</i>
A Seyfert 1 at $z = 0.0506$ (Zaznabin et al. 2021b).	In the LMC.
<i>SRGA J043510.5–752749</i>	<i>SRGA J053043.5–665424</i>
Likely associated with CRTS J043509.7–752743, a variable star of RR Lyr type. The exact nature of the X-ray emission is unknown.	In the LMC.
<i>SRGA J043522.9+552234</i>	<i>SRGA J053232.1–655141</i>
X-ray transient SRGA J043520.9+552226 = SRGE J043523.3+552234 discovered by <i>SRG/ART-XC</i> and eROSITA, associated with the optical transient ATLAS19bcxp. An LMXB, BH candidate (Mereminskiy et al. 2020b; Yao et al. 2020; Mereminskiy et al. 2021).	In the LMC.
<i>SRGA J043830.9–681205</i>	<i>SRGA J053249.3–662220</i>
Likely associated with the galaxy 2MASS J04383119–6812003, with infrared colors (WISE) typical of AGN.	In the LMC.
<i>SRGA J045050.1+301450</i>	<i>SRGA J053525.0–691621</i>
A Seyfert 1.9 at $z = 0.0331$ (Zaznabin et al. 2021b).	In the LMC.
<i>SRGA J045254.2–585353</i>	<i>SRGA J053739.1+210826</i>
A blazar candidate based on radio and infrared properties (D’Abrusco et al. 2019).	A binary Be star.
<i>SRGA J050021.6+523801</i>	<i>SRGA J053749.8–691016</i>
Associated with the gamma-ray source 3FGL J0500.3+5237, likely a blazar (Chang et al. 2019).	In the LMC.
<i>SRGA J050810.6–660657</i>	<i>SRGA J053857.2–640503</i>
A new Be X-ray binary eRASSU J050810.4–660653 discovered by <i>SRG/eROSITA</i> in LMC (Haberl et al. 2020), previously detected during the ROSAT all-sky survey (2RXS J050810.2–660645).	In the LMC.
<i>SRGA J051514.3–142701</i>	<i>SRGA J053939.4–694440</i>
Associated with the infrared source WISEA J051514.91–142718.6, with colors typical of AGN.	In the LMC.
<i>SRGA J052029.0–715733</i>	<i>SRGA J054010.9–692001</i>
In the LMC.	In the LMC.
<i>SRGA J052410.7–662045</i>	<i>SRGA J055053.7–621457</i>
In the LMC.	Associated with the galaxy LEDA 178653, with infrared colors (WISE) typical of AGN.
<i>SRGA J060241.1–595152</i>	<i>SRGA J060651.8–624550</i>
	Associated with the galaxy LEDA 178859, with infrared colors (WISE) typical of AGN.
	Associated with the galaxy LEDA 340165, with infrared colors (WISE) typical of AGN.

SRGA J060728.9–614836

Heavily obscured AGN (Goulding & Alexander 2009; Annmar et al. 2020) in an edge-on galaxy.

SRGA J061322.9–290027

Associated with the galaxy LEDA 734640, with infrared (WISE) colors typical of AGN.

SRGA J061619.2–705228

Possibly associated with the infrared source WISEA J061617.13–705228.7 based on the position of the X-ray source 4XMM J061617.1-705229.

SRGA J062109.8–680554

Associated with the galaxy LEDA 179145, with infrared (WISE) colors typical of AGN.

SRGA J062627.2+072734

Associated with the galaxy LEDA 136513, with infrared (WISE) colors typical of AGN.

SRGA J062945.0–834426

Likely associated with the infrared source WISEA J062948.62–834421.6, with colors typical of AGN.

SRGA J062953.4–033505

Likely associated with the star Gaia EDR3 3105034928633782400 at $D \sim 670$ pc. Possibly a CV based on X-ray and optical photometric properties.

SRGA J063558.6+075528

Associated with the bright star TYC 733-2098-1 at $D \sim 200$ pc. Coronally active or a CV?

SRGA J064849.9–694524

A blazar candidate (Chang et al. 2019).

SRGA J065513.5–012846

Likely associated with the bright star V520 Mon (long-period variable) at $D \sim 4000$ pc. Possibly an HMXB or a symbiotic X-ray binary.

SRGA J070636.4+635109

Associated with the galaxy UGC 3660. Classified as a Seyfert 1 based on follow-up spectroscopy (Zaznabin et al., in preparation).

SRGA J071739.0–710349

Associated with the infrared source WISEA J071740.40–710347.3, with colors typical of AGN.

SRGA J072041.5–552614

Associated with the galaxy LEDA 409410, with infrared (WISE) colors typical of AGN.

SRGA J072823.5–440823

Associated with the galaxy 2MASS J07282338–4408241, with infrared colors (WISE) typical of AGN.

SRGA J080735.3+023517

Likely associated with the star Gaia EDR3 3090944824560398208 at $D \sim 1400$ pc. Possibly a CV based on X-ray and optical photometric properties.

SRGA J082625.5–703138

Likely a nonmagnetic CV (Parisi et al. 2012).

SRGA J084434.0–375747

Likely associated with the bright star HD 74771 at $D \sim 170$ pc. Coronally active?

SRGA J085040.6–421156

Likely associated with the bright star UCAC2 13726137 at $D \sim 12$ kpc. Possibly an HMXB or a symbiotic X-ray binary.

SRGA J091511.9–752345

Associated with the galaxy 2MASS J09151520–7523498, with infrared colors (WISE) typical of AGN. Also a radio source (SUMSS).

SRGA J092021.6+860249

Associated with the galaxy LEDA 2790304, with infrared (WISE) colors typical of AGN; a radio source (NVSS).

SRGA J092418.4–314218

An LMXB or a CV (Tomsick et al. 2017).

SRGA J104450.9–602446

Likely an AGN (Clavel et al. 2019).

SRGA J104833.4–390227

A Seyfert 1.5 at $z = 0.0446$ (Masetti et al. 2018).

SRGA J111153.2–611826

A massive star-forming region. Very many point X-ray sources and diffuse X-ray emission (*Chandra*, Townsley et al. 2014).

SRGA J111457.9–611432

A massive star-forming region. Very many point X-ray sources and diffuse X-ray emission (*Chandra*, Townsley et al. 2014).

SRGA J111821.7–543730

Likely an LMXB and not an HMXB (Coleiro et al. 2013).

SRGA J114721.9–495309

Possible confusion of two known X-ray sources: XMMSL2 J114720.7–495302 (14'' from the ART-XC position) and XMMSL2 J114724.7–495303 (27'', the brighter one). There is also 1RXS J114724.3–495250 at 29''. The weaker XMM source is associated with the emission-line star TWA 19B, while the brighter XMM source is associated with the young stellar object HD 102458.

SRGA J120413.4–294646

Likely associated with the infrared source WISEA J120412.71–294709.1, with colors typical of AGN.

SRGA J123629.1–664554

In addition to XMMSL2 J123629.8–664549, there is another nearby source 2SXPS J123632.4–664557.

SRGA J123821.8–253205

A bright, short-duration X-ray transient SRGt J123822.3–253206 discovered by ART-XC and eROSITA (Semena et al. 2020; Wilms et al. 2020).

SRGA J124249.6–630348

A Be star or Be star–white dwarf binary (Tsujimoto et al. 2018).

SRGA J124640.6+543222

A Seyfert 2 (Parisi et al. 2012).

SRGA J131239.5–624256

A Wolf-Rayet star. The most likely physical picture is that of colliding stellar winds in a wide binary system, with the unseen secondary star being another WR star or a luminous blue variable (Zhekov et al. 2014).

SRGA J132032.4–701437

Associated with the bright star Gaia EDR3 5844075864125790464 at $D \sim 2300$ pc. Possibly an HMXB or a symbiotic X-ray binary.

SRGA J133949.9–643019

Possibly associated with IGR J13402–6428 at 2.8 arcmin from the ART-XC position, but the latter is inconsistent with those of two *Chandra* sources, CXOU J133935.8–642537

and CXOU J133959.2–642444 (located at 5.0 and 4.3 arcmin, respectively, from the *INTEGRAL* position), which have been suggested as possible soft X-ray counterparts of IGR J13402–6428 (Tomsick et al. 2012).

SRGA J140654.9–52749

Associated with the galaxy NGC 5472, a radio source.

SRGA J141249.5–402141

A CV of VY Scl-type (Greiner et al. 2010).

SRGA J152100.6+320405

A Seyfert 2 at $z = 0.1143$ (Zaznabin et al. 2021b).

SRGA J153414.5+625852

A Seyfert 1 at $z = 0.26$ (Campbell et al. 2015).

SRGA J153814.0–554219

Likely an LMXB (Degenaar et al. 2012).

SRGA J154805.3–473806

Associated with the galaxy LEDA 141863, with infrared colors (WISE) typical of AGN.

SRGA J160050.0–514249

A colliding-wind Wolf-Rayet binary (Callingham et al. 2019).

SRGA J160456.1–722318

Likely associated with the star Gaia EDR3 5806631686386070144 at $D \sim 580$ pc. Possibly a CV based on X-ray and optical photometric properties.

SRGA J160901.4–390519

Likely associated with the star THA 15-35 at $D \sim 160$ pc.

SRGA J161017.3–634243

A Seyfert 1.5, at $z = 0.2094$ (Stephen et al. 2018).

SRGA J161156.7–603826

Part of cluster A3627, together with SRGA J161415.5–605124.

SRGA J161201.8–464616

Likely associated with the star Gaia EDR3 5990098842316868352 at $D \sim 400$ pc. Possibly a CV based on X-ray and optical photometric properties.

SRGA J161415.5–605124

Part of cluster A3627, together with SRGA J161156.7–603826.

SRGA J163529.2–480558

Bright star at $D \sim 1100$ pc. Possibly an HMXB or a symbiotic X-ray binary.

SRGA J174009.6–284714

Likely a CV rather than an LMXB (Lo et al. 2014).

SRGA J174028.2–365545

An intermediate polar (Clavel et al. 2019).

SRGA J174046.4+060353

A CV (Halpern & Thorstensen 2015).

SRGA J174446.1–295057

Symbiotic X-ray binary (Bahramian et al. 2014).

SRGA J174450.9–323321

Massive cluster of galaxies at $z = 0.055$, with some contribution from a background blazar in the hard X-ray band (Barrière et al. 2015).

SRGA J175721.3–304400

Likely an LMXB with a giant companion (Maeda et al. 2013).

SRGA J180849.4+663432

A flat-spectrum radio source (Massaro et al. 2014).

SRGA J181228.0–181235

A burster, an ultra-compact LMXB (Goodwin et al. 2019).

SRGA J181239.6–221924

Discovered by MAXI, likely an LMXB (Negoro et al. 2018).

SRGA J181637.1–391248

Likely associated with V371 CrA, a variable star of Mira Cet type. A symbiotic X-ray binary?

SRGA J182156.2+642036

Powerful AGN in the central galaxy of a rich cluster. The X-ray luminosities of the quasar and cluster are comparable according to previous observations, in particular, *Chandra* (Russell et al. 2010; Reynolds et al. 2014).

SRGA J182511.1+645018

KO giant star with blended double lines in the optical spectrum (Sperauskas et al. 2019), thus most likely a coronally active binary.

SRGA J182919.6–121301

Likely an intermediate polar (Clavel et al. 2016).

SRGA J183605.4–192217

Possibly associated with 3MAXI J1836–194 at 2.0 arcmin from the ART-XC position.

SRGA J183754.6+155438

Likely associated with the bright star Gaia EDR3 4510001297611019392 at $D \sim 500$ pc.

SRGA J183907.1–571456

Suggested to be associated with the infrared source WISEA J183905.95–571505.1, with colors typical of AGN, and also has an absorbed X-ray spectrum (Landi et al. 2017). However, the optical counterpart appears to have a high proper motion in Gaia (Gaia EDR3 6637527637032850176).

SRGA J184117.8–045612

Magnetar 1E 1841–045 in the supernova remnant Kes 73, which are both bright in X-rays (An et al. 2013; Kumar et al. 2014) and consistent with the ART-XC position.

SRGA J184554.7–003937

A Be X-ray binary, pulsar (Kennea et al. 2019; McCollum & Laine 2019).

SRGA J185421.6+083844

Likely associated with the infrared source CatWISE J185422.29+083846.1, with infrared colors typical of AGN.

SRGA J190140.2+012627

Likely an LMXB (Karasev et al. 2008; Torrejón et al. 2010).

SRGA J190722.0–204635

Likely an intermediate polar (Xu et al. 2019).

SRGA J191456.9+103647

Likely an HMXB (Cusumano et al. 2015).

SRGA J192501.3+504309

A Seyfert 1.2 at $z = 0.068$ (Masetti et al. 2013).

SRGA J194638.9+704552

A CV, likely an intermediate polar ([Zaznabin et al. 2021a](#)).

SRGA J195702.4+615036

Associated with the galaxy LEDA 2625686, with infrared (WISE) colors typical of AGN.

SRGA J195928.3+404358

There must be a significant contribution of the central AGN to the X-ray luminosity of the cluster ([Young et al. 2002](#)).

SRGA J201118.2+600421

Suggested to be an AGN ([Warwick et al. 2012](#)), but likely associated with the star Gaia EDR3 2236896418906579072 at $D \sim 1.5$ kpc based on the position of XMMSL2 J201116.8+600431. Possibly a CV based on X-ray and optical photometric properties.

SRGA J202932.4–614903

Associated with the galaxy LEDA 352109, with infrared (WISE) colors typical of AGN.

SRGA J204149.6–373345

Blazar candidate ([Chang et al. 2019](#)) or a cluster of galaxies ([Schwope et al. 2000](#)).

SRGA J204319.7+443821

Galactic X-ray transient SRGA J204318.2+443815 = SRGE J204319.0+443820 discovered by *SRG/ART-XC* and *EROSITA* ([Mereminskiy et al. 2020a](#)), an X-ray pulsar in a Be system ([Lutovinov et al. 2021](#)).

SRGA J204547.8+672642

A CV ([Zaznabin et al. 2021a](#)).

SRGA J211747.6+513850

Blazar candidate based on infrared (WISE) colors ([Maselli et al. 2013](#)).

SRGA J221913.2+362014

Associated with the infrared source WISEA J221914.50+362010.5, with colors typical of AGN; a radio source (NVSS).

SRGA J223714.9+402939

Associated with the galaxy LEDA 5060459, with infrared (WISE) colors typical of AGN.

SRGA J225412.8+690658

A CV ([Zaznabin et al. 2021a](#)).

SRGA J230630.9+155637

Apparently a Seyfert 2 based on a visual inspection of the SDSS DR16 spectrum.

SRGA J232037.8+482329

Associated with the galaxy LEDA 2316409, a radio source.

SRGA J235250.6–170449

Associated with the galaxy 2MASS J23525142–1704372, with infrared colors (WISE) typical of AGN.

1. Source catalog

In Table 1, we present the catalog of sources detected during the first year of the *SRG/ART-XC* all-sky survey.

Table A.1. Catalog of sources^{a)} detected during the first year of the SRG/ART-XC all-sky survey.

Id	Name SRGA	RA (J2000)	Dec (J2000)	S/N	Flux (10^{-12} erg s $^{-1}$ cm $^{-2}$)	Common name	Redshift	Class
N001	J000132.7+240242	0.3861	24.0449	5.3	4.7($-2.3 + 3.1$)		0.1045	BLAZAR? ^{c)}
N002	J000632.2-690029	1.6340	-69.0081	7.1	5.0($-2.0 + 2.6$)			CV
N003	J001124.6-112841	2.8525	-11.4782	5.3	8.3($-2.5 + 3.0$)	WW Cet		CV
N004	J001315.3+774824	3.3138	77.8066	5.3	4.6($-1.5 + 1.8$)	8C 0010+775	0.3260	BLAZAR? ^{c)}
N005	J001704.0+813451	4.2667	81.5810	7.3	3.8($-1.4 + 1.7$)	6C 001403+811827	3.3660	BLAZAR
N006	J002021.4-042502	5.0893	-4.4171	5.2	2.8($-2.1 + 3.0$)			UNIDENT
N007	J002202.7+254008	5.5113	25.6689	5.1	4.4($-2.2 + 2.9$)	XMMSL1 J002202.9+254004	0.1292	SEYFERT ^{c)}
N008	J002256.7+614104	5.7362	61.6845	6.2	4.4($-1.6 + 1.9$)	V1033 Cas		CV
N009	J002301.7-394555	5.7570	-39.7652	5.7	7.3($-3.0 + 4.1$)			UNIDENT
N010	J002512.3+640822 ^{b)}	6.3013	64.1393		~40	Tycho SNR		SNR
N011	J002513.7+415305	6.3069	41.8848	5.3	2.5($-1.6 + 2.1$)			UNIDENT
N012	J002848.3+591714	7.2013	59.2871	19.1	39.0($-3.6 + 3.9$)	V709 Cas		CV
N013	J003552.7+595005	8.9694	59.8347	11.0	16.3($-2.5 + 2.8$)	1ES 0033+59.5	0.0860	BLAZAR
N014	J003708.1+612144	9.2837	61.3623	10.3	12.1($-2.2 + 2.5$)	IGR J00370+6122		HMXB
N015	J004013.4+405005	10.0560	40.8347	5.8	4.1($-1.8 + 2.3$)	5C 3.76		BLAZAR
N016	J004144.3+413415	10.4345	41.5707	5.1	4.1($-1.8 + 2.3$)	1E 0039.0+4118		LMXB? ^{c)}
N017	J004241.1+411603 ^{b)}	10.6711	41.2674		~10	M31		GALAXY ^{c)}
N018	J004242.6-813521	10.6777	-81.5891	5.1	3.8($-1.8 + 2.3$)			UNIDENT
N019	J004506.7+620747	11.2781	62.1296	5.0	1.9($-1.2 + 1.6$)	1RXS J004504.8+620803		AGN ^{c)}
N020	J004546.3+413951	11.4430	41.6642	5.7	3.3($-1.7 + 2.2$)	2E 0042.9+4123		X-RAY BINARY ^{c)}
N021	J004752.5+544745	11.9687	54.7960	4.9	3.9($-1.6 + 2.0$)	1RXS J004754.5+544758		BLAZAR
N022	J004800.8+001626	12.0035	0.2738	4.8	6.4($-2.6 + 3.4$)			UNIDENT
N023	J004846.8+315732	12.1950	31.9589	11.5	20.3($-3.4 + 3.9$)	NGC 262	0.0150	SEYFERT
N024	J005155.4+172552	12.9810	17.4312	6.5	8.4($-2.7 + 3.5$)	Mrk 1148	0.0640	SEYFERT
N025	J005456.3-722646	13.7346	-72.4460	10.7	15.4($-2.8 + 3.3$)	2E 0053.2-7242		HMXB ^{c)}
N026	J005520.0+461300	13.8331	46.2165	9.7	18.7($-3.0 + 3.4$)	V515 And		CV
N027	J005642.5+604302	14.1773	60.7172	29.1	107.2($-5.9 + 6.3$)	gam Cas		STAR ^{c)}
N028	J005953.3+314942	14.9721	31.8282	9.2	9.9($-2.5 + 3.1$)	Mrk 352	0.0149	SEYFERT
N029	J010324.9-295758	15.8539	-29.9662	4.9	4.0($-2.2 + 3.1$)			UNIDENT
N030	J010545.6-343200	16.4400	-34.5332	4.9	4.8($-1.8 + 2.3$)	HE 0103-3447	0.0570	SEYFERT
N031	J010650.3-225126	16.7096	-22.8573	5.9	8.5($-3.0 + 3.8$)	CS Cet		STAR
N032	J010743.2+540843 ^{b)}	16.9302	54.1453		~20	RXC J0107.7+5408	0.1066	CLUSTER
N033	J010744.2+574428	16.9341	57.7412	5.4	1.3($-1.3 + 1.7$)	XMMSL2 J010743.2+574429		UNIDENT
N034	J010942.8+731146	17.4285	73.1960	5.5	6.5($-1.9 + 2.3$)	3C 33.1	0.1810	SEYFERT
N035	J011244.1-310937	18.1840	-31.1602	5.0	4.0($-2.2 + 3.0$)			UNIDENT
N036	J011407.2-323841	18.5302	-32.6447	4.8	4.5($-2.1 + 2.7$)	IC 1657	0.0120	SEYFERT
N037	J011511.9+882912	18.7998	88.4867	5.7	2.6($-1.3 + 1.6$)	1RXS J011523.1+882923		STAR? ^{c)}
N038	J011704.7-732637	19.2694	-73.4435	43.3	296.0($-11.2 + 11.6$)	SMC X-1		HMXB ^{c)}
N039	J011802.6+651729	19.5110	65.2914	24.2	82.8($-5.8 + 6.2$)	4U 0114+65		HMXB
N040	J011832.3+634437	19.6346	63.7435	59.7	222.9($-6.2 + 6.3$)	4U 0115+63		HMXB
N041	J012308.6+342043	20.7859	34.3452	10.0	13.8($-2.8 + 3.3$)	1ES 0120+340	0.2720	BLAZAR
N042	J012345.0-584819	20.9375	-58.8053	10.6	13.8($-2.6 + 3.0$)	Fairall 9	0.0470	SEYFERT

Table A.1. Continued.

Id	Name SRGA	RA (J2000)	Dec (J2000)	S/N	Flux (10^{-12} erg s $^{-1}$ cm $^{-2}$)	Common name	Redshift	Class
N043	J012354.2-350403	20.9758	-35.0676	13.9	28.3(-4.8 + 5.5)	NGC 526	0.0190	SEYFERT
N044	J012428.1+334757	21.1171	33.7991	6.7	6.1(-2.0 + 2.5)	NGC 513	0.0196	SEYFERT
N045	J012531.2+320807	21.3800	32.1352	6.5	7.0(-2.2 + 2.7)	Mrk 993	0.0155	SEYFERT
N046	J012806.4-184823	22.0265	-18.8063	5.4	7.6(-2.7 + 3.5)	MCG -03-04-072	0.0430	SEYFERT
N047	J014622.4+614501	26.5934	61.7503	7.3	9.9(-2.4 + 2.8)	4U 0142+61		MAGNETAR
N048	J014701.1+612126	26.7546	61.3571	12.5	26.0(-3.5 + 3.9)	RX J0146.9+6121		HMXB
N049	J014944.1+194158	27.4339	19.6995	4.9	4.3(-1.9 + 2.5)			UNIDENT
N050	J014950.5+711910	27.4602	71.3195	5.3	4.8(-1.8 + 2.2)			UNIDENT
N051	J015639.0-835828	29.1625	-83.9745	5.8	5.7(-1.9 + 2.3)	1RXS J015634.6-835836		CV? ^c
N052	J015657.8-530201	29.2407	-53.0337	9.1	7.8(-2.2 + 2.7)	RBS 259		BLAZAR
N053	J020457.9-170113	31.2412	-17.0201	5.7	7.1(-2.2 + 2.7)	PKS 0202-17	1.7395	BLAZAR
N054	J020653.1+151738	31.7215	15.2939	10.7	18.0(-3.2 + 3.7)	TT Ari		CV
N055	J020916.6+444925	32.3192	44.8237	6.1	8.2(-2.3 + 2.8)	1RXS J020917.6+444951		BLAZAR
N056	J020932.9-742718	32.3871	-74.4549	12.7	21.2(-3.0 + 3.4)	RX J0209.6-7427		HMXB
N057	J020937.9+522647	32.4080	52.4463	12.5	14.3(-2.4 + 2.7)	2E 0206.3+5212	0.0492	SEYFERT
N058	J020948.6-631838	32.4525	-63.3107	7.2	5.2(-1.6 + 1.9)	WX Hyi		CV
N059	J022235.8+250816	35.6493	25.1377	7.3	5.2(-2.0 + 2.5)	SWIFT J0222.3+2509	0.0620	AGN ^c
N060	J022624.9+592741	36.6036	59.4614	5.1	4.6(-1.9 + 2.5)	SWIFT J0225.8+5946		AGN ^c
N061	J022745.0-693133	36.9377	-69.5259	9.4	5.9(-1.7 + 2.1)	CL Hyi		STAR? ^c
N062	J022814.9+311841	37.0622	31.3114	11.6	17.7(-3.3 + 3.9)	NGC 931	0.0163	SEYFERT
N063	J023005.5-085941	37.5229	-8.9946	7.2	10.7(-2.6 + 3.1)	Mrk 1044	0.0161	SEYFERT
N064	J023054.0-684157	37.7251	-68.6990	6.0	3.8(-1.5 + 1.9)	CW Hyi		CV
N065	J023248.2+201712	38.2007	20.2868	5.5	5.3(-2.1 + 2.6)	1ES 0229+200	0.1400	BLAZAR
N066	J023420.4+323019	38.5851	32.5054	7.5	11.3(-2.7 + 3.3)	NGC 973	0.0167	SEYFERT
N067	J023437.9-084711	38.6581	-8.7865	6.3	11.2(-2.6 + 3.1)	NGC 985	0.0427	SEYFERT
N068	J023821.6-521142	39.5901	-52.1949	6.9	4.9(-1.8 + 2.2)	ESO 198-G024	0.0452	SEYFERT
N069	J023832.3-311654	39.6347	-31.2817	7.0	8.5(-2.1 + 2.5)	RBS 337	0.2329	BLAZAR
N070	J023843.2-611719	39.6801	-61.2886	5.5	5.8(-1.8 + 2.2)	SWIFT J0238.5-6119	0.0540	SEYFERT
N071	J024032.0+611344	40.1332	61.2288	5.9	9.4(-2.5 + 3.0)	LS I +61 303		HMXB
N072	J024239.8-000103	40.6658	-0.0174	7.0	10.4(-2.6 + 3.1)	NGC 1068	0.0038	SEYFERT
N073	J024252.0+564137	40.7165	56.6935	7.2	6.8(-2.4 + 3.1)	PT Per		CV
N074	J024458.1+622805	41.2420	62.4680	10.5	16.3(-3.1 + 3.6)	4U 0241+61	0.0440	SEYFERT
N075	J025025.8+464745	42.6074	46.7957	6.4	11.8(-2.9 + 3.6)	SWIFT J0250.2+4650	0.0210	SEYFERT
N076	J025234.3+431004	43.1429	43.1678	4.9	2.7(-1.8 + 2.3)	2SXPS J025233.8+431001	0.0518	AGN ^c
N077	J025426.6+413325 ^b	43.6108	41.5570		~40	AWM 7	0.0172	CLUSTER
N078	J025504.7-285537	43.7694	-28.9268	4.9	2.2(-1.4 + 1.8)			UNIDENT
N079	J025608.3+192633	44.0345	19.4426	7.0	8.3(-2.3 + 2.8)	XY Ari		CV
N080	J025621.4-321101	44.0890	-32.1835	8.6	7.5(-1.9 + 2.3)	ESO 417-G006	0.0163	SEYFERT
N081	J025659.0+303612	44.2458	30.6032	5.0	6.2(-2.3 + 2.9)			UNIDENT
N082	J025710.8-153418	44.2950	-15.5717	4.9	0.1(-0.1 + 1.7)			UNIDENT
N083	J025850.3+133406 ^b	44.7094	13.5685		~30	Abell 401	0.0737	CLUSTER
N084	J025929.8-001950	44.8741	-0.3305	5.0	2.1(-1.6 + 2.1)	LBQS 0256-0031	1.9999	BLAZAR
N085	J030003.4-104924	45.0143	-10.8233	11.1	17.8(-3.1 + 3.5)	MCG-02-08-038	0.0326	SEYFERT

Article number, page 22 of 40
Table A.1. Continued.

Id	Name SRGA	RA (J2000)	Dec (J2000)	S/N	Flux (10^{-12} erg s $^{-1}$ cm $^{-2}$)	Common name	Redshift	Class
N086	J030736.3-725012	46.9014	-72.8366	5.2	4.3(-1.4 + 1.7)	1H 0307-722	0.0280	SEYFERT
N087	J030810.6+405725	47.0440	40.9569	5.9	10.3(-2.8 + 3.5)	bet Per		STAR
N088	J030838.1-552041	47.1589	-55.3446	5.2	4.8(-1.5 + 1.9)		0.0814	AGN ^{c)}
N089	J031102.9-440232	47.7620	-44.0421	5.1	2.8(-1.3 + 1.6)	1RXS J031104.2-440245		BLAZAR? ^{c)}
N090	J031131.8-315251	47.8825	-31.8808	6.2	4.5(-1.6 + 2.0)	2QZ J031130.9-315250		CV ^{c)}
N091	J031150.3-585355	47.9597	-58.8987	5.0	0.7(-0.7 + 1.1)			UNIDENT
N092	J031202.4+502913	48.0099	50.4868	5.5	7.1(-2.4 + 3.0)	1RXS J031202.7+502922	0.0620	SEYFERT
N093	J031752.9-441507 ^{b)}	49.4706	-44.2518		~10	Abell 3112	0.0759	CLUSTER
N094	J031947.6+413054 ^{b)}	49.9482	41.5150		~600	Perseus Cluster	0.0176	CLUSTER
N095	J031952.5+184538	49.9689	18.7607	10.8	19.3(-3.7 + 4.4)	QSO B0317+18	0.1900	BLAZAR
N096	J032317.0-481805	50.8209	-48.3015	5.4	2.4(-1.2 + 1.5)	1RXS J032320.6-481808	0.1550	AGN
N097	J032324.2-255007	50.8510	-25.8353	4.9	2.6(-1.4 + 1.8)			UNIDENT
N098	J032512.0+404157	51.2999	40.6993	5.0	3.6(-2.0 + 2.7)	IGR J03249+4041	0.0475	SEYFERT
N099	J032524.7-563554	51.3530	-56.5985	8.6	6.3(-1.6 + 1.8)	1RXS J032521.8-563543	0.0602	BLAZAR
N100	J032635.6+284248	51.6483	28.7134	9.3	16.1(-3.5 + 4.2)	UX Ari		STAR
N101	J033012.8-053250	52.5532	-5.5471	5.5	4.2(-2.0 + 2.6)	NGC 1346	0.0134	SEYFERT
N102	J033110.5-504241	52.7939	-50.7114	4.9	2.9(-1.2 + 1.4)			UNIDENT
N103	J033112.4+435416	52.8017	43.9045	7.7	10.9(-2.9 + 3.6)	GK Per		CV
N104	J033319.9+371810	53.3328	37.3027	5.2	7.3(-2.5 + 3.2)	IGR J03334+3718	0.0547	SEYFERT
N105	J033335.7-360832	53.3986	-36.1422	13.1	18.0(-2.5 + 2.8)	NGC 1365	0.0055	SEYFERT
N106	J033623.7-034724	54.0985	-3.7901	4.9	3.6(-1.9 + 2.6)	1RXS J033623.3-034727	0.1618	BLAZAR
N107	J033623.8-605853	54.0993	-60.9813	5.7	2.0(-1.1 + 1.4)	1RXS J033624.5-605848	0.4710	AGN
N108	J033630.6+321806	54.1275	32.3016	5.4	8.2(-2.7 + 3.4)	4C 32.14	1.2580	BLAZAR
N109	J033647.8+003517	54.1992	0.5880	4.9	6.6(-2.3 + 2.9)	HD 22468		STAR
N110	J033845.3+095835 ^{b)}	54.6889	9.9764		~10	2A 0335+096	0.0349	CLUSTER
N111	J034203.6-211436	55.5150	-21.2432	6.5	4.1(-1.7 + 2.1)	ESO 548-G81	0.0145	SEYFERT
N112	J034307.5-533809 ^{b)}	55.7814	-53.6359		~20	Abell 3158	0.0597	CLUSTER
N113	J034510.3-393435	56.2931	-39.5764	4.8	1.8(-1.2 + 1.5)	TOL 0343-397	0.0430	SEYFERT
N114	J034553.7-004300	56.4737	-0.7168	5.1	1.5(-1.5 + 2.3)			UNIDENT
N115	J034923.8-115914	57.3492	-11.9871	7.7	11.7(-2.7 + 3.2)	1ES 0347-121	0.1850	BLAZAR
N116	J035023.8-501802	57.5993	-50.3006	5.2	2.8(-1.1 + 1.3)	ESO 201-IG004	0.0359	SEYFERT ^{c)}
N117	J035141.7-402759	57.9236	-40.4663	6.3	3.6(-1.3 + 1.6)	Fairall 1116	0.0586	SEYFERT
N118	J035256.5-683118	58.2355	-68.5218	6.1	3.6(-1.2 + 1.4)	PKS 0352-686	0.0870	BLAZAR
N119	J035522.6+310241	58.8441	31.0446	38.9	329.0(-13.8 + 14.3)	X Per		HMXB
N120	J040501.8-371116	61.2577	-37.1878	7.2	7.4(-1.8 + 2.1)	ESO 359-G019	0.0552	SEYFERT
N121	J040748.0-121128	61.9500	-12.1910	5.7	5.1(-2.1 + 2.7)	PKS 0405-12	0.5726	SEYFERT
N122	J040850.8-791418	62.2116	-79.2384	6.2	4.7(-1.5 + 1.9)	2SXPS J040848.1-791405		CV? ^{c)}
N123	J040941.9-075325	62.4245	-7.8904	8.9	15.3(-3.3 + 3.9)	EI Eri		STAR
N124	J041242.1-471231	63.1752	-47.2087	7.0	3.7(-1.2 + 1.4)	1RXS J041242.5-471238	0.1320	SEYFERT
N125	J041324.8+102752 ^{b)}	63.3532	10.4644		~30	Abell 478	0.0881	CLUSTER
N126	J041328.3-061446	63.3679	-6.2460	5.2	2.9(-1.9 + 2.6)	1RXS J041327.9-061502	0.1586	BLAZAR ^{c)}
N127	J041452.4-075527	63.7185	-7.9243	7.7	12.4(-3.0 + 3.6)	2E 0412.4-0802	0.0382	SEYFERT

Table A.1. Continued.

Id	Name SRGA	RA	Dec	S/N	Flux	Common name	Redshift	Class
		(J2000)	(J2000)		(10^{-12} erg s $^{-1}$ cm $^{-2}$)			
N128	J041732.7-525316	64.3864	-52.8878	5.0	1.7(-0.9 + 1.1)		0.0456	AGN? ^{c)}
N129	J041821.5+380141	64.5896	38.0280	12.6	29.9(-4.5 + 5.1)	3C 111	0.0485	SEYFERT
N130	J041835.3+662157	64.6472	66.3658	5.8	4.5(-1.9 + 2.4)			UNIDENT
N131	J042000.7-545613	65.0027	-54.9370	11.1	8.6(-1.3 + 1.5)	NGC 1566	0.0050	SEYFERT
N132	J042202.5-415333	65.5104	-41.8925	5.3	4.4(-1.2 + 1.5)	CTS B26.08	0.0621	SEYFERT
N133	J042224.4-561329	65.6018	-56.2248	4.9	2.0(-0.9 + 1.0)	ESO 157-G023	0.0433	SEYFERT
N134	J042309.8-310633	65.7909	-31.1093	5.1	2.8(-1.5 + 2.0)			UNIDENT
N135	J042340.6+040802	65.9193	4.1338	4.8	2.6(-1.8 + 2.5)	IRAS 04210+0400	0.0461	SEYFERT
N136	J042555.8-194545	66.4824	-19.7625	5.1	3.7(-1.9 + 2.4)	IW Eri		CV
N137	J042601.6-571158	66.5069	-57.1995	12.1	11.0(-1.4 + 1.5)	1H 0419-577	0.1040	SEYFERT
N138	J042616.9-592322	66.5705	-59.3893	5.0	2.6(-0.8 + 1.0)	XMMSL2 J042617.5-592334		AGN ^{c)}
N139	J042746.6+131433	66.9440	13.2425	5.0	2.2(-1.8 + 2.5)			UNIDENT
N140	J043126.3-612517 ^{b)}	67.8598	-61.4214		~40	Abell 3266	0.0589	CLUSTER
N141	J043209.5+354927	68.0394	35.8243	7.7	11.1(-3.0 + 3.7)	1WGA J0432.1+3549	0.0506	SEYFERT ^{c)}
N142	J043310.8+052115	68.2950	5.3542	13.5	30.8(-4.5 + 5.1)	3C 120	0.0330	SEYFERT
N143	J043340.8-131434 ^{b)}	68.4202	-13.2428		~30	Abell 496	0.0328	CLUSTER
N144	J043510.5-752749	68.7939	-75.4635	8.2	7.6(-1.5 + 1.7)	1RXS J043509.8-752732		STAR? ^{c)}
N145	J043522.9+552234	68.8452	55.3760	59.5	243.7(-6.8 + 6.9)			LMXB ^{c)}
N146	J043554.4-363634	68.9765	-36.6095	5.7	4.4(-1.6 + 2.0)	CTS A29.15	0.1398	SEYFERT
N147	J043622.0-102243	69.0917	-10.3787	6.3	4.9(-2.0 + 2.6)	Mrk 618	0.0352	SEYFERT
N148	J043729.2-471132	69.3715	-47.1922	4.9	4.1(-1.3 + 1.5)	1ES 0435-472	0.0510	SEYFERT
N149	J043827.0-614759	69.6125	-61.7996	6.4	3.4(-0.9 + 1.0)	1RXS J043830.0-614758	0.0690	SEYFERT
N150	J043830.9-681205	69.6289	-68.2015	4.9	0.7(-0.7 + 0.8)	4XMM J043831.1-681201		AGN? ^{c)}
N151	J044017.9-433312	70.0746	-43.5534	5.5	4.0(-1.4 + 1.7)	PKS 0438-43	2.8520	BLAZAR
N152	J044059.4+443153	70.2474	44.5314	9.7	14.0(-3.2 + 3.9)	RX J0440.9+4431		HMXB
N153	J044605.6-072148	71.5235	-7.3633	4.9	3.6(-1.9 + 2.5)			UNIDENT
N154	J044925.1-435008	72.3546	-43.8356	7.2	4.7(-1.5 + 1.8)	PKS 0447-439	0.1070	BLAZAR
N155	J045013.9+450317 ^{b)}	72.5581	45.0547		~50	4U 0446+44	0.0210	CLUSTER
N156	J045050.1+301450	72.7089	30.2471	5.0	7.1(-2.6 + 3.3)	SWIFT J0450.6+3015	0.0331	SEYFERT ^{c)}
N157	J045144.8-581058	72.9366	-58.1827	8.3	3.9(-0.8 + 1.0)	1RXS J045145.2-581058	0.0907	SEYFERT
N158	J045254.2-585353	73.2260	-58.8981	6.1	1.3(-0.7 + 0.8)	1RXS J045254.2-585351		BLAZAR? ^{c)}
N159	J045442.9-431416	73.6789	-43.2377	5.0	3.6(-1.4 + 1.7)	1RXS J045444.4-431427	0.0877	SEYFERT
N160	J045556.3-753225	73.9846	-75.5403	5.3	3.8(-1.2 + 1.4)	ESO 033-G002	0.0184	SEYFERT
N161	J045709.0+452752	74.2876	45.4645	7.0	8.1(-2.7 + 3.4)	1RXS J045707.4+452751		CV
N162	J045818.8-751638	74.5785	-75.2772	5.7	4.1(-1.2 + 1.4)	YY Men		STAR
N163	J045958.5-611507	74.9936	-61.2519	5.9	2.1(-0.6 + 0.7)	1RXS J045958.1-611506	0.0860	SEYFERT
N164	J050021.6+523801	75.0898	52.6335	6.0	9.6(-2.7 + 3.4)	1RXS J050020.8+523747		BLAZAR ^{c)}
N165	J050209.3+033140	75.5387	3.5277	8.3	12.2(-3.1 + 3.7)	2E 0459.5+0327	0.0160	SEYFERT
N166	J050227.0+244518	75.6125	24.7550	8.9	13.6(-3.3 + 4.0)	V1062 Tau		CV
N167	J050258.9+225940	75.7456	22.9945	7.1	11.4(-3.1 + 3.8)	1RXS J050258.5+225949	0.0577	SEYFERT
N168	J050302.5-663352	75.7603	-66.5645	5.7	1.7(-0.7 + 0.8)	1RXS J050304.8-663345	0.0640	SEYFERT
N169	J050434.3-734943	76.1430	-73.8286	5.0	3.6(-1.1 + 1.2)	IGR J05053-7343	0.0452	SEYFERT

Article number, page 24 of 40
Table A.1. Continued.

Id	Name	RA	Dec	S/N	Flux (10^{-12} erg s $^{-1}$ cm $^{-2}$)	Common name	Redshift	Class
	SRGA	(J2000)	(J2000)					
N170	J050541.3–231302	76.4222	-23.2173	5.1	2.9($-1.7 + 2.2$)			UNIDENT
N171	J050547.7–090116	76.4489	-9.0212	4.9	2.7($-1.8 + 2.4$)			UNIDENT
N172	J050648.6–193700	76.7026	-19.6165	5.1	4.3($-1.9 + 2.4$)	1RXS J050648.5-193651	0.0941	SEYFERT
N173	J050757.2+673728	76.9882	67.6245	5.9	5.3($-2.0 + 2.6$)	1ES 0502+675	0.3140	BLAZAR
N174	J050810.6–660657	77.0440	-66.1158	10.3	4.9($-0.7 + 0.8$)	2RXS J050810.2-660645		HMXB ^{c)}
N175	J050957.0–641744	77.4875	-64.2957	9.3	4.2($-0.7 + 0.8$)	RBS 625		BLAZAR
N176	J051045.3+162956	77.6887	16.4989	9.7	23.4($-4.3 + 5.0$)	4U 0517+17	0.0179	SEYFERT
N177	J051300.1–252326	78.2503	-25.3906	4.9	4.3($-1.8 + 2.3$)			UNIDENT
N178	J051327.5–654705	78.3648	-65.7848	7.0	2.8($-0.7 + 0.7$)	SWIFT J0513.4-6547		HMXB
N179	J051344.1–165034	78.4336	-16.8429	4.9	2.5($-1.7 + 2.2$)			UNIDENT
N180	J051406.1–400240	78.5253	-40.0445	21.4	52.0($-4.0 + 4.3$)	4U 0513-40		LMXB
N181	J051514.3–142701	78.8098	-14.4503	4.9	2.8($-1.8 + 2.4$)	XMM SL2 J051515.2-142719		AGN ^{c)}
N182	J051611.2–000902	79.0468	-0.1505	10.3	21.6($-3.9 + 4.6$)	Ark 120	0.0323	SEYFERT
N183	J051621.1–103342	79.0877	-10.5615	6.4	5.6($-2.2 + 2.8$)	MCG -02-14-009	0.0289	SEYFERT
N184	J051637.5–514640	79.1561	-51.7777	5.4	3.7($-1.1 + 1.2$)	RBS 635	0.2220	SEYFERT
N185	J051901.7+630338	79.7572	63.0606	5.1	3.3($-1.9 + 2.5$)	1RXS J051905.3+630335		STAR
N186	J051935.4–323925	79.8973	-32.6569	8.6	6.4($-1.9 + 2.3$)	ESO 362-G018	0.0126	SEYFERT
N187	J051950.0–454650	79.9583	-45.7804	8.3	7.9($-1.6 + 1.8$)	Pictor A	0.0340	SEYFERT
N188	J052029.0–715733	80.1208	-71.9591	73.7	241.0($-5.4 + 5.5$)	LMC X-2		LMXB ^{c)}
N189	J052139.0–355257	80.4124	-35.8824	5.2	1.3($-1.2 + 1.6$)			UNIDENT
N190	J052257.6–362746	80.7399	-36.4627	7.9	6.0($-1.8 + 2.1$)	PKS 0521-36	0.0550	BLAZAR
N191	J052410.7–662045	81.0444	-66.3458	4.8	0.8($-0.4 + 0.5$)	RX J0524.2-6620		HMXB ^{c)}
N192	J052430.6+424448	81.1274	42.7467	4.9	5.4($-2.4 + 3.1$)	Paloma		CV
N193	J052505.4–693853	81.2727	-69.6481	5.2	2.5($-0.7 + 0.8$)	SNR J052501-693842		SNR ^{c)}
N194	J052522.2+241340	81.3425	24.2277	5.3	10.1($-3.0 + 3.8$)	RX J0525.3+2413		CV
N195	J052627.9–211714	81.6162	-21.2873	5.0	3.0($-1.8 + 2.3$)	SWIFT J0526.2-2118	0.0278	SEYFERT
N196	J052832.9+283832	82.1369	28.6422	5.0	4.9($-2.4 + 3.1$)	1RXS J052832.5+283824		CV
N197	J052845.1–652655	82.1877	-65.4486	13.5	4.7($-0.6 + 0.6$)	AB Dor		STAR
N198	J052925.4–324905	82.3559	-32.8181	16.4	40.1($-4.0 + 4.3$)	TV Col		CV
N199	J052947.3–655645	82.4472	-65.9458	21.2	12.3($-0.8 + 0.9$)	RX J0529.8-6556		HMXB ^{c)}
N200	J052959.8–340157	82.4993	-34.0325	4.9	4.6($-1.7 + 2.0$)	XMM SL2 J052958.9-340159	0.0790	AGN
N201	J053043.5–665424	82.6814	-66.9067	10.3	3.7($-0.6 + 0.6$)	SWIFT J053041.9-665426		HMXB ^{c)}
N202	J053218.5+214212	83.0771	21.7034	5.0	2.3($-2.3 + 2.9$)			UNIDENT
N203	J053231.6+624800	83.1319	62.7998	5.4	4.5($-2.0 + 2.6$)	V391 Cam		CV
N204	J053232.1–655141	83.1339	-65.8613	5.9	0.9($-0.4 + 0.4$)	RX J0532.5-6551		HMXB ^{c)}
N205	J053249.3–662220	83.2055	-66.3722	27.7	21.1($-0.9 + 1.0$)	LMC X-4		HMXB ^{c)}
N206	J053431.3–601610	83.6306	-60.2694	6.2	1.8($-0.6 + 0.7$)	1RXS J053431.9-601613	0.0570	SEYFERT
N207	J053431.8+220103 ^{b)}	83.6324	22.0174	213.8	13900	Crab		SNR / PULSAR
N208	J053450.8–580143	83.7118	-58.0287	19.3	18.6($-1.5 + 1.6$)	TW Pic		CV
N209	J053451.5+573950	83.7145	57.6639	5.0	3.7($-2.0 + 2.6$)			UNIDENT
N210	J053456.9+282843	83.7369	28.4786	6.1	3.0($-1.9 + 2.7$)	SWIFT J0535.2+2830		CV
N211	J053516.8–052315	83.8201	-5.3876	10.0	24.0($-4.1 + 4.8$)	Orion Nebula		SFR

Table A.1. Continued.

Id	Name SRGA	RA	Dec	S/N	Flux	Common name	Redshift	Class
		(J2000)	(J2000)		(10^{-12} erg s $^{-1}$ cm $^{-2}$)			
N212	J053525.0-691621	83.8541	-69.2724	5.0	0.5(-0.5 + 0.6)	SN 1987A		SNR ^{c)}
N213	J053601.5+360004	84.0064	36.0012	4.8	4.9(-2.3 + 3.1)			UNIDENT
N214	J053739.1+210826	84.4128	21.1404	7.9	16.3(-3.8 + 4.5)	zet Tau		STAR ^{c)}
N215	J053749.8-691016	84.4574	-69.1711	8.4	3.5(-0.6 + 0.7)	PSR J0537-6910		SNR / PULSAR ^{c)}
N216	J053854.3+261856	84.7261	26.3156	25.1	118.1(-8.7 + 9.3)	A 0535+26		HMXB
N217	J053857.2-640503	84.7383	-64.0843	115.9	129.6(-1.9 + 1.9)	LMC X-3		HMXB ^{c)}
N218	J053939.4-694440	84.9140	-69.7444	75.7	104.6(-2.3 + 2.3)	LMC X-1		HMXB ^{c)}
N219	J054010.9-692001	85.0455	-69.3336	28.3	20.5(-1.1 + 1.1)	PSR B0540-69		SNR / PULSAR ^{c)}
N220	J054248.3+605136	85.7014	60.8601	11.0	22.5(-3.8 + 4.4)	BY Cam		CV
N221	J054319.9-410155	85.8330	-41.0319	12.1	13.3(-2.2 + 2.5)	TX Col		CV
N222	J054356.6-553211	85.9858	-55.5365	11.4	8.5(-1.2 + 1.4)	RBS 679	0.2730	BLAZAR
N223	J054422.3+590748	86.0928	59.1299	5.5	3.6(-1.9 + 2.6)	SWIFT J0544.4+5909	0.0674	SEYFERT
N224	J054641.2-641529	86.6719	-64.2581	6.3	0.9(-0.4 + 0.4)	RBS 681	0.3230	BLAZAR
N225	J054920.2-181122	87.3343	-18.1895	5.1	2.8(-1.8 + 2.3)			UNIDENT
N226	J054920.9-620525	87.3371	-62.0903	7.1	3.1(-0.6 + 0.6)	1RXS J054919.1-620511	0.3760	CLUSTER
N227	J055034.8-663655	87.6450	-66.6152	5.0	0.7(-0.2 + 0.2)	2E 0550.6-6637	0.0752	SEYFERT
N228	J055040.1-321623	87.6671	-32.2732	8.5	10.5(-2.3 + 2.7)	PKS 0548-322	0.0690	BLAZAR
N229	J055053.7-621457	87.7238	-62.2492	6.3	1.4(-0.5 + 0.5)	1RXS J055054.2-621454	0.0587	AGN ^{c)}
N230	J055211.1-072723	88.0461	-7.4565	16.9	53.3(-5.8 + 6.4)	NGC 2110	0.0076	SEYFERT
N231	J055225.6-640213	88.1065	-64.0370	7.4	1.5(-0.4 + 0.4)	PKS 0552-640	0.6840	BLAZAR
N232	J055227.3+592837	88.1138	59.4769	6.2	9.2(-3.0 + 3.8)	1RXS J055229.5+592842	0.0585	SEYFERT
N233	J055327.8-815704	88.3660	-81.9510	5.1	1.7(-1.1 + 1.4)	1RXS J055327.9-815650		STAR
N234	J055453.1+462621	88.7213	46.4392	12.2	38.2(-5.9 + 6.8)	MCG +08-11-11	0.0205	SEYFERT
N235	J055646.4-331031	89.1932	-33.1752	15.5	38.5(-4.4 + 4.9)	MAXI J0556-332		LMXB
N236	J055759.4+535340	89.4974	53.8945	7.4	12.4(-3.4 + 4.2)	V405 Aur		CV
N237	J055801.4-382006	89.5059	-38.3349	7.2	9.5(-2.3 + 2.7)	4U 0557-38	0.0340	SEYFERT
N238	J055807.1-383839	89.5294	-38.6443	5.1	5.7(-1.9 + 2.4)	EXO 0556.4-3838	0.3020	BLAZAR
N239	J055947.0-502653	89.9456	-50.4482	9.4	9.3(-1.9 + 2.1)	PKS 0558-504	0.1370	BLAZAR
N240	J060210.5+282811	90.5439	28.4697	7.7	15.6(-4.6 + 5.9)	RX J0602.1+2828	0.0326	SEYFERT
N241	J060241.1-595152	90.6713	-59.8644	6.2	2.5(-0.8 + 0.9)	XMMSL2 J060241.6-595149	0.1005	AGN ^{c)}
N242	J060651.8-624550	91.7159	-62.7639	7.1	2.3(-0.7 + 0.7)	1RXS J060650.3-624539		AGN ^{c)}
N243	J060728.9-614836	91.8704	-61.8101	7.8	3.1(-0.8 + 0.9)	ESO 121-G006	0.0040	AGN ^{c)}
N244	J060859.6+693626	92.2481	69.6073	4.9	3.8(-2.2 + 3.1)			UNIDENT
N245	J060916.9-560657	92.3204	-56.1158	5.9	3.0(-1.1 + 1.3)	CTS H34.06	0.0318	SEYFERT
N246	J061007.3-624317	92.5305	-62.7215	5.4	2.0(-0.7 + 0.7)	1RXS J061006.6-624311	0.1570	SEYFERT
N247	J061146.3-814929	92.9427	-81.8247	6.0	5.2(-1.4 + 1.6)	AH Men		CV
N248	J061148.3-662439	92.9511	-66.4109	10.9	2.4(-0.3 + 0.3)	IGR J06117-6625	0.2300	SEYFERT
N249	J061322.9-290027	93.3455	-29.0076	7.2	12.4(-3.2 + 3.9)	1RXS J061324.2-290029	0.0706	AGN ^{c)}
N250	J061323.1+474420	93.3463	47.7390	10.4	17.4(-3.6 + 4.3)	SS Aur		CV
N251	J061539.5+710217	93.9144	71.0381	5.8	7.0(-2.6 + 3.4)	Mrk 3	0.0130	SEYFERT
N252	J061619.2-705228	94.0800	-70.8743	5.3	0.7(-0.5 + 0.5)	1RXS J061617.6-705237		UNIDENT ^{c)}
N253	J061707.7+090814	94.2823	9.1371	39.4	624.4(-25.8 + 26.9)	4U 0614+09		LMXB

Article number, page 26 of 40
Table A.1. Continued.

Id	Name	RA	Dec	S/N	Flux	Common name	Redshift	Class
					(10^{-12} erg s $^{-1}$ cm $^{-2}$)			
N254	J062039.8+264348	95.1658	26.7299	4.8	3.8($-2.7 + 4.0$)	RX J0620.6+2644		BLAZAR
N255	J062109.8-680554	95.2909	-68.0983	7.1	1.0($-0.3 + 0.3$)		0.0651	AGN ^{c)}
N256	J062309.2-643630	95.7884	-64.6083	5.8	1.3($-0.5 + 0.6$)	PMN J0623-6436	0.1290	BLAZAR
N257	J062345.2-605845	95.9382	-60.9790	8.0	3.7($-0.9 + 1.0$)	IGR J06239-6052	0.0405	SEYFERT
N258	J062405.2-093905	96.0216	-9.6514	5.6	6.4($-3.0 + 4.1$)	2MAXI J0623-095		CV
N259	J062517.1+733440	96.3213	73.5779	7.2	9.0($-2.5 + 3.1$)	MU Cam		CV
N260	J062627.2+072734	96.6132	7.4595	5.1	1.7($-1.7 + 3.6$)	SWIFT J0626.6+0729		AGN ^{c)}
N261	J062945.0-834426	97.4374	-83.7405	5.1	3.4($-1.2 + 1.4$)	SWIFT J0628.7-8346		AGN? ^{c)}
N262	J062953.4-033505	97.4723	-3.5847	5.3	8.8($-3.3 + 4.4$)	1RXS J062954.6-033520		CV? ^{c)}
N263	J063107.7+112740	97.7823	11.4612	5.4	8.7($-3.7 + 5.0$)	SWIFT J0630.9+1129		UNIDENT
N264	J063114.7+615435	97.8112	61.9096	4.9	2.8($-2.1 + 3.0$)			UNIDENT
N265	J063200.6-540458	98.0026	-54.0829	5.0	2.7($-1.2 + 1.5$)	1ES 0630-540	0.2036	BLAZAR
N266	J063324.9-561424	98.3539	-56.2399	5.1	3.4($-1.2 + 1.4$)	1RXS J063326.3-561430	0.0478	AGN
N267	J063545.9-751617	98.9412	-75.2714	8.3	4.2($-0.9 + 1.0$)	PKS 0637-75	0.6590	BLAZAR
N268	J063558.6+075528	98.9943	7.9245	7.6	10.6($-3.8 + 5.1$)	2E 0633.2+0757		STAR? ^{c)}
N269	J064117.9+324935	100.3245	32.8263	6.0	11.0($-4.0 + 5.3$)	SWIFT J0641.3+3257	0.0470	SEYFERT
N270	J064421.5-662620	101.0894	-66.4388	5.5	0.6($-0.5 + 0.5$)	1RXS J064422.9-662625	0.0784	AGN
N271	J064517.6-165136	101.3232	-16.8600	8.4	13.2($-3.6 + 4.6$)	HL CMa		CV
N272	J064849.9-694524	102.2077	-69.7566	6.1	1.1($-0.5 + 0.5$)	1RXS J064850.3-694519		BLAZAR? ^{c)}
N273	J065212.3+742535	103.0511	74.4263	5.5	9.0($-2.8 + 3.6$)	Mrk 6	0.0187	SEYFERT
N274	J065252.9+383350	103.2203	38.5639	5.4	3.6($-2.7 + 3.9$)			UNIDENT
N275	J065513.5-012846	103.8061	-1.4795	5.9	5.9($-2.8 + 3.9$)	2SXPS J065512.4-012855		X-RAY BINARY? ^{c)}
N276	J065548.7+395957	103.9528	39.9992	6.1	8.4($-3.4 + 4.6$)	SWIFT J0655.8+3957	0.0172	SEYFERT
N277	J065643.0-670222	104.1791	-67.0393	4.9	1.2($-0.6 + 0.7$)			UNIDENT
N278	J065806.5-174433	104.5269	-17.7425	8.1	16.9($-4.1 + 5.0$)	1RXS J065806.3-174427		CV
N279	J065826.9-555821	104.6120	-55.9725	4.9	4.4($-1.4 + 1.6$)	Bullet Cluster	0.2960	CLUSTER
N280	J070511.8-670515	106.2992	-67.0876	4.9	1.2($-0.6 + 0.7$)			UNIDENT
N281	J070636.4+635109	106.6516	63.8525	5.1	5.4($-2.6 + 3.6$)		0.0143	SEYFERT ^{c)}
N282	J070649.8+032442	106.7074	3.4117	5.3	7.8($-3.5 + 4.7$)	PBC J0706.7+0327		CV
N283	J070658.6-590949	106.7442	-59.1635	5.0	1.3($-0.9 + 1.1$)			UNIDENT
N284	J070712.3+643552	106.8012	64.5978	4.9	4.7($-2.5 + 3.5$)	VII Zw 118	0.0795	SEYFERT
N285	J070842.6-464244	107.1773	-46.7122	6.6	5.4($-1.9 + 2.3$)	SWIFT J0709.0-4642	0.0469	SEYFERT
N286	J070912.9-360115	107.3039	-36.0210	6.1	6.2($-2.3 + 3.0$)	PKS 0707-35	0.1100	SEYFERT
N287	J071739.0-710349	109.4126	-71.0637	7.9	4.0($-0.7 + 0.8$)	2E 0718.2-7057		AGN? ^{c)}
N288	J071802.0+440540	109.5082	44.0944	6.4	10.9($-3.8 + 4.9$)	RX J0718.0+4405	0.0634	SEYFERT
N289	J072041.5-552614	110.1728	-55.4371	5.4	4.6($-1.5 + 1.8$)	XMMSSL2 J072041.2-552616		AGN ^{c)}
N290	J072820.5-490846	112.0854	-49.1462	5.3	2.2($-1.4 + 1.8$)	1RXS J072823.4-490830		STAR
N291	J072823.5-440823	112.0979	-44.1397	4.9	4.6($-1.9 + 2.5$)	1RXS J072822.3-440819	0.0817	AGN ^{c)}
N292	J072854.3-260638	112.2263	-26.1106	9.5	22.6($-4.4 + 5.2$)	3A 0726-260		HMXB
N293	J073128.9+095619	112.8704	9.9387	5.8	10.6($-3.9 + 5.2$)	BG CMi		CV
N294	J073237.7-133104	113.1572	-13.5178	7.8	15.0($-4.0 + 5.0$)	SWIFT J0732.5-1331		CV
N295	J074233.4+494852	115.6393	49.8146	6.5	10.8($-3.6 + 4.6$)	Mrk 79	0.0223	SEYFERT

Table A.1. Continued.

Id	Name SRGA	RA	Dec	S/N	Flux	Common name	Redshift	Class
		(J2000)	(J2000)		(10^{-12} erg s $^{-1}$ cm $^{-2}$)			
N296	J074458.8-525715	116.2451	-52.9542	6.0	4.7(-1.6 + 1.9)	V436 Car		CV
N297	J074732.4-191823 ^{b)}	116.8848	-19.3065		~40	4U 0739-19	0.1028	CLUSTER
N298	J074905.5-233351	117.2729	-23.5641	5.2	5.2(-2.6 + 3.5)	BV Pup		CV
N299	J075117.9+144431	117.8246	14.7418	7.5	17.1(-4.8 + 6.0)	PQ Gem		CV
N300	J075152.6+494833	117.9691	49.8091	5.6	9.8(-3.4 + 4.4)	MCG +08-15-009	0.0244	SEYFERT
N301	J075504.1+220005	118.7672	22.0013	6.2	11.8(-4.1 + 5.3)	U Gem		CV
N302	J075941.7-384405	119.9237	-38.7347	8.9	13.4(-3.0 + 3.6)	IGR J07597-3842	0.0400	SEYFERT
N303	J080159.8-494639	120.4993	-49.7774	7.5	6.2(-1.9 + 2.3)	ESO 209-G012	0.0403	SEYFERT
N304	J080407.5+050656	121.0312	5.1156	6.8	14.1(-4.2 + 5.3)	Mrk 1210	0.0130	SEYFERT
N305	J080456.5-565451	121.2356	-56.9141	4.9	2.1(-1.1 + 1.4)			UNIDENT
N306	J080525.5+753432	121.3563	75.5757	7.4	16.7(-3.6 + 4.3)	RBS 690	0.1210	BLAZAR
N307	J080735.3+023517	121.8971	2.5881	5.0	6.3(-3.0 + 4.2)			CV? ^{c)}
N308	J081006.7-193903	122.5278	-19.6508	5.0	5.6(-2.8 + 3.7)			UNIDENT
N309	J081726.1-073113 ^{b)}	124.3588	-7.5202		~20	Abell 644	0.0704	CLUSTER
N310	J081820.1-142544	124.5837	-14.4290	5.6	9.4(-3.3 + 4.3)	1RXS J081820.4-142555	0.1070	SEYFERT
N311	J081857.0-225256	124.7377	-22.8823	4.9	5.0(-2.5 + 3.3)	RX J0818.9-2252	0.0350	SEYFERT
N312	J082625.5-703138	126.6062	-70.5273	7.2	4.3(-1.0 + 1.1)	1ES 0826-703		CV ^{c)}
N313	J082628.9-640406	126.6204	-64.0684	6.4	3.9(-1.2 + 1.4)	1RXS J082627.1-640421		BLAZAR
N314	J083521.2-451031	128.8382	-45.1752	12.1	36.0(-4.4 + 4.9)	Vela Pulsar		SNR / PULSAR
N315	J083821.9+483816	129.5913	48.6379	6.4	11.2(-3.7 + 4.7)	EI UMa		CV
N316	J083831.0-355929	129.6293	-35.9915	6.9	9.2(-2.8 + 3.4)	Fairall 1146	0.0318	SEYFERT
N317	J083848.7-483115	129.7028	-48.5210	4.9	5.8(-2.1 + 2.7)	IGR J08390-4833		CV
N318	J083950.2-121437	129.9593	-12.2437	6.2	12.5(-3.8 + 4.7)	3C 206	0.1978	SEYFERT
N319	J084123.8+705333	130.3493	70.8926	7.2	11.8(-3.3 + 4.0)	4C +71.07	2.1720	BLAZAR
N320	J084434.0-375747	131.1417	-37.9631	9.5	15.6(-3.4 + 4.1)	1RXS J084433.5-375738		STAR? ^{c)}
N321	J084518.8+142052	131.3283	14.3477	5.5	8.0(-3.3 + 4.5)	PBC J0845.3+1421	0.0606	SEYFERT
N322	J085040.6-421156	132.6693	-42.1988	5.7	8.8(-2.6 + 3.2)	SWIFT J0850.8-4219		X-RAY BINARY? ^{c)}
N323	J085740.9-554227	134.4202	-55.7075	5.2	4.1(-1.6 + 2.0)	2RXS J085738.9-554156		UNIDENT
N324	J090207.2-403313	135.5299	-40.5535	81.9	1518.4(-30.8 + 31.4)	Vela X-1		HMXB
N325	J090236.0-481325	135.6502	-48.2237	7.7	6.7(-2.5 + 3.1)	IGR J09026-4812	0.0390	SEYFERT
N326	J090632.4+401501	136.6349	40.2503	5.2	4.2(-2.8 + 4.0)			UNIDENT
N327	J090705.1+470919	136.7713	47.1553	6.8	8.0(-3.3 + 4.4)	RBS 741		STAR
N328	J090914.8-094035 ^{b)}	137.3118	-9.6763		~60	Abell 754	0.0535	CLUSTER
N329	J091203.4-645200	138.0141	-64.8664	30.1	81.6(-4.4 + 4.6)	MAXI J0911-655		LMXB
N330	J091324.3-573638	138.3513	-57.6107	5.0	0.9(-0.9 + 1.7)			UNIDENT
N331	J091511.9-752345	138.7997	-75.3957	4.9	1.9(-0.8 + 1.0)	RX J0915.3-7523		AGN ^{c)}
N332	J091609.8-621920	139.0409	-62.3224	10.7	14.4(-2.2 + 2.4)	IRAS 09149-6206	0.0571	SEYFERT
N333	J092021.6+860249	140.0898	86.0469	5.0	5.1(-2.0 + 2.5)	1RXS J092015.3+860254		AGN ^{c)}
N334	J092027.9-551213	140.1163	-55.2035	27.7	72.3(-4.3 + 4.5)	4U 0919-54		LMXB
N335	J092046.3-080322	140.1930	-8.0561	7.8	16.6(-4.2 + 5.2)	MCG -01-24-012	0.0198	SEYFERT
N336	J092234.6-631738	140.6442	-63.2938	18.0	29.3(-2.9 + 3.1)	2S 0921-630		LMXB
N337	J092343.5+225439	140.9313	22.9109	7.1	13.8(-4.1 + 5.2)	MCG +04-22-04	0.0332	SEYFERT
N338	J092418.4-314218	141.0766	-31.7049	19.4	82.0(-8.0 + 8.8)	NuSTAR J092418-3142.2		LMXB? ^{c)}

Table A.1. Continued.

Id	Name	RA SRGA	Dec (J2000)	S/N	Flux (10^{-12} erg s $^{-1}$ cm $^{-2}$)	Common name	Redshift	Class
N339	J092514.1+521654	141.3088	52.2817	7.2	12.9($-3.8 + 4.8$)	Mrk 110	0.0355	SEYFERT
N340	J092547.2+692747	141.4465	69.4631	5.8	6.7($-2.6 + 3.4$)	IGR J09253+6929	0.0398	SEYFERT
N341	J092615.3-842119	141.5638	-84.3552	5.9	4.9($-1.4 + 1.6$)	IRAS 09305-8408	0.0629	SEYFERT
N342	J092752.9-694439	141.9705	-69.7442	5.9	5.3($-1.2 + 1.4$)	PBC J0927.8-6945		CV
N343	J093451.4+312206	143.7143	31.3684	5.0	4.2($-2.6 + 3.7$)			UNIDENT
N344	J094542.2-141940	146.4258	-14.3278	7.8	17.2($-4.3 + 5.3$)	NGC 2992	0.0073	SEYFERT
N345	J094718.3-380408	146.8262	-38.0689	5.1	4.6($-2.5 + 3.5$)			UNIDENT
N346	J094740.3-305655	146.9181	-30.9486	16.4	50.8($-5.6 + 6.2$)	ESO 434-G040	0.0082	SEYFERT
N347	J095155.3-064911	147.9803	-6.8197	5.7	6.4($-3.0 + 4.1$)	NGC 3035	0.0146	SEYFERT
N348	J095243.1-200912	148.1795	-20.1532	4.9	6.6($-3.0 + 4.1$)			UNIDENT
N349	J095551.0+694055	148.9625	69.6819	7.3	9.8($-2.9 + 3.7$)	M82 X-1		ULX
N350	J095838.2-411040	149.6592	-41.1779	5.0	4.7($-2.2 + 2.9$)	ICRF J095838.2-411033	2.9340	BLAZAR
N351	J095929.6-224926	149.8735	-22.8239	7.3	10.6($-3.0 + 3.7$)	NGC 3081	0.0080	SEYFERT
N352	J100229.7-020820	150.6239	-2.1388	5.6	4.2($-2.6 + 3.7$)			UNIDENT
N353	J100617.1-701349	151.5711	-70.2302	5.1	1.8($-1.0 + 1.2$)	OY Car		CV
N354	J100947.3-581735	152.4471	-58.2930	22.7	32.2($-2.5 + 2.7$)	GRO J1008-57		HMXB
N355	J101012.0-565517	152.5501	-56.9214	8.2	8.2($-2.0 + 2.4$)	IGR J10100-5655		HMXB
N356	J101103.1-574802	152.7628	-57.8006	8.3	8.4($-2.0 + 2.3$)	IGR J10109-5746		CV
N357	J101116.2+321713	152.8176	32.2868	4.8	9.3($-3.4 + 4.4$)			UNIDENT
N358	J101132.4-442258	152.8849	-44.3828	4.9	3.8($-1.6 + 2.0$)	1RXS J101130.7-442241		UNIDENT
N359	J101223.8-194516	153.0991	-19.7543	4.9	3.1($-2.2 + 3.1$)			UNIDENT
N360	J102330.5+195149	155.8771	19.8637	9.6	23.7($-5.1 + 6.2$)	NGC 3227	0.0037	SEYFERT
N361	J102347.6+003835	155.9482	0.6429	7.5	14.4($-4.2 + 5.3$)	PSR J1023+0038		LMXB
N362	J103152.1-345116	157.9670	-34.8544	5.0	8.1($-2.7 + 3.4$)	NGC 3281	0.0107	SEYFERT
N363	J103447.6-432155	158.6983	-43.3652	5.2	0.9($-0.9 + 2.0$)			UNIDENT
N364	J103735.5-564747	159.3981	-56.7963	14.5	31.3($-3.6 + 3.9$)	4U 1036-56		HMXB
N365	J103843.9-494659	159.6828	-49.7829	6.2	6.1($-2.0 + 2.5$)	SWIFT J1038.8-4942	0.0600	SEYFERT
N366	J104450.9-602446	161.2122	-60.4128	5.4	5.2($-1.5 + 1.8$)	IGR J10447-6027		AGN? ^{c)}
N367	J104503.3-594104	161.2638	-59.6846	31.9	111.6($-5.7 + 5.9$)	eta Car		STAR
N368	J104802.0+245619	162.0083	24.9387	4.9	7.6($-3.2 + 4.4$)			UNIDENT
N369	J104833.4-390227	162.1390	-39.0408	5.6	1.0($-1.0 + 2.2$)	SWIFT J1048.6-3901	0.0446	SEYFERT ^{c)}
N370	J105501.7-145127	163.7569	-14.8576	4.9	5.4($-2.7 + 3.7$)			UNIDENT
N371	J105946.7+650408	164.9444	65.0688	6.3	8.6($-2.8 + 3.6$)	PBC J1059.9+6505	0.0836	SEYFERT
N372	J110019.9-073854	165.0831	-7.6482	5.4	8.4($-3.2 + 4.3$)	RX J1100.3-0738	0.0655	SEYFERT
N373	J110337.9-232936	165.9080	-23.4934	6.0	10.9($-3.1 + 3.8$)	2A 1058-226	0.1860	BLAZAR
N374	J110350.0-203446	165.9582	-20.5795	5.0	4.7($-2.5 + 3.3$)			UNIDENT
N375	J110427.9+381234	166.1161	38.2095	24.9	155.5($-11.8 + 12.7$)	Mrk 421	0.0310	BLAZAR
N376	J110647.4+723410	166.6974	72.5694	9.8	16.0($-3.4 + 4.0$)	NGC 3516	0.0088	SEYFERT
N377	J111153.2-611826	167.9718	-61.3072	5.7	2.3($-1.2 + 1.5$)	NGC 3576		SFR ^{c)}
N378	J111157.9-611432	168.7411	-61.2422	5.4	4.0($-1.4 + 1.7$)	NGC 3603		SFR ^{c)}
N379	J111182.7-543730	169.5905	-54.6250	5.1	4.0($-1.5 + 1.9$)	IGR J11187-5438		LMXB? ^{c)}
N380	J112048.4-431531	170.2016	-43.2587	6.5	6.6($-2.4 + 3.0$)	ESO 265-G023	0.0566	SEYFERT
N381	J112115.0-603722	170.3124	-60.6227	179.3	1319.3($-12.4 + 12.5$)	Cen X-3		HMXB

Table A.1. Continued.

Id	Name SRGA	RA	Dec	S/N	Flux	Common name	Redshift	Class
		(J2000)	(J2000)		(10^{-12} erg s $^{-1}$ cm $^{-2}$)			
N382	J112120.9–742648	170.3372	-74.4467	5.5	2.2(-1.1 + 1.4)			UNIDENT
N383	J112437.6–591620	171.1568	-59.2723	7.1	4.4(-1.5 + 1.8)	PSR J1124-5916		SNR / PULSAR
N384	J113034.0–780048	172.6417	-78.0133	6.9	5.1(-1.5 + 1.8)	RX J1130.5-7800		BLAZAR
N385	J113154.2–343639	172.9757	-34.6109	5.5	5.0(-2.3 + 2.9)	1RXS J113155.7-343632		STAR
N386	J113257.7+634402	173.2404	63.7339	5.0	5.5(-2.3 + 2.9)			UNIDENT
N387	J113631.2+673702	174.1299	67.6173	6.5	9.0(-2.6 + 3.2)	RBS 1004	0.1342	BLAZAR
N388	J113851.7–232118	174.7153	-23.3551	5.0	6.0(-2.6 + 3.5)	HE 1136-2304	0.0270	SEYFERT
N389	J113901.9–374410	174.7581	-37.7360	13.5	35.7(-5.1 + 5.8)	NGC 3783	0.0098	SEYFERT
N390	J113910.4+591216	174.7934	59.2044	4.8	4.3(-2.2 + 2.9)	SBS 1136+594	0.0610	SEYFERT
N391	J113930.3–652350	174.8764	-65.3973	7.1	6.5(-1.6 + 1.9)	GT Mus		STAR
N392	J114122.9–641025	175.3452	-64.1735	13.0	16.2(-2.3 + 2.6)	V1033 Cen		CV
N393	J114339.0+714123	175.9127	71.6896	12.6	26.9(-4.1 + 4.7)	DO Dra		CV
N394	J114347.8–690528 ^{b)}	175.9490	-69.0911		~60	PSZ2 G296.91-07.00	0.3100	CLUSTER
N395	J114359.4–610730	175.9973	-61.1251	10.8	15.8(-2.4 + 2.7)	IGR J11435-6109		HMXB
N396	J114430.2+365308	176.1259	36.8857	5.6	4.4(-1.9 + 2.5)	KUG 1141+371	0.0382	SEYFERT
N397	J114446.2+053312	176.1927	5.5533	4.9	4.3(-2.5 + 3.4)			UNIDENT
N398	J114515.8+794052	176.3158	79.6810	5.1	6.6(-2.2 + 2.7)	1ES 1141+79.9	0.0673	SEYFERT
N399	J114541.3–182709	176.4222	-18.4524	7.0	11.3(-3.3 + 4.1)	H 1143-182	0.0328	SEYFERT
N400	J114552.1–695358	176.4673	-69.8995	5.0	4.0(-1.4 + 1.7)	PKS 1143-696	0.2434	BLAZAR
N401	J114721.9–495309	176.8413	-49.8858	10.1	14.8(-2.6 + 3.0)	XMMSL2 J114724.7-495303		UNIDENT ^{c)}
N402	J114728.3–615715	176.8679	-61.9541	34.3	131.8(-6.2 + 6.5)	1E 1145.1-6141		HMXB
N403	J114759.5–621229	176.9979	-62.2081	8.3	6.8(-1.8 + 2.1)	4U 1145-619		HMXB
N404	J115224.4–673841	178.1018	-67.6448	6.1	4.3(-1.4 + 1.6)	1RXS J115222.9-673815		UNIDENT
N405	J115526.2–564144	178.8592	-56.6956	11.0	13.5(-2.3 + 2.7)	V1040 Cen		CV
N406	J115755.3+552721	179.4802	55.4557	5.1	6.3(-2.5 + 3.2)	NGC 3998	0.0036	SEYFERT
N407	J115949.1+464206	179.9545	46.7017	4.9	3.2(-2.2 + 3.1)			UNIDENT
N408	J120232.4–194814	180.6350	-19.8040	4.9	7.0(-2.6 + 3.3)			UNIDENT
N409	J120247.4–535003	180.6976	-53.8340	10.4	13.5(-2.4 + 2.8)	IGR J12026-5349	0.0284	SEYFERT
N410	J120310.6+443139	180.7941	44.5275	6.4	9.4(-3.1 + 3.9)	NGC 4051	0.0022	SEYFERT
N411	J120413.4–294646	181.0558	-29.7794	5.7	3.2(-2.0 + 2.7)			AGN ^{c)}
N412	J121033.1+392421	182.6380	39.4059	17.8	98.9(-10.2 + 11.2)	NGC 4151	0.0033	SEYFERT
N413	J121225.1–580028	183.1044	-58.0078	6.5	4.3(-1.6 + 1.9)	IGR J12123-5802		CV
N414	J121314.9–645231	183.3120	-64.8754	35.2	137.9(-6.3 + 6.6)	4U 1210-64		HMXB
N415	J121323.9–261756	183.3496	-26.2990	4.9	2.8(-2.0 + 2.7)	RBS 1080	0.2780	BLAZAR
N416	J121356.7+440847	183.4862	44.1464	4.9	6.5(-2.4 + 3.1)			UNIDENT
N417	J121710.5+071120	184.2938	7.1890	6.5	11.7(-3.5 + 4.4)	NGC 4235	0.0074	SEYFERT
N418	J122143.8+751830	185.4324	75.3084	6.6	7.7(-2.3 + 2.8)	Mrk 205	0.0708	SEYFERT
N419	J122547.1+123938	186.4462	12.6605	12.1	38.8(-5.9 + 6.8)	NGC 4388	0.0086	SEYFERT
N420	J122617.6+190920	186.5735	19.1556	4.9	3.7(-1.9 + 2.4)		0.1213	SEYFERT
N421	J122637.1–624613	186.6545	-62.7702	93.1	922.9(-16.5 + 16.8)	GX 301-2		HMXB
N422	J122643.2+104935	186.6798	10.8265	5.1	3.2(-2.6 + 3.8)			UNIDENT
N423	J122708.5+263416	186.7853	26.5710	4.9	5.9(-2.6 + 3.5)			UNIDENT
N424	J122906.1+020316	187.2756	2.0545	14.1	49.7(-6.4 + 7.2)	3C 273	0.1583	BLAZAR

Article number, page 30 of 40
Table A.1. Continued.

Id	Name	RA	Dec	S/N	Flux (10^{-12} erg s $^{-1}$ cm $^{-2}$)	Common name	Redshift	Class
	SRGA	(J2000)	(J2000)					
N425	J123002.8+691205	187.5116	69.2013	4.8	3.2($-1.8 + 2.3$)	4 Dra		CV
N426	J123047.8+122307 ^{b)}	187.6991	12.3852		~ 50	Virgo Cluster	0.0038	CLUSTER
N427	J123136.9-475757	187.9038	-47.9658	5.2	2.2($-1.5 + 2.0$)	1RXS J123137.4-475800	0.0279	SEYFERT
N428	J123536.8-395438	188.9031	-39.9104	9.6	16.0($-2.9 + 3.3$)	NGC 4507	0.0119	SEYFERT
N429	J123629.1-664554	189.1214	-66.7651	6.1	5.6($-1.6 + 1.9$)	XMMSL2 J123629.8-664549		UNIDENT ^{c)}
N430	J123815.9-384254	189.5661	-38.7150	5.1	4.0($-1.8 + 2.3$)	V1025 Cen		CV
N431	J123821.8-253205	189.5910	-25.5346	11.6	20.4($-3.8 + 4.5$)			UNIDENT ^{c)}
N432	J123855.1-271830	189.7297	-27.3082	6.2	8.8($-2.8 + 3.5$)	ESO 506-G027	0.0252	SEYFERT
N433	J124124.4-574953	190.3518	-57.8314	10.1	10.9($-2.2 + 2.5$)	IGR J12415-5750	0.0242	SEYFERT
N434	J124249.6-630348	190.7066	-63.0632	5.4	4.3($-1.6 + 2.0$)	1H 1249-637		STAR? ^{c)}
N435	J124640.6+543222	191.6690	54.5394	5.5	5.2($-2.3 + 3.0$)	NGC 4686	0.0167	SEYFERT ^{c)}
N436	J124849.2-411817 ^{b)}	192.2051	-41.3047		~ 60	Centaurus Cluster	0.0110	CLUSTER
N437	J124939.4-590514	192.4140	-59.0871	16.5	29.2($-3.2 + 3.6$)	4U 1246-58		LMXB
N438	J125224.3-291456	193.1011	-29.2488	16.5	47.0($-5.0 + 5.5$)	EX Hya		CV
N439	J125342.1-393157	193.4256	-39.5324	7.1	6.7($-2.1 + 2.6$)	1RXS J125341.2-393200	0.1785	BLAZAR
N440	J125611.4-054714	194.0474	-5.7872	7.0	9.4($-2.9 + 3.7$)	3C 279	0.5362	BLAZAR
N441	J125737.0-691719	194.4044	-69.2886	49.5	318.4($-10.5 + 10.9$)	4U 1254-69		LMXB
N442	J125927.3-041049 ^{b)}	194.8636	-4.1804		~ 10	Abell 1651	0.0838	CLUSTER
N443	J130115.7-613620	195.3154	-61.6054	6.6	5.8($-1.8 + 2.2$)	GX 304-1		HMXB
N444	J130353.6+453542	195.9735	45.5951	5.0	1.7($-1.7 + 2.5$)			UNIDENT
N445	J130526.0-492816	196.3582	-49.4712	4.8	8.9($-2.1 + 2.6$)	NGC 4945	0.0018	SEYFERT
N446	J130755.5+535120	196.9812	53.8555	4.9	7.1($-2.8 + 3.7$)	EV UMa		CV
N447	J131045.7-555220	197.6904	-55.8722	5.2	3.3($-1.5 + 1.9$)	IGR J13109-5552	0.1040	SEYFERT
N448	J131239.5-624256	198.1647	-62.7155	6.1	4.1($-1.4 + 1.6$)	WR 48a		STAR ^{c)}
N449	J131503.1-423653	198.7628	-42.6148	5.0	4.1($-1.8 + 2.3$)	1E 1312-4221	0.1050	BLAZAR
N450	J131654.1-715521	199.2254	-71.9225	4.9	5.4($-1.8 + 2.2$)	IGR J13168-7157	0.0700	SEYFERT
N451	J132032.4-701437	200.1352	-70.2437	6.4	5.7($-1.8 + 2.2$)	1RXS J132032.3-701451		X-RAY BINARY ^{c)}
N452	J132425.6-620133	201.1066	-62.0259	4.9	3.3($-1.6 + 2.0$)	SAX J1324.4-6200		HMXB
N453	J132436.0-573255 ^{b)}	201.1502	-57.5487		~ 10	RXC J1324.7-5736	0.0190	CLUSTER
N454	J132527.9-430111	201.3663	-43.0197	33.3	180.5($-8.8 + 9.2$)	Cen A	0.0018	SEYFERT
N455	J132636.9-620809	201.6539	-62.1358	25.1	64.9($-4.3 + 4.5$)	4U 1323-62		LMXB
N456	J132803.3-313135 ^{b)}	202.0135	-31.5265		~ 50	Abell 3558	0.0469	CLUSTER
N457	J132858.1-363909	202.2423	-36.6525	4.9	2.8($-1.7 + 2.2$)			UNIDENT
N458	J133113.9-252402	202.8078	-25.4005	7.6	8.8($-2.4 + 2.9$)	ESO 509-G038	0.0261	SEYFERT
N459	J133118.4-545830	202.8266	-54.9750	7.6	10.8($-2.4 + 2.8$)	BV Cen		CV
N460	J133226.7+513522	203.1112	51.5894	5.0	1.4($-1.4 + 2.3$)			UNIDENT
N461	J133428.4-362533	203.6183	-36.4257	4.8	2.5($-1.6 + 2.1$)			UNIDENT
N462	J133554.1-341745	203.9754	-34.2958	13.4	25.6($-3.7 + 4.1$)	ESO 383-G035	0.0076	SEYFERT
N463	J133815.8+043232	204.5658	4.5423	10.5	21.6($-4.1 + 4.8$)	NGC 5252	0.0229	SEYFERT
N464	J133936.9-174148	204.9036	-17.6968	4.9	3.0($-1.8 + 2.4$)			UNIDENT
N465	J133949.9-643019	204.9580	-64.5052	5.3	3.5($-1.5 + 1.9$)			UNIDENT ^{c)}
N466	J134448.4-360429	206.2018	-36.0746	4.8	0.3($-0.3 + 1.8$)	ESO 383-G069	0.0374	SEYFERT

Table A.1. Continued.

Id	Name SRGA	RA (J2000)	Dec (J2000)	S/N	Flux (10^{-12} erg s $^{-1}$ cm $^{-2}$)	Common name	Redshift	Class
N467	J134649.2-602422	206.7048	-60.4061	6.5	7.7(-2.2 + 2.7)	Cen B	0.0121	SEYFERT
N468	J134732.4-325012 ^{b)}	206.8848	-32.8367		~100	Abell 3571	0.0397	CLUSTER
N469	J134736.5-603700	206.9019	-60.6164	13.9	26.0(-3.6 + 4.0)	4U 1344-60	0.0130	SEYFERT
N470	J134847.4+263455 ^{b)}	207.1974	26.5820		~50	Abell 1795	0.0630	CLUSTER
N471	J134919.3-301830	207.3303	-30.3082	23.4	79.3(-6.2 + 6.7)	IC 4329A	0.0161	SEYFERT
N472	J134953.3+020445	207.4723	2.0792	6.2	8.3(-2.4 + 3.0)	UM 614	0.0329	SEYFERT
N473	J135305.9+691822	208.2745	69.3062	7.8	9.1(-2.2 + 2.6)	Mrk 279	0.0305	SEYFERT
N474	J140044.8-632540	210.1866	-63.4277	7.6	6.9(-2.1 + 2.6)	IGR J14003-6326		SNR / PULSAR
N475	J140103.4+025221	210.2643	2.8725	5.6	5.5(-2.1 + 2.7)	Abell 1835	0.2506	CLUSTER
N476	J140146.9-501333	210.4456	-50.2259	6.0	4.2(-1.6 + 2.0)			UNIDENT
N477	J140429.6-614707	211.1233	-61.7854	5.0	5.7(-2.0 + 2.5)	IGR J14043-6148		UNIDENT
N478	J140504.4-534139	211.2683	-53.6942	4.9	3.9(-1.4 + 1.8)			UNIDENT
N479	J140654.9-052749	211.7288	-5.4635	5.1	3.8(-1.8 + 2.4)	2SXPS J140655.3-052735	0.0095	AGN ^{c)}
N480	J140740.6+222836	211.9192	22.4767	4.9	5.1(-2.1 + 2.8)			UNIDENT
N481	J140908.0-451716	212.2833	-45.2877	9.4	10.9(-2.6 + 3.1)	V834 Cen		CV
N482	J141245.9-442932	213.1913	-44.4924	4.9	3.3(-1.7 + 2.3)			UNIDENT
N483	J141249.5-402141	213.2064	-40.3613	7.0	7.3(-2.3 + 2.8)	V504 Cen		CV ^{c)}
N484	J141309.0-652021	213.2877	-65.3391	10.5	17.0(-3.0 + 3.4)	Circinus Galaxy	0.0014	SEYFERT
N485	J141315.2-031226	213.3133	-3.2073	18.7	50.6(-5.2 + 5.7)	NGC 5506	0.0059	SEYFERT
N486	J141650.0-115857	214.2083	-11.9826	5.1	6.7(-2.2 + 2.7)	1RXS J141650.6-1158	0.0990	SEYFERT
N487	J141759.0+250808	214.4958	25.1356	10.9	20.3(-3.2 + 3.6)	NGC 5548	0.0163	SEYFERT
N488	J141904.9-131034	214.7704	-13.1761	5.0	4.1(-1.9 + 2.4)	PG 1416-129	0.1293	SEYFERT
N489	J141909.8+075500	214.7908	7.9168	5.2	5.3(-2.0 + 2.5)	SWIFT J1419.1+0790	0.0560	SEYFERT
N490	J142112.7-624202	215.3031	-62.7005	16.9	40.8(-4.5 + 5.0)	4U 1416-62		HMXB
N491	J142131.0+474724	215.3791	47.7899	5.2	4.1(-1.8 + 2.3)	2A 1418+485	0.0730	SEYFERT
N492	J142148.2-630135	215.4510	-63.0264	5.0	2.6(-1.7 + 2.2)	2E 1418.0-6247		UNIDENT
N493	J142422.5+243653	216.0936	24.6147	4.9	4.2(-1.8 + 2.2)	SWIFT J1424.3+2435	0.0169	SEYFERT
N494	J142557.4+374954	216.4892	37.8316	5.1	9.6(-2.4 + 2.9)	Abell 1914	0.1660	CLUSTER
N495	J142721.7-681513	216.8403	-68.2537	5.1	1.7(-1.4 + 1.9)			UNIDENT
N496	J142748.7-203659	216.9531	-20.6163	4.8	2.4(-1.6 + 2.2)			UNIDENT
N497	J142833.1+424011	217.1378	42.6698	10.0	10.1(-2.5 + 3.0)	4U 1444+43	0.1292	BLAZAR
N498	J142906.2+011710	217.2759	1.2862	7.2	8.7(-2.4 + 2.9)	Mrk 1383	0.0860	SEYFERT
N499	J142958.9-671438	217.4954	-67.2439	8.2	6.8(-2.1 + 2.5)	IGR J14298-6715		LMXB
N500	J143307.5-611544	218.2812	-61.2621	5.9	5.3(-2.0 + 2.6)	IGR J14331-6112		HMXB
N501	J143649.4-161341	219.2059	-16.2281	5.8	2.6(-1.7 + 2.3)	HE 1434-1600	0.1445	SEYFERT
N502	J143739.7-361324	219.4156	-36.2233	8.3	8.3(-2.1 + 2.6)	XMMSL2 J143739.7-361331		STAR
N503	J144037.4-384649	220.1559	-38.7803	8.7	9.0(-2.1 + 2.5)	1RXS J144037.4-384658		BLAZAR
N504	J144223.1-171505	220.5961	-17.2514	4.9	3.4(-1.7 + 2.2)	NGC 5728	0.0095	SEYFERT
N505	J144248.5+120053	220.7022	12.0147	7.4	12.2(-2.6 + 3.1)	1ES 1440+122	0.1631	BLAZAR
N506	J144712.9-631719	221.8036	-63.2887	4.9	4.4(-1.9 + 2.4)	IGR J14471-6319	0.0380	SEYFERT
N507	J144851.0-400843	222.2126	-40.1451	5.9	6.2(-2.2 + 2.7)	IGR J14488-4008	0.1230	SEYFERT
N508	J145742.4-430811	224.4266	-43.1364	5.5	4.7(-2.2 + 2.8)	IGR J14579-4308	0.0166	SEYFERT
N509	J145804.3-390945	224.5178	-39.1626	5.1	3.5(-1.6 + 2.0)	ESO 327-G035	0.0381	SEYFERT

Table A.1. Continued.

Id	Name SRGA	RA (J2000)	Dec (J2000)	S/N	Flux (10^{-12} erg s $^{-1}$ cm $^{-2}$)	Common name	Redshift	Class
N510	J150340.6-154116	225.9192	-15.6879	12.3	19.0(-2.9 + 3.3)	EGR J1504-1539		BLAZAR
N511	J150341.0+271027	225.9209	27.1741	4.9	1.9(-1.4 + 1.8)			UNIDENT
N512	J150401.7+102619	226.0070	10.4385	8.2	11.8(-2.6 + 3.0)	Mrk 841	0.0364	SEYFERT
N513	J150407.4-024811	226.0307	-2.8030	5.7	9.9(-2.6 + 3.1)	RBS 1460	0.2153	CLUSTER
N514	J150926.2-664924	227.3590	-66.8233	9.2	11.4(-2.5 + 3.0)	IGR J15094-6649		CV
N515	J151003.9+333057 ^{b)}	227.5163	33.5158		~50	Abell 2034	0.1132	CLUSTER
N516	J151054.2+054422	227.7257	5.7396	6.3	20.3(-3.3 + 3.8)	Abell 2029	0.0773	CLUSTER
N517	J151250.8-090611	228.2116	-9.1030	5.9	5.1(-1.8 + 2.2)	PKS 1510-08	0.3600	BLAZAR
N518	J151347.6-590754 ^{b)}	228.4482	-59.1318		~60	PSR B1509-58		SNR / PULSAR
N519	J151433.2-455920 ^{b)}	228.6383	-45.9889		~30	RXC J1514.6-4558	0.0580	CLUSTER
N520	J151442.7-812321	228.6780	-81.3891	5.9	3.9(-1.6 + 1.9)	SWIFT J1513.8-8125	0.0690	SEYFERT
N521	J151747.5+652529	229.4479	65.4249	5.0	4.9(-1.7 + 2.0)	H 1517+656	0.7020	BLAZAR
N522	J152040.8-571002	230.1702	-57.1673	140.6	3373.0(-40.2 + 40.7)	Cir X-1		HMXB
N523	J152100.6+320405	230.2526	32.0681	5.2	5.5(-1.7 + 2.0)	2SXPS J152101.8+320415	0.1143	SEYFERT ^{c)}
N524	J152148.8+074341 ^{b)}	230.4532	7.7280		~10	MKW 3s	0.0450	CLUSTER
N525	J152222.6+274420 ^{b)}	230.5944	27.7389		~10	Abell 2065	0.0731	CLUSTER
N526	J152345.6+633923	230.9401	63.6565	4.9	2.6(-1.2 + 1.5)	4C +63.22	0.2040	SEYFERT
N527	J153414.5+625852	233.5604	62.9810	6.0	3.5(-1.2 + 1.5)	1RXS J153412.6+625902	0.2600	SEYFERT ^{c)}
N528	J153550.9+575358	233.9620	57.8995	7.8	5.8(-1.4 + 1.6)	Mrk 290	0.0302	SEYFERT
N529	J153814.0-554219	234.5583	-55.7052	6.3	7.4(-2.3 + 2.9)	AX J1538.3-5541		LMXB ^{c)}
N530	J153937.0-833503	234.9040	-83.5841	5.4	4.5(-1.6 + 2.0)	RXC J1539.5-8335	0.0728	CLUSTER
N531	J154223.2-522307	235.5966	-52.3851	44.4	385.5(-14.2 + 14.7)	4U 1538-52		HMXB
N532	J154500.2-664200	236.2507	-66.7001	4.9	3.3(-1.7 + 2.2)	1RXS J154458.3-664153		BLAZAR
N533	J154753.6-623411	236.9734	-62.5696	23.5	87.1(-6.5 + 7.0)	4U 1543-624		LMXB
N534	J154805.3-473806	237.0220	-47.6349	4.9	3.4(-1.9 + 2.6)	1RXS J154807.4-473830	0.0206	AGN ^{c)}
N535	J154814.2-452847	237.0592	-45.4797	10.6	22.4(-3.7 + 4.3)	NY Lup		CV
N536	J154824.5-134519	237.1020	-13.7552	7.6	11.1(-3.1 + 3.8)	NGC 5995	0.0254	SEYFERT
N537	J154849.9-225050	237.2078	-22.8473	11.5	23.1(-4.1 + 4.8)	PMN J1548-2251	0.1920	BLAZAR
N538	J155247.0+185641	238.1957	18.9447	5.3	4.7(-1.7 + 2.0)	PG 1550+191		CV
N539	J155342.9+234827	238.4288	23.8075	5.8	5.5(-1.9 + 2.3)	4C +23.42	0.1176	SEYFERT
N540	J155519.3-353019	238.8306	-35.5052	4.9	4.6(-2.1 + 2.8)			UNIDENT
N541	J155543.6+111125	238.9315	11.1902	7.6	6.5(-1.9 + 2.3)	PG 1553+11	0.3600	BLAZAR
N542	J155700.0-791406	239.2499	-79.2349	4.9	2.8(-1.5 + 1.9)	PKS 1549-79	0.1500	BLAZAR
N543	J155826.5+271352 ^{b)}	239.6103	27.2311		~50	Abell 2142	0.0903	CLUSTER
N544	J155929.5+255512	239.8730	25.9201	5.9	3.0(-1.3 + 1.6)	T CrB		CV
N545	J160050.0-514249	240.2084	-51.7135	4.9	3.2(-1.9 + 2.5)	2XMM J160050.7-514245		STAR ^{c)}
N546	J160102.4-604419	240.2602	-60.7385	28.9	160.6(-8.9 + 9.4)	4U 1556-60		LMXB
N547	J160252.1-240200	240.7169	-24.0334	6.0	3.6(-2.0 + 2.6)	RX J1602.8-2401B		STAR
N548	J160456.1-722318	241.2338	-72.3884	5.4	4.4(-1.8 + 2.2)	1RXS J160454.5-722312		CV? ^{c)}
N549	J160545.7+255200	241.4404	25.8664	5.2	3.6(-1.6 + 2.1)	2E 1603.6+2600		LMXB
N550	J160613.9+101915	241.5580	10.3209	5.0	2.7(-1.9 + 2.5)			UNIDENT
N551	J160901.4-390519	242.2558	-39.0885	5.3	0.5(-0.5 + 2.2)	1RXS J160838.1-390526		STAR? ^{c)}

Table A.1. Continued.

Id	Name SRGA	RA (J2000)	Dec (J2000)	S/N	Flux	Common name	Redshift	Class
					(10^{-12} erg s $^{-1}$ cm $^{-2}$)			
N552	J161006.9+035233	242.5289	3.8758	6.9	9.5($-2.8 + 3.4$)	V519 Ser		CV
N553	J161017.3-634243	242.5722	-63.7118	5.6	8.7($-2.4 + 2.9$)	1RXS J161017.3-634234	0.2094	SEYFERT ^{c)}
N554	J161156.7-603826 ^{b)}	242.9862	-60.6404		~ 30	Abell 3627	0.0163	CLUSTER ^{c)}
N555	J161201.8-464616	243.0074	-46.7711	5.3	5.2($-2.2 + 2.8$)	1WGA J1612.0-4646		CV? ^{c)}
N556	J161243.0-522526	243.1790	-52.4238	40.0	332.3($-13.5 + 14.1$)	4U 1608-52		LMXB
N557	J161358.4+654314	243.4931	65.7205	8.2	5.5($-1.2 + 1.4$)	Mrk 876	0.1385	SEYFERT
N558	J161415.5-605124 ^{b)}	243.5645	-60.8566		~ 90	Abell 3627	0.0163	CLUSTER ^{c)}
N559	J161515.4-283729	243.8140	-28.6248	7.0	7.0($-2.5 + 3.2$)	V893 Sco		CV
N560	J161637.4-495849	244.1558	-49.9804	9.5	17.5($-3.4 + 4.1$)	IGR J16167-4957		CV
N561	J161741.9+322239	244.4244	32.3776	6.3	8.0($-2.0 + 2.4$)	3C 332	0.1510	SEYFERT
N562	J161932.0-494431	244.8835	-49.7419	14.8	40.0($-4.9 + 5.5$)	IGR J16195-4945		HMXB
N563	J161947.3+435834	244.9469	43.9762	4.9	1.0($-1.0 + 1.3$)			UNIDENT
N564	J161954.6-153821	244.9775	-15.6392	562.5	115240.9($-346.4 + 347.4$)	Sco X-1		LMXB
N565	J162046.4-513013	245.1935	-51.5037	11.2	22.2($-3.8 + 4.4$)	IGR J16207-5129		HMXB
N566	J162145.3+542718	245.4389	54.4551	9.1	5.0($-1.1 + 1.2$)	SBS 1620+545	0.0520	SEYFERT
N567	J162521.1+852947	246.3379	85.4964	5.9	4.8($-1.7 + 2.1$)	IRAS 16360+8536	0.0629	SEYFERT
N568	J162626.2-332941 ^{b)}	246.6092	-33.4948		~ 10	RXC J1626.3-3329	0.1098	CLUSTER
N569	J162718.7-244145	246.8280	-24.6957	7.3	8.9($-2.8 + 3.5$)	SR 12		STAR
N570	J162802.8-491156	247.0115	-49.1988	61.7	809.3($-21.7 + 22.3$)	4U 1624-49		LMXB
N571	J162803.5+514629	247.0147	51.7746	10.2	6.7($-1.2 + 1.4$)	Mrk 1498	0.0556	SEYFERT
N572	J162834.5+393226 ^{b)}	247.1439	39.5405		~ 60	Abell 2199	0.0309	CLUSTER
N573	J163147.1-484901	247.9461	-48.8168	7.2	9.2($-2.7 + 3.3$)	IGR J16318-4848		HMXB
N574	J163202.0-475231	248.0083	-47.8753	23.8	106.9($-8.0 + 8.6$)	IGR J16320-4751		HMXB
N575	J163217.0-672738	248.0708	-67.4605	34.7	214.7($-10.0 + 10.5$)	4U 1626-67		LMXB
N576	J163243.1-750756 ^{b)}	248.1796	-75.1321		~ 20	Abell 3628	0.1492	CLUSTER
N577	J163247.7+053419	248.1988	5.5718	5.3	11.4($-2.8 + 3.4$)	Abell 2204	0.1511	CLUSTER
N578	J163401.3-472339	248.5056	-47.3940	44.0	425.2($-15.8 + 16.4$)	4U 1630-47		LMXB
N579	J163529.2-480558	248.8715	-48.0995	7.6	10.1($-2.8 + 3.5$)	2E 1631.7-4759		X-RAY BINARY? ^{c)}
N580	J163813.2-642121 ^{b)}	249.5549	-64.3559		~ 100	Triangulum Australis Cluster	0.0510	CLUSTER
N581	J163827.5-441440	249.6146	-44.2445	5.0	2.4($-1.8 + 2.5$)			UNIDENT
N582	J163829.5-205530	249.6228	-20.9249	5.8	6.9($-2.6 + 3.3$)	IGR J16385-2057	0.0268	SEYFERT
N583	J163905.1-464208	249.7713	-46.7022	12.2	33.2($-4.7 + 5.3$)	AX J1639.0-4642		HMXB
N584	J164035.9+065533	250.1496	6.9259	5.0	4.2($-2.0 + 2.6$)			UNIDENT
N585	J164055.5-534508	250.2312	-53.7523	55.1	618.6($-18.5 + 19.0$)	4U 1636-536		LMXB
N586	J164151.5-453227	250.4644	-45.5407	13.8	34.9($-5.0 + 5.6$)	IGR J16418-4532		HMXB
N587	J164548.1-453643	251.4504	-45.6118	170.2	6197.0($-61.1 + 61.8$)	GX 340+0		LMXB
N588	J164635.9-450715	251.6495	-45.1207	8.4	17.2($-4.1 + 4.8$)	IGR J16465-4507		HMXB
N589	J164641.4-602405	251.6726	-60.4014	5.0	3.9($-1.9 + 2.5$)	CIZA J1646.6-6023	0.1480	CLUSTER
N590	J164806.4-451216	252.0266	-45.2044	8.6	22.5($-4.4 + 5.0$)	IGR J16479-4514		HMXB
N591	J164927.8-434912	252.3657	-43.8200	16.1	50.0($-5.7 + 6.3$)	IGR J16493-4348		HMXB
N592	J164955.8-330656	252.4826	-33.1156	4.9	9.6($-2.9 + 3.6$)	IGR J16500-3307		CV
N593	J165042.1+043618	252.6755	4.6050	6.0	9.4($-2.7 + 3.4$)	NGC 6230	0.0326	SEYFERT
N594	J165219.6+555423	253.0818	55.9065	6.5	2.8($-0.9 + 1.0$)	SBS 1651+559	0.0290	SEYFERT

Table A.1. Continued.

Id	Name	RA SRGA (J2000)	Dec (J2000)	S/N	Flux (10^{-12} erg s $^{-1}$ cm $^{-2}$)	Common name	Redshift	Class
N595	J165246.7–591257	253.1944	-59.2158	7.0	11.1($-2.7 + 3.3$)	NGC 6221	0.0050	SEYFERT
N596	J165309.5–594128 ^{b)}	253.2895	-59.6910		~50	CIZA J1653.0-5943	0.0480	CLUSTER
N597	J165351.4+394539	253.4642	39.7609	11.6	17.3($-2.6 + 3.0$)	Mrk 501	0.0330	BLAZAR
N598	J165443.8–191638	253.6823	-19.2772	6.8	16.1($-3.5 + 4.2$)	IGR J16547-1916		CV
N599	J165602.2+211245	254.0090	21.2125	6.1	7.6($-2.3 + 2.8$)	1RXS J165602.3+211239	0.0492	SEYFERT
N600	J165606.2–520339	254.0257	-52.0608	9.3	18.7($-3.6 + 4.2$)	IGR J16558-5203	0.0540	SEYFERT
N601	J165749.5+352028	254.4561	35.3410	23.1	61.4($-4.6 + 5.0$)	Her X-1		LMXB
N602	J165833.5+051516	254.6398	5.2544	6.3	6.4($-2.3 + 2.9$)	PKS 1656+053	0.8800	BLAZAR
N603	J170004.3–415800	255.0180	-41.9668	5.7	7.2($-2.7 + 3.4$)	AX J1740.1-2847		HMXB
N604	J170048.7–413923	255.2028	-41.6563	39.7	371.3($-15.2 + 15.9$)	OAO 1657-41		HMXB
N605	J170053.1+400356	255.2211	40.0655	5.2	1.7($-1.2 + 1.5$)	V1237 Her		CV
N606	J170144.3–405130	255.4347	-40.8582	31.9	246.3($-12.4 + 13.1$)	XTE J1701-407		LMXB
N607	J170249.0–484727	255.7042	-48.7908	16.4	50.9($-5.7 + 6.4$)	GX 339-4		LMXB
N608	J170318.6–630500	255.8275	-63.0833	5.1	4.1($-2.0 + 2.5$)			UNIDENT
N609	J170337.5+783723 ^{b)}	255.9064	78.6230		~40	Abell 2256	0.0583	CLUSTER
N610	J170356.7–375038	255.9863	-37.8440	112.3	2892.7($-43.1 + 43.7$)	4U 1700-37		HMXB
N611	J170412.1–443138	256.0503	-44.5272	6.3	8.9($-2.8 + 3.4$)	1RXS J170410.9-443131		UNIDENT
N612	J170433.6–483051	256.1399	-48.5140	4.8	3.6($-2.1 + 2.7$)			UNIDENT
N613	J170442.4+604435	256.1767	60.7430	5.8	1.7($-0.6 + 0.7$)	3C 351	0.3715	SEYFERT
N614	J170544.3–362521	256.4345	-36.4224	181.3	7510.9($-69.6 + 70.3$)	GX 349+2		LMXB
N615	J170615.2–430211	256.5633	-43.0364	46.9	519.8($-18.1 + 18.8$)	4U 1702-429		LMXB
N616	J170616.4–614239	256.5685	-61.7107	15.0	33.7($-4.4 + 4.9$)	IGR J17062-6143		LMXB
N617	J170634.1+235819	256.6421	23.9719	16.3	38.0($-4.3 + 4.7$)	4U 1700+24		LMXB
N618	J170806.7–314923	257.0278	-31.8230	5.3	5.1($-2.4 + 3.1$)			UNIDENT
N619	J170846.1–400856	257.1919	-40.1488	7.6	7.9($-2.7 + 3.4$)	1RXS J170849.0-400910		MAGNETAR
N620	J170855.1–321849	257.2295	-32.3137	5.5	5.1($-2.4 + 3.1$)	4U 1705-32		LMXB
N621	J170855.1–440612	257.2298	-44.1034	39.7	362.2($-14.9 + 15.5$)	4U 1705-44		LMXB
N622	J170930.5–263925	257.3770	-26.6571	5.2	10.6($-3.1 + 3.8$)	XTE J1709-267		LMXB
N623	J171012.8–280751	257.5533	-28.1310	9.6	20.6($-4.0 + 4.7$)	XTE J1710-281		LMXB
N624	J171223.6–405036	258.0982	-40.8432	21.2	76.6($-7.2 + 7.9$)	4U 1708-40		LMXB
N625	J171226.3–232138 ^{b)}	258.1097	-23.3606		~500	Oph Cluster	0.0280	CLUSTER
N626	J171236.8–241449	258.1535	-24.2470	14.4	43.6($-5.6 + 6.3$)	V2400 Oph		CV
N627	J171237.0–373843	258.1541	-37.6451	13.9	49.6($-5.8 + 6.5$)	SAX J1712.6-3739		LMXB
N628	J171256.0+640406 ^{b)}	258.2333	64.0683		~20	Abell 2255	0.0801	CLUSTER
N629	J171334.5–252010	258.3937	-25.3362	5.3	7.8($-2.7 + 3.5$)	1RXS J171333.8-252018		UNIDENT
N630	J171516.9+031034 ^{b)}	258.8205	3.1761		~20	RXC J1715.2+0309	0.1647	CLUSTER
N631	J171659.8–624919	259.2493	-62.8219	7.8	12.1($-2.8 + 3.4$)	NGC 6300	0.0037	SEYFERT
N632	J171936.0–410052	259.8998	-41.0146	10.5	23.1($-4.1 + 4.8$)	IGR J17195-4100		CV
N633	J172005.9–311658	260.0246	-31.2829	10.2	16.7($-3.7 + 4.4$)	IGR J17200-3116		LMXB
N634	J172202.6+431532	260.5108	43.2588	6.2	4.3($-1.4 + 1.7$)	RBS 1640	0.1390	SEYFERT
N635	J172307.2–124810	260.7800	-12.8028	15.0	39.6($-5.3 + 6.0$)	RY Ser		CV
N636	J172321.0+341755	260.8373	34.2985	5.3	6.6($-1.9 + 2.3$)	4C +34.47	0.2060	SEYFERT
N637	J172324.5+362958	260.8522	36.4996	6.2	5.6($-1.7 + 2.1$)	IRAS 17216+3633	0.0400	SEYFERT

Table A.1. Continued.

Id	Name SRGA	RA (J2000)	Dec (J2000)	S/N	Flux	Common name	Redshift	Class
					$(10^{-12} \text{ erg s}^{-1} \text{ cm}^{-2})$			
N638	J172525.9–325713	261.3578	-32.9537	9.8	23.0($-4.3 + 5.1$)	IGR J17254-3257		LMXB
N639	J172733.4–304801	261.8892	-30.8002	25.8	130.2($-9.5 + 10.2$)	4U 1722-30		LMXB
N640	J172818.3+501309	262.0765	50.2192	6.4	2.5($-1.1 + 1.3$)	6C 172704+501607	0.0550	BLAZAR
N641	J173022.0–055928	262.5916	-5.9910	10.1	22.3($-4.0 + 4.7$)	V2731 Oph		CV
N642	J173043.4–212854 ^{b)}	262.6807	-21.4817		~20	Kepler SNR		SNR
N643	J173144.2–165747	262.9341	-16.9630	101.0	2427.8($-40.1 + 40.8$)	GX 9+9		LMXB
N644	J173158.0–334958	262.9917	-33.8329	62.3	931.1($-24.7 + 25.3$)	GX 354-0		LMXB
N645	J173202.0–244448	263.0084	-24.7466	30.9	258.7($-13.5 + 14.2$)	GX 1+4		LMXB
N646	J173250.9–273000	263.2121	-27.5001	11.0	22.5($-4.2 + 4.9$)	IGR J17329-2731		LMXB
N647	J173253.7–440731	263.2239	-44.1253	4.9	7.0($-2.6 + 3.4$)	2SXPS J173253.9-440728		UNIDENT
N648	J173324.0–332319	263.3500	-33.3886	34.8	312.9($-14.6 + 15.3$)	Rapid Burster		LMXB
N649	J173527.1–325554	263.8628	-32.9316	8.7	19.4($-4.0 + 4.8$)	IGR J17354-3255		HMXB
N650	J173547.1–302859	263.9464	-30.4829	17.9	74.8($-7.4 + 8.2$)	XB 1732-304		LMXB
N651	J173549.3+223747	263.9556	22.6297	4.9	3.0($-1.7 + 2.2$)			UNIDENT
N652	J173728.9–290801	264.3705	-29.1336	14.1	45.2($-5.8 + 6.5$)	GRS 1734-292	0.0210	SEYFERT
N653	J173759.5–374620	264.4978	-37.7721	11.1	27.2($-4.6 + 5.3$)	IGR J17379-3747		LMXB
N654	J173817.6–265939	264.5735	-26.9941	25.0	172.4($-11.0 + 11.7$)	SLX 1735-269		LMXB
N655	J173858.5–442701	264.7438	-44.4503	102.8	2473.6($-40.2 + 40.8$)	4U 1735-444		LMXB
N656	J173953.4–282943	264.9723	-28.4952	16.4	57.5($-6.5 + 7.3$)	XTE J1739-285		LMXB
N657	J174009.6–284714	265.0401	-28.7872	5.3	4.4($-2.4 + 3.2$)	AX J1740.1-2847		CV? ^{c)}
N658	J174025.2+514944	265.1051	51.8290	5.7	3.2($-1.1 + 1.2$)	2E 1739.2+5151	0.0610	SEYFERT
N659	J174028.2–365545	265.1176	-36.9292	5.6	11.8($-3.2 + 3.9$)	IGR J17404-3655		CV ^{c)}
N660	J174046.4+060353	265.1932	6.0647	8.9	14.0($-3.3 + 3.9$)	PBC J1740.7+0603		CV ^{c)}
N661	J174128.8+034854	265.3699	3.8151	5.3	6.6($-2.5 + 3.2$)	RX J1741.4+0348	0.0230	SEYFERT
N662	J174155.6–121207	265.4815	-12.2018	7.5	11.0($-3.1 + 3.9$)	2E 1739.1-1210	0.0370	SEYFERT
N663	J174217.7+635124	265.5738	63.8568	5.9	0.4($-0.3 + 0.4$)	RX J1742.2+6351	0.4019	SEYFERT
N664	J174354.7–294444	265.9780	-29.7456	26.3	175.1($-11.1 + 11.8$)	1E1740.7-2942		LMXB
N665	J174400.1–035013	266.0004	-3.8371	4.9	5.5($-2.4 + 3.2$)	PKS 1741-03	1.0540	BLAZAR
N666	J174446.1–295057	266.1919	-29.8492	6.4	11.2($-3.5 + 4.3$)	XMMU J174445.5-29504		LMXB ^{c)}
N667	J174450.9–323321 ^{b)}	266.2120	-32.5558		~50	IGR J17448-3232	0.0550	CLUSTER ^{c)}
N668	J174502.3–285441	266.2598	-28.9115	12.4	35.5($-5.5 + 6.2$)	GRS 1741.9-2853		LMXB
N669	J174503.2+141104	266.2632	14.1845	4.9	1.2($-1.2 + 2.2$)			UNIDENT
N670	J174535.6–290134	266.3984	-29.0260	20.9	143.9($-10.4 + 11.1$)	1A 1742-289		LMXB
N671	J174605.3–293052	266.5220	-29.5145	56.7	842.6($-24.5 + 25.2$)	1A 1742-294		LMXB
N672	J174621.1–284338	266.5879	-28.7274	21.9	116.9($-9.3 + 10.0$)	1E 1743.1-2843		LMXB
N673	J174700.1+683626	266.7505	68.6072	6.6	0.9($-0.4 + 0.5$)	VII Zw 742	0.0631	SEYFERT
N674	J174726.0–300002	266.8584	-30.0006	19.2	101.0($-8.6 + 9.3$)	SLX 1744-299		LMXB
N675	J174726.2–300245	266.8592	-30.0458	29.4	212.8($-12.2 + 12.9$)	SLX 1744-300		LMXB
N676	J174729.8–225250	266.8740	-22.8806	6.1	7.8($-2.8 + 3.5$)	IGR J17476-2253	0.0470	SEYFERT
N677	J174756.3–263347	266.9846	-26.5631	109.4	2964.6($-45.3 + 46.0$)	GX 3+1		LMXB
N678	J174834.1–290514	267.1423	-29.0873	4.9	1.1($-1.1 + 2.7$)			UNIDENT
N679	J174838.6–233523	267.1610	-23.5897	5.3	7.5($-2.7 + 3.5$)	IGR J17488-2338	0.2400	SEYFERT
N680	J174854.1–325447	267.2253	-32.9130	7.0	10.2($-3.1 + 3.8$)	IGR J17488-3253	0.0200	SEYFERT

Table A.1. Continued.

Id	Name SRGA	RA (J2000)	Dec (J2000)	S/N	Flux (10^{-12} erg s $^{-1}$ cm $^{-2}$)	Common name	Redshift	Class
N681	J175003.8-322546	267.5159	-32.4295	10.0	26.2(-4.6 + 5.4)	2E 1746.7-3225		LMXB
N682	J175013.0-370305	267.5540	-37.0513	28.1	160.8(-10.8 + 11.5)	4U 1746-371		LMXB
N683	J175340.6+654240	268.4193	65.7112	5.6	0.4(-0.2 + 0.2)	7C 1753+6543	0.1400	BLAZAR
N684	J175713.1+703340	269.3044	70.5611	5.2	0.9(-0.5 + 0.6)	2E 1757.7+7034	0.4060	BLAZAR
N685	J175721.3-304400	269.3388	-30.7333	5.9	15.4(-4.1 + 5.1)	1RXS J175721.2-304405		LMXB ^{c)}
N686	J175840.6-334827	269.6693	-33.8074	27.0	179.7(-12.4 + 13.2)	4U 1755-33		LMXB
N687	J180007.7+663700	270.0320	66.6166	16.4	1.0(-0.1 + 0.1)	NGC 6552	0.0265	SEYFERT
N688	J180036.1+081015	270.1503	8.1710	7.9	11.2(-3.3 + 4.1)	V2301 Oph		CV
N689	J180108.7-250443	270.2863	-25.0786	193.5	11319.7(-98.3 + 99.2)	GX 5-1		LMXB
N690	J180112.4-254437	270.3019	-25.7435	29.9	310.2(-16.7 + 17.6)	GRS 1758-258		LMXB
N691	J180132.6-203145	270.3859	-20.5292	177.1	9333.3(-88.5 + 89.4)	GX 9+1		LMXB
N692	J180147.2+663835	270.4467	66.6430	9.2	0.2(-0.1 + 0.1)	RX J1801.7+6638		BLAZAR
N693	J180241.5-201714	270.6730	-20.2873	9.8	32.0(-6.8 + 7.7)	IGR J18027-2016		HMXB
N694	J180328.3+673813	270.8681	67.6368	8.1	0.6(-0.2 + 0.2)	QSO B1803+6737	0.1354	SEYFERT
N695	J180651.3+694926	271.7138	69.8240	10.6	3.1(-0.5 + 0.6)	3C 371	0.0510	BLAZAR
N696	J180751.9+055147	271.9663	5.8631	11.6	25.4(-4.7 + 5.6)	V426 Oph		CV
N697	J180835.6+101034	272.1482	10.1760	5.8	6.8(-2.7 + 3.5)	1RXS J180834.7+101041		CV
N698	J180849.4+663432	272.2057	66.5755	4.9	0.5(-0.2 + 0.2)	RX J1808.7+6634	0.6970	BLAZAR ^{c)}
N699	J181021.4-190413	272.5890	-19.0703	20.0	97.7(-9.6 + 10.6)	XTE J1810-189		LMXB
N700	J181228.0-181235	273.1167	-18.2097	38.3	491.0(-20.8 + 21.7)	XTE J1812-182		LMXB ^{c)}
N701	J181239.6-221924	273.1650	-22.3232	19.3	81.6(-8.8 + 9.7)	MAXI J1810-222		LMXB? ^{c)}
N702	J181431.3-170923	273.6303	-17.1564	101.7	3673.9(-60.3 + 61.3)	GX 13+1		LMXB
N703	J181506.4-120548	273.7766	-12.0967	21.0	137.0(-11.8 + 12.9)	4U 1812-12		LMXB
N704	J181601.7-140209	274.0072	-14.0357	149.6	8516.4(-95.5 + 96.5)	GX 17+2		LMXB
N705	J181611.0+423955	274.0460	42.6654	6.8	8.0(-2.2 + 2.6)	MCG +07-37-031	0.0412	SEYFERT
N706	J181613.0+495203	274.0542	49.8676	28.2	84.4(-5.1 + 5.4)	AM Her		CV
N707	J181637.1-391248	274.1546	-39.2134	4.9	8.9(-3.4 + 4.5)	IGR J18165-3912		X-RAY BINARY? ^{c)}
N708	J181800.0-160745	274.4998	-16.1292	5.4	12.9(-4.2 + 5.3)	SWIFT J1818.0-1607		MAGNETAR
N709	J181829.1+674121	274.6213	67.6892	8.0	0.6(-0.3 + 0.3)	2E 1818.6+6740	0.3140	SEYFERT
N710	J181921.8-252418	274.8408	-25.4049	10.5	29.1(-5.8 + 7.0)	V4641 Sgr		HMXB
N711	J182155.0-134713	275.4794	-13.7870	7.3	19.0(-5.1 + 6.4)	IGR J18219-1347		HMXB
N712	J182156.2+642036	275.4843	64.3434	14.2	8.4(-0.8 + 0.9)	H 1821+643	0.2970	SEYFERT ^{c)}
N713	J182340.5-302138	275.9189	-30.3606	85.3	2903.4(-56.6 + 57.7)	4U 1820-30		LMXB
N714	J182511.1+645018	276.2964	64.8383	9.1	4.0(-0.6 + 0.7)	2E 1824.9+6448		STAR ^{c)}
N715	J182522.3-000041	276.3431	-0.0113	22.3	122.6(-11.2 + 12.2)	4U 1822-00		LMXB
N716	J182547.0-370617	276.4459	-37.1048	32.9	426.5(-21.0 + 22.0)	4U 1822-37		LMXB
N717	J182606.8-041144	276.5284	-4.1957	5.1	4.7(-2.8 + 4.0)			UNIDENT
N718	J182848.6+502218	277.2026	50.3716	8.8	8.5(-1.9 + 2.3)	Ark 539	0.0164	SEYFERT
N719	J182919.6-121301	277.3318	-12.2169	5.1	6.2(-3.1 + 4.2)	IGR J18293-1213		CV? ^{c)}
N720	J182928.8-234748	277.3699	-23.7967	71.3	2033.1(-47.2 + 48.3)	GS 1826-24		LMXB
N721	J183022.8+731314	277.5949	73.2206	10.7	5.2(-0.8 + 0.9)	IRAS F18315+7310	0.1230	SEYFERT
N722	J183050.2-123223	277.7090	-12.5397	6.1	13.0(-4.3 + 5.6)	IGR J18308-1232		CV
N723	J183334.0-103401	278.3915	-10.5670	11.9	45.4(-7.1 + 8.3)	SNR 021.5-00.9		SNR / PULSAR

Table A.1. Continued.

Id	Name	RA SRGA	Dec (J2000)	S/N	Flux (10^{-12} erg s $^{-1}$ cm $^{-2}$)	Common name	Redshift	Class
N724	J183341.1-210333	278.4212	-21.0592	7.1	12.1(-4.2 + 5.5)	PKS 1830-21	2.5070	BLAZAR
N725	J183504.0+324147	278.7667	32.6963	9.8	18.3(-3.6 + 4.3)	3C 382	0.0581	SEYFERT
N726	J183543.9-325918	278.9329	-32.9882	6.6	12.0(-4.0 + 5.2)	XB 1832-330		LMXB
N727	J183605.4-192217	279.0226	-19.3713	5.1	6.5(-3.1 + 4.3)			UNIDENT ^{c)}
N728	J183613.0-350922	279.0543	-35.1560	5.1	5.4(-3.0 + 4.2)			UNIDENT
N729	J183658.0-592400	279.2418	-59.4001	6.7	15.0(-4.0 + 5.0)	Fairall 49	0.0200	SEYFERT
N730	J183754.6+155438	279.4776	15.9105	6.3	8.3(-3.1 + 4.0)	1RXS J183753.8+155433		STAR? ^{c)}
N731	J183811.3+655451	279.5472	65.9141	5.2	1.0(-0.5 + 0.5)	HS 1838+6552	0.2310	AGN
N732	J183821.5-652543	279.5897	-65.4287	8.8	17.4(-4.1 + 4.9)	ESO 103-G035	0.0132	SEYFERT
N733	J183907.1-571456	279.7797	-57.2488	6.7	9.2(-3.3 + 4.3)	PBC J1838.9-5714		UNIDENT ^{c)}
N734	J183957.8+050213	279.9910	5.0369	267.0	2777.1(-17.5 + 17.6)	Ser X-1		LMXB
N735	J184117.8-045612	280.3243	-4.9366	18.4	14.7(-1.6 + 1.8)	1E 1841-045/Kes 73		MAGNETAR ^{c)}
N736	J184209.1+794613	280.5378	79.7703	15.7	17.1(-1.8 + 2.0)	3C 390.3	0.0561	SEYFERT
N737	J184239.8-042410	280.6659	-4.4027	7.9	13.9(-4.2 + 5.3)			UNIDENT
N738	J184527.3+721104	281.3637	72.1845	8.5	3.6(-0.7 + 0.8)	CGCG 341-006	0.0461	SEYFERT
N739	J184554.7-003937	281.4778	-0.6603	6.2	8.8(-3.7 + 4.9)	SWIFT J1845.7-0037		HMXB ^{c)}
N740	J184625.3-025830	281.6053	-2.9751	6.2	16.1(-4.8 + 6.0)	PSR J1846-0258		SNR / PULSAR
N741	J184817.8-031020	282.0741	-3.1722	11.7	37.2(-6.5 + 7.6)	IGR J18483-0311		HMXB
N742	J184823.1+653654	282.0961	65.6151	6.3	1.5(-0.6 + 0.6)	1RXS J184822.6+653700	0.3640	BLAZAR
N743	J184855.6+003447	282.2315	0.5798	5.1	11.0(-3.8 + 5.0)	V603 Aql		CV
N744	J185304.6-084223	283.2692	-8.7064	14.3	55.8(-8.1 + 9.3)	4U 1850-086		LMXB
N745	J185354.7+682253	283.4780	68.3814	5.1	1.0(-0.5 + 0.5)	Abell 2312	0.0930	CLUSTER
N746	J185421.6+083844	283.5900	8.6456	5.0	6.7(-3.0 + 4.0)	IGR J18544+0839		AGN? ^{c)}
N747	J185501.8-310955	283.7576	-31.1652	10.3	30.2(-6.1 + 7.3)	V1223 Sgr		CV
N748	J185530.4-023614	283.8767	-2.6038	23.7	150.9(-12.4 + 13.4)	XTE J1855-026		HMXB
N749	J185707.5-782826	284.2812	-78.4740	5.5	7.1(-2.5 + 3.2)	2E 1849.2-7832	0.0433	SEYFERT
N750	J190140.2+012627	285.4176	1.4407	8.5	19.0(-4.8 + 5.9)	XTE J1901+014		LMXB? ^{c)}
N751	J190614.0-535110	286.5584	-53.8529	5.3	3.2(-2.4 + 3.5)			UNIDENT
N752	J190629.5-044654	286.6227	-4.7816	5.5	7.9(-3.4 + 4.5)			UNIDENT
N753	J190722.0-204635	286.8415	-20.7764	9.3	25.5(-5.6 + 6.7)	V1082 Sgr		CV? ^{c)}
N754	J190824.0+522559	287.1001	52.4329	5.2	2.3(-1.3 + 1.6)	V1762 Cyg		STAR
N755	J190938.1+094942	287.4088	9.8284	26.0	186.6(-13.5 + 14.5)	4U 1907+09		HMXB
N756	J191048.4+073552	287.7018	7.5978	26.9	203.6(-14.0 + 14.9)	4U 1909+07		HMXB
N757	J191109.5+090621	287.7894	9.1059	6.9	27.1(-5.5 + 6.5)	W49B		SNR
N758	J191115.6+003502	287.8152	0.5839	32.8	456.7(-22.5 + 23.6)	Aql X-1		LMXB
N759	J191149.6+045850	287.9566	4.9806	15.2	58.1(-7.7 + 8.7)	SS 433		HMXB
N760	J191404.4+095300	288.5182	9.8833	11.0	28.7(-5.5 + 6.5)	IGR J19140+0951		HMXB
N761	J191456.9+103647	288.7372	10.6131	8.5	19.8(-4.7 + 5.7)	IGR J19149+1036		HMXB? ^{c)}
N762	J191511.1+105648	288.7963	10.9466	25.2	176.4(-13.2 + 14.2)	GRS 1915+105		LMXB
N763	J191847.6-051417	289.6984	-5.2382	26.9	218.8(-14.9 + 16.0)	4U 1916-053		LMXB
N764	J191927.5-295801	289.8646	-29.9668	5.6	9.2(-3.6 + 4.8)	PKS 1916-300	0.1668	SEYFERT
N765	J192114.0+435657 ^{b)}	290.3084	43.9493		~100	Abell 2319	0.0559	CLUSTER
N766	J192114.1-584017	290.3086	-58.6713	8.4	17.3(-4.1 + 4.9)	ESO 141-G055	0.0371	SEYFERT

Article number, page 38 of 40
Table A.1. Continued.

Id	Name	RA	Dec	S/N	Flux	Common name	Redshift	Class
					(10^{-12} erg s $^{-1}$ cm $^{-2}$)			
N767	J192214.5+691111	290.5604	69.1865	7.8	2.6($-0.7 + 0.7$)	4C 69.26	0.0970	SEYFERT
N768	J192433.0+501434	291.1373	50.2429	11.2	15.3($-2.5 + 2.9$)	CH Cyg		CV
N769	J192501.3+504309	291.2554	50.7192	6.1	4.4($-1.5 + 1.8$)	2E 1923.7+5037	0.0670	SEYFERT ^{c)}
N770	J192502.3+281534	291.2597	28.2594	5.0	4.6($-2.2 + 3.1$)	1RXS J192502.7+281540		BLAZAR
N771	J192748.3+735752	291.9514	73.9644	5.0	4.2($-0.9 + 1.1$)	4C 73.18	0.3021	BLAZAR
N772	J192955.4+181831	292.4809	18.3086	5.2	4.1($-2.5 + 3.5$)	IGR J19294+1816		HMXB
N773	J193345.9+325421	293.4412	32.9058	5.2	10.3($-3.3 + 4.2$)	SWIFT J1933.9+3258	0.0565	SEYFERT
N774	J193355.6+654021	293.4815	65.6724	5.3	1.3($-0.8 + 0.9$)	6C 193337+653350	1.6870	BLAZAR
N775	J193732.5-061303	294.3855	-6.2176	7.4	20.9($-5.1 + 6.3$)	1H 1934-063	0.0103	SEYFERT
N776	J193927.4+700748	294.8641	70.1300	6.2	2.2($-0.7 + 0.8$)	1RXS J193929.8+700752	0.1200	SEYFERT
N777	J194010.7-102528	295.0444	-10.4246	8.8	22.4($-5.4 + 6.7$)	V1432 Aql		CV
N778	J194241.4-101932	295.6723	-10.3256	9.3	26.2($-5.6 + 6.7$)	NGC 6814	0.0052	SEYFERT
N779	J194638.9+704552	296.6620	70.7643	11.1	6.8($-0.9 + 1.0$)	1RXS J194639.7+704552		CV ^{c)}
N780	J194649.6-233834	296.7067	-23.6428	4.9	4.8($-2.9 + 4.2$)			UNIDENT
N781	J194719.9+444942	296.8328	44.8285	7.0	6.2($-2.1 + 2.5$)	XSS J19459+4508	0.0530	SEYFERT
N782	J194753.2+102000	296.9718	10.3334	4.9	3.9($-2.5 + 3.6$)			UNIDENT
N783	J195541.9+320549	298.9247	32.0970	27.7	156.2($-10.2 + 10.9$)	4U 1954+31		LMXB
N784	J195702.4+615036	299.2601	61.8435	6.0	3.4($-1.2 + 1.4$)	1RXS J195702.3+615038		AGN ^{c)}
N785	J195815.4-301050	299.5641	-30.1806	5.1	6.0($-3.2 + 4.5$)	1RXS J195815.6-301119	0.1193	BLAZAR
N786	J195822.1+351205	299.5920	35.2015	141.1	4063.7($-48.3 + 48.8$)	Cyg X-1		HMXB
N787	J195834.2+182656	299.6426	18.4489	5.0	5.9($-2.8 + 3.8$)			UNIDENT
N788	J195923.6+114224	299.8484	11.7067	26.2	172.2($-13.2 + 14.3$)	4U 1957+115		LMXB
N789	J195928.3+404358	299.8678	40.7328	14.8	42.9($-4.8 + 5.4$)	Cyg A	0.0561	CLUSTER ^{c)}
N790	J195958.1+650858	299.9920	65.1493	39.8	97.7($-4.0 + 4.2$)	1ES 1959+650	0.0470	BLAZAR
N791	J200021.7+321122	300.0906	32.1894	8.0	13.4($-3.2 + 3.9$)	IGR J20006+3210		HMXB
N792	J200845.7-610615	302.1906	-61.1042	5.2	6.7($-2.9 + 3.9$)	NGC 6860	0.0152	SEYFERT
N793	J200910.7+323354	302.2947	32.5650	5.3	10.1($-3.2 + 4.0$)	1RXS J200912.0+323344		STAR
N794	J201118.2+600421	302.8258	60.0726	5.2	3.3($-1.3 + 1.6$)	1RXS J201117.9+600421		CV? ^{c)}
N795	J202835.3+254404	307.1473	25.7344	6.0	11.5($-3.3 + 4.2$)	MCG +04-48-002	0.0148	SEYFERT
N796	J202932.4-614903	307.3852	-61.8176	5.3	3.0($-2.2 + 3.2$)	XMMSL1 J202931.2-614858		AGN ^{c)}
N797	J203215.7+373813	308.0655	37.6371	7.3	14.0($-3.2 + 3.8$)	EXO 2030+375		HMXB
N798	J203225.6+405729	308.1068	40.9580	119.8	2996.2($-41.8 + 42.4$)	Cyg X-3		HMXB
N799	J203430.7-303728	308.6280	-30.6245	7.3	19.2($-4.9 + 6.0$)	1RXS J203433.1-303731	0.0194	SEYFERT
N800	J204149.6-373345	310.4566	-37.5626	5.2	11.7($-4.0 + 5.3$)	RBS 1691	0.0985	BLAZAR? ^{c)}
N801	J204237.3+750802	310.6554	75.1339	14.8	15.1($-1.7 + 1.8$)	4C 74.26	0.1040	SEYFERT
N802	J204319.7+443821	310.8319	44.6392	6.5	5.4($-2.1 + 2.7$)			HMXB ^{c)}
N803	J204405.6+394132	311.0233	39.6923	5.1	2.4($-1.8 + 2.4$)			UNIDENT
N804	J204409.3-104325	311.0388	-10.7235	9.7	26.1($-5.7 + 6.9$)	Mrk 509	0.0341	SEYFERT
N805	J204547.8+672642	311.4490	67.4451	6.1	3.5($-1.0 + 1.2$)	1RXS J204549.1+672615		CV ^{c)}
N806	J205642.5+494008	314.1772	49.6689	12.6	19.8($-3.7 + 4.3$)	1RXS J205644.3+494011		BLAZAR
N807	J210302.8-435148	315.7617	-43.8634	4.8	5.9($-2.9 + 4.2$)			UNIDENT
N808	J210336.2+454507	315.9010	45.7520	29.8	143.3($-7.6 + 8.1$)	SAX J2103.5+4545		HMXB
N809	J210845.3-051328	317.1887	-5.2243	4.8	2.4($-2.3 + 3.4$)			UNIDENT

Table A.1. Continued.

Id	Name	RA	Dec	S/N	Flux	Common name	Redshift	Class
	SRGA	(J2000)	(J2000)		(10^{-12} erg s $^{-1}$ cm $^{-2}$)			
N810	J211333.7+542227	318.3905	54.3742	7.7	7.7(-2.0 + 2.4)	1RXS J211336.1+542226		CV
N811	J211401.1+820452	318.5045	82.0811	10.0	8.7(-1.6 + 1.8)	S5 2116+81	0.0860	SEYFERT
N812	J211747.6+513850	319.4485	51.6471	8.8	8.7(-2.3 + 2.7)	IGR J21178+5139		BLAZAR? ^{c)}
N813	J212438.7+505820	321.1612	50.9723	18.2	47.5(-4.6 + 5.0)	4C +50.55	0.0200	SEYFERT
N814	J212745.1+565645	321.9379	56.9457	9.4	10.8(-2.4 + 2.9)	IGR J21277+5656	0.0147	SEYFERT
N815	J212901.1+363109	322.2548	36.5192	5.9	2.8(-1.8 + 2.4)	1RXS J212902.0+363103		UNIDENT
N816	J212912.4-153830	322.3017	-15.6417	5.1	7.7(-3.2 + 4.3)	PKS 2126-158	3.2680	BLAZAR
N817	J212958.5+121000	322.4939	12.1666	18.0	80.4(-8.5 + 9.4)	4U 2129+12		LMXB
N818	J213136.0-120707	322.9000	-12.1187	5.4	5.6(-2.9 + 4.0)	PKS 2128-12	0.5010	BLAZAR
N819	J213151.5+491400	322.9647	49.2334	5.1	4.0(-1.8 + 2.3)			UNIDENT
N820	J213203.0-334249	323.0126	-33.7135	5.2	11.5(-3.8 + 4.9)	CTS 109	0.0300	SEYFERT
N821	J213343.3+510729	323.4304	51.1248	9.6	15.3(-2.8 + 3.2)	RX J2133.7+5107		CV
N822	J213419.5+473758	323.5814	47.6328	13.7	31.1(-4.3 + 4.9)	IGR J21347+4737		HMXB
N823	J213551.9+472758	323.9661	47.4661	4.8	4.8(-2.1 + 2.7)	RX J2135.9+4728	0.0252	SEYFERT
N824	J213622.9-622400	324.0953	-62.4000	6.9	9.9(-3.2 + 4.0)	1RXS J213623.1-622400	0.0586	SEYFERT
N825	J213806.2+261955	324.5257	26.3319	4.9	3.2(-2.2 + 3.2)	V627 Peg		CV
N826	J213822.1+282723	324.5921	28.4563	4.9	9.3(-3.1 + 4.0)			UNIDENT
N827	J214149.4-501919	325.4559	-50.3219	4.8	4.7(-2.6 + 3.6)			UNIDENT
N828	J214243.4+433509	325.6807	43.5860	32.1	229.8(-11.6 + 12.1)	SS Cyg		CV
N829	J214441.2+381917	326.1715	38.3214	129.9	5182.6(-66.8 + 67.6)	Cyg X-2		LMXB
N830	J215659.1+624928	329.2463	62.8245	5.3	0.6(-0.6 + 1.3)			UNIDENT
N831	J220201.3-315159	330.5054	-31.8664	6.6	15.5(-4.1 + 5.2)	NGC 7172	0.0086	SEYFERT
N832	J220755.4+543118	331.9806	54.5216	23.1	25.1(-1.9 + 2.0)	4U 2206+543		HMXB
N833	J220841.2+454434	332.1715	45.7427	8.6	5.4(-1.7 + 2.1)	AR Lac		STAR
N834	J221023.5-361058	332.5979	-36.1827	5.0	6.5(-2.9 + 3.9)			UNIDENT
N835	J221144.8-034933	332.9366	-3.8258	5.3	11.6(-3.9 + 5.0)	MCXC J2211.7-0349	0.3970	CLUSTER
N836	J221401.4+124217	333.5058	12.7047	4.8	4.1(-2.2 + 3.0)	RU Peg		CV
N837	J221754.8-082104	334.4783	-8.3511	10.4	31.7(-6.1 + 7.3)	FO Aqr		CV
N838	J221913.2+362014	334.8051	36.3373	4.9	5.4(-2.3 + 3.0)			AGN ^{c)}
N839	J222320.8+021841	335.8368	2.3114	5.4	4.7(-2.7 + 3.9)			UNIDENT
N840	J222446.5+220432	336.1937	22.0754	4.9	7.1(-3.4 + 4.7)			UNIDENT
N841	J222914.6+664650	337.3109	66.7806	7.4	4.5(-1.3 + 1.5)	IGR J22292+6647	0.1130	SEYFERT
N842	J223452.7-843445	338.7198	-84.5791	4.9	3.6(-1.8 + 2.4)	1RXS J223455.8-843450		AGN
N843	J223546.4-260300	338.9432	-26.0501	6.6	13.7(-4.1 + 5.2)	NGC 7314	0.0048	SEYFERT
N844	J223714.9+402939	339.3120	40.4942	5.2	5.0(-2.3 + 2.9)	1RXS J223716.6+403021	0.0580	AGN ^{c)}
N845	J224548.5+394127	341.4522	39.6910	5.3	2.6(-1.8 + 2.5)	3C 452	0.0811	SEYFERT
N846	J225051.5-085457	342.7144	-8.9158	5.7	7.8(-2.9 + 3.8)	2MASX J22505170-0854572	0.0649	SEYFERT
N847	J225355.4+624335	343.4810	62.7264	7.8	4.5(-1.4 + 1.7)	IGR J22534+6243		HMXB
N848	J225405.5-173459	343.5231	-17.5830	10.4	27.2(-5.5 + 6.5)	MR 2251-178	0.0640	SEYFERT
N849	J225412.8+690658	343.5534	69.1161	5.8	2.7(-1.1 + 1.3)	1RXS J225415.8+690654		CV ^{c)}
N850	J225517.8-031037	343.8241	-3.1769	11.5	41.0(-7.3 + 8.6)	AO Psc		CV
N851	J230109.9+585254	345.2913	58.8818	5.2	1.2(-1.1 + 1.4)	1E 2259+586		MAGNETAR
N852	J230200.0+155755	345.5000	15.9653	5.8	8.7(-3.1 + 4.0)	NGC 7465	0.0065	SEYFERT

Table A.1. Continued.

Id	Name SRGA	RA (J2000)	Dec (J2000)	S/N	Flux	Common name	Redshift	Class
					$(10^{-12} \text{ erg s}^{-1} \text{ cm}^{-2})$			
N853	J230315.4+085239	345.8143	8.8776	8.3	17.9($-4.4 + 5.4$)	NGC 7469	0.0159	SEYFERT
N854	J230443.8-084118	346.1825	-8.6884	7.5	19.7($-5.4 + 6.7$)	Mrk 926	0.0470	SEYFERT
N855	J230630.9+155637	346.6286	15.9435	5.5	6.6($-2.7 + 3.7$)		0.4386	SEYFERT ^{c)}
N856	J230703.5+043258	346.7647	4.5494	7.8	11.4($-3.8 + 4.9$)	PG 2304+042	0.0420	SEYFERT
N857	J230832.7+394232	347.1360	39.7090	4.9	3.5($-2.0 + 2.6$)			UNIDENT
N858	J232035.4+643046	350.1474	64.5128	5.7	5.7($-1.5 + 1.8$)	IGR J23206+6431	0.0717	SEYFERT
N859	J232037.8+482329	350.1573	48.3914	5.2	1.6($-1.5 + 2.0$)	2RXS J232039.7+482317	0.0415	AGN ^{c)}
N860	J232116.0-265903	350.3168	-26.9841	4.9	8.3($-2.6 + 3.3$)	HD 220096		STAR
N861	J232326.0+584841 ^{b)}	350.8584	58.8113		~ 200	Cas A		SNR
N862	J232901.1-294708	352.2547	-29.7854	5.2	8.8($-2.9 + 3.6$)	VY Scl		CV
N863	J234023.7+123725	355.0986	12.6235	5.0	6.5($-2.8 + 3.7$)	HX Peg		CV
N864	J234704.3+514212	356.7681	51.7035	5.2	2.0($-1.4 + 1.8$)	1ES 2344+514	0.0440	BLAZAR
N865	J234754.0+543630	356.9750	54.6085	6.1	5.9($-1.8 + 2.1$)	3FHL J2347.9+5435		BLAZAR
N866	J235250.6-170449	358.2108	-17.0804	6.0	6.6($-3.0 + 4.0$)	SWIFT J2352.6-1707		AGN ^{c)}
N867	J235908.3-303800	359.7847	-30.6331	5.1	7.5($-3.5 + 4.8$)	H 2356-309	0.1654	BLAZAR

Notes. ^(a) For the description of columns see §4. Online version of this catalog is available at <http://srg.cosmos.ru>. ^(b) Spatial extension of the source is detected. ^(c) Additional information on the source identification/classification is provided in Sect. 1.